國立臺灣大學工學院材料科學與工程學研究所

碩士論文

Department of Materials Science and Engineering

College of Engineering

National Taiwan University

Master Thesis

二氧化鈦奈米晶體之表面改質應用於有機無機混摻

太陽能電池之研究

Study of Surface Modification of TiO$_2$ Nanorod in

Organic/Inorganic Hybrid Solar Cells

徐瑞鴻

Jui-Hung Hsu

指導教授：林唯芳　博士

Advisor: Wei-Fang Su, Ph.D.

中華民國　九十八　年　七　月

July, 2009

摘要

　　本研究探討導電高分子 P3HT 與二氧化鈦奈米桿的混摻系統中,二氧化鈦奈米桿的表面改質研究。預期藉由奈米桿的表面改質,提昇有機無機混摻太陽能電池的能量轉換效率。在此,表面改質乃是利用化學置換反應,去除原本存附於二氧化鈦奈米桿表面的非導電分子,並分別吸附二種導電性的界面改質分子(interface modifier),即酞菁銅(CuPc)的衍生物 Cudye 及末端具羧酸基的己基噻吩寡體(oligomer 3HT-COOH),以增進載子在予體、受體界面的傳輸性質。由定性及定量分析結果,可確認表面改質分子可於二氧化鈦奈米桿表面產生有效吸附。雖然由於其較少的吸附量,改質分子的存在不足以額外提昇混摻系統對光子的吸收,但系統中的激子分離效率卻可在改質後獲得很大程度的提昇;電子與電洞的再結合亦可被有效抑制。另外,在表面改質後,P3HT 與二氧化鈦間顯示了更為相近的親疏水性,混摻薄膜中的高分子也具備較佳的結晶排列,因此可推測表面改質亦有助於提昇混摻系統中,有機相(P3HT)與無機相(二氧化鈦奈米桿)之間的相容性。藉由釐清表面改質分子在有機太陽能電池作用層中的角色與功能,本研究提供了一提昇太陽能電池效率的可行途徑。

關鍵字:有機太陽能電池、聚三己基噻吩、二氧化鈦奈米桿、異質接面結構、表面改質、表面改質分子

Abstract

   This work presents the study of surface modification of TiO_2 nanorod in bulk heterojunction composites based on poly(3-hexylthiophene) (P3HT) and TiO_2 nanorods, trying to improve the performance of organic/inorganic hybrid solar cells. Surface modification of TiO_2 was performed by replacing the insulating surface ligand (oleic acid) with two kinds of conductive, novel interface modifiers: the derivative of copper phthalocyanine (Cudye) and the regioregular 3-hexylthiophene oligomer with carboxylic end functional groups (oligomer 3HT–COOH). As surface modification was carried out, the hybrid system exhibited an improved charge separation by showing a more pronounced PL quenching. Also, back recombination between electrons and holes can be suppressed from the transient photo-voltage measurement, revealing a longer charge carrier lifetime. Furthermore, the compatibility between P3HT and TiO_2 can also be improved after surface modification, as P3HT and modified TiO_2 exhibited a more similar surface hydrophobicity (by contact angle measurement) and higher polymer crystallinity in the hybrid films (by XRD). All the data show that the oligomer 3HT-COOH is the better performed interface modifier than Cudye. By clarifying the functions and roles of interface modifier in the active layer of photovoltaic devices, this study provides a possible route for increasing the efficiency of organic solar cells.

Key words: organic solar cell, poly (3-hexylthiophene), TiO_2 nanorod, bulk heterojunction structure, surface modification, interface modifier

Contents

List of Figures

List of Tables

Chapter 1 Introduction

1.1 Solar energy - a promising renewable energy source

Energy and environment have become the most widely concerned issues in recent years. Nowadays, over 80% of energy supplies are rely on the consuming of fossil fuels, such as petroleum, coal and gas. However, it is estimated that the fossil fuels are going to run out in several ten years; their limited supply has led to considerably increased oil prices. Furthermore, the burning of fossil fuels keeps deteriorating our global environment, leading to severe environmental degradation such as global warming, green house effect and acid rains. For these reasons, humans are in search of various kinds of renewable energy sources (such as wind, biomass, tidal energy of water and solar energy), which are environmental friendly and theoretically unlimited, to take the place of fossil fuels.

Among all the renewable energy sources, solar energy is a promising choice, for it is abundant and clean. The sun delivers a tremendous amount of power to the surface of the earth, which at peak power is almost 1 GW/km^2. Utilization of solar energy has almost no harmful effect to the environment. In addition, solar energy has relatively low geographical limitations and can be applied at remote sites where the generation and distribution of electric power remains a problem. Therefore, solar energy as a renewable

energy source is of great potential, and is expected to grow at a rate of 15 to 20% per year over the next few decades. Many efforts have been devoted by researchers to convert solar energy to electricity in a more efficient and cheap way.

1.2   Solar cell classifications

Solar cells (also called "photovoltaic devices") are the devices that harvest sunlight and convert it into electrical power in the form of photo-generated current and voltage. They can be simply classified into two categories: conventional inorganic solar cells and organic solar cells.

1.2.1   Conventional inorganic solar cells

Inorganic solar cells have been developed for more than 50 years, first demonstrated by Chapin et al. at the Bell Laboratories. Inorganic solar cells are based on inorganic semiconductors such as silicon, cadmium telluride, gallium arsenide and copper indium gallium selenide. After years of development, their power conversion efficiencies have increased from the original 6% to as much as 24% [Green, 2005], which is already close to the theoretical limit (30%). In spite of the high efficiency, the fabrication of inorganic solar cells involves various energy intensive processing steps at high temperature (300 ℃-1400℃); high vacuum condition with several lithographic steps is required, leading

to their relatively high manufacturing costs. Evidently, what we are pursuing today is to lower the fabrication costs of photovoltaic devices while maintaining moderate power conversion efficiency.

1.2.2 *Organic solar cells*

The development of organic semiconductors during the 1970s and 1980s offers an alternative route to solar cell technology. Thanks to the extensive research in the field of organic displays based on organic light emitting diodes, the physical and chemical properties of organic semiconductors become widely understood, contributing a lot to the development of organic photovoltaics. The first organic solar cell was demonstrated by Tang in 1986 [C. W. Tang, 1986], and an efficiency of about 1% was presented. After about 20 years of development, the efficiency of organic solar cell has achieved approximately 6% [A. J. Heeger, 2009]. Although the performance is not as good as the inorganic counterparts until today, organic photovoltaics do have several favorable advantages: they are lightweight, easy to fabricate and manipulate, and can be made on flexible substrates. Most important of all, simple fabrication processes at relatively low temperature and rather low manufacturing costs can be achieved on large-scale production. This makes organic photovoltaic a potent competitor to inorganic solar cells, and it is deserved to be studied in a more extensive way.

1.3   Working principles of organic solar cells

The processes for an organic solar cell to convert light into electricity can be divided into six steps (Figure 1.1):
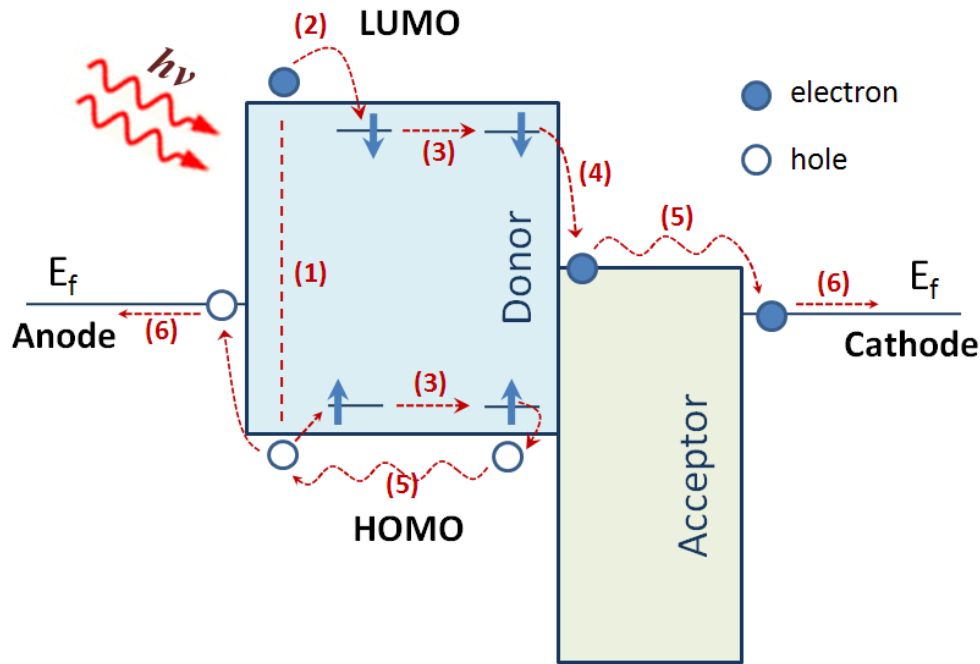
Figure 1.1   Mechanisms of photo-carrier generation in organic solar cells.

(1)   Photon absorption

The incident photons are absorbed mainly by the p-type donor material (often a conjugated polymer), causing electron transition from π-HOMO level to π*-LUMO level of the donor material. The number of photons absorbed is determined by the absorption coefficient and film thickness of the active layer materials.

(2)   Generation of excitons

The primary photo-excitation of organic materials does not directly lead to free

charge carriers, but result in electron-hole pairs bonded by Coulomb force, termed

excitons (exciton binding energy is around 0.1 to 1 eV in organics) [B.A. Gregg, 2003].

(3) Exciton diffusion

Within the lifetime excitons can diffuse in the donor material. It was estimated that

the exciton diffusion lengths are typically 10~20nm [J.M. Nunzi, 2002].

(4) Exciton dissociation

If an exciton can diffuse and meets an internal field within its lifetime, dissociation of

exciton into free charge carriers could occur. For efficient dissociation of excitons,

strong electric fields are needed. Generally, the built in field (on an order of 10^{6}-10^7 V/m)

in a device originated from the work function difference of the two electrodes is not

large enough to split excitons. However, at the donor/acceptor interface where abrupt

potential change occurs, excitons can be dissociated effectively by the strong local

electric field. The dissociation process that photo-excited electrons are transferred from

the LUMO of the donor to the conduction band of the acceptor is termed

"photo-induced charge transfer". Noted that for efficient exciton dissociation (or charge

separation), the donor/acceptor phase separation length in active layer should be

comparable to the exciton diffusion length, or recombination of electron-hole pairs

could occur via radiative or non-radiative routes before they reach the interface.

(5) Charge carrier transport towards the electrodes

After exciton dissociation the created electrons and holes can transport to their respective electrodes with the aid of internal electric fields. Yet the free charge carriers could undergo a fate of recombination during the journey to the electrodes if they meet together, largely limiting the lifetime of free charge carriers.

(6) Charge collection at the respective electrodes

At the last step, charge carriers are extracted from the device through the respective electrodes. To achieve efficient charge collection, the following conditions must be fulfilled:

$$(E_f)_{cathode} < (E_{LUMO})_{acceptor} \quad ; \quad (E_f)_{anode} > (E_{HOMO})_{donor}$$

where E_f denotes the Fermi level of a material.

From the working principles presented above, requirements for an organic solar cell to have promising performance are provided: first of all the active layer should absorb the incident photons as effective as possible, and the generated excitons should be dissociated successfully at the donor/acceptor interface. Subsequently, efficient charge carrier transport towards the electrodes without undergoing large scale recombination is required. Finally, the charge carriers should be effectively collected by electrodes with properly aligned energy levels.

1.4 Device architectures of organic solar cells

In the history of organic solar cells, various kinds of device architectures have been proposed. The most important among them are: single-layered architecture, bi-layered heterojunction architecture and bulk heterojunction architecture. The main differences between the three architectures are: the locations where exciton dissociation or charge separation takes place, and the consecutive charge transport process to the electrodes.

1.4.1 Single layer structure

Organic solar cell of the first generation was based on a single organic layer sandwiched between two metal electrodes of distinct work functions, generally referred to as Schottky type devices since charge separation occurs at the rectifying (Schottky) junction with one electrode (Figure 1.2). Quantum efficiencies of single layered solar cells are quite low, for it is estimated that only 10% of the photo-excitations lead to free charge carriers [A. J. Heeger, 2001]. Moreover, since photo-generated electrons and holes travel through the same material, recombination losses are usually high. Therefore, the reported power conversion efficiencies were generally poor.
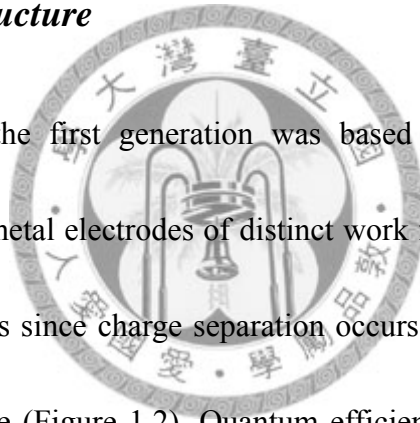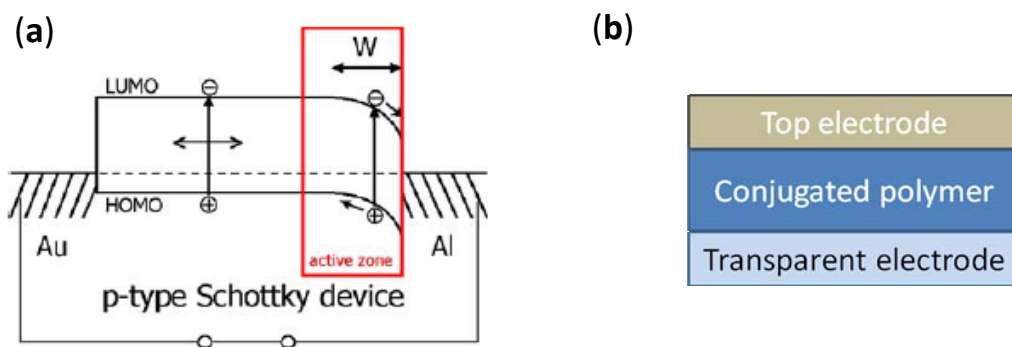
Figure 1.2 (a) Energy band diagram and (b) device architecture of single-layered devices. In single layer single material devices, charge carriers can only be dissociated at the Schottky junction. Therefore only excitons generated close to the depletion region W can contribute to the photocurrent (denoted as the "active zone"). [H. Hoppe, 2007]

1.4.2 Bi-layered heterojunction structure

To improve the poor performance of single-layered devices, the bi-layered heterojunction concept was introduced (Figure 1.3). In this case, two organic layers with specific hole or electron transporting properties (called donor and acceptor, respectively) were stacked together between electrodes with a planar interface. Charge separation is substantially facilitated by the large potential drop between donor and acceptor and the generated free charge carriers can transport within their respective transporting materials. This architecture benefits from that holes and electrons are effectively separated from each other and recombination between them can be largely reduced. Nevertheless, in bi-layered heterojunction the donor/acceptor interface is relatively small. Only excitons generated within their diffusion lengths from the interface can reach it and get dissociated. In other words, photons absorbed out of the "active region"

are lost and cannot contribute to power generation. For this reason quantum efficiencies of bi-layered devices are still not high.
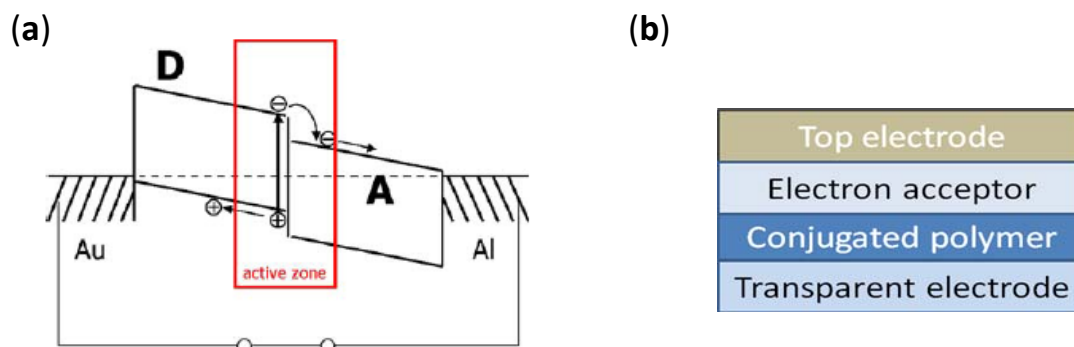
Figure 1.3   (a) Energy band diagram and (b) device architecture of bi-layered devices. Charge carriers can be dissociated at the donor (D)–acceptor (A) material heterojunction. Only excitons generated within diffusion distance to the interface can contribute to the photocurrent. [H. Hoppe, 2007]

1.4.3   Bulk heterojunction structure

The concept of bulk heterojunction is to intimately mix the donor and acceptor components together to provide a substantial interfacial area between them (Figure 1.4). In this case, efficient charge separation in the whole volume of the active layer is ensured, provided that the domain sizes of each component of the heterojunction are comparable to the diffusion length of excitons so that each exciton can reach the interface and get dissociated. In bulk heterojunction devices a key issue is that percolated pathways formed by the hole and electron transporting phases are required to effectively mediate charge carriers to the electrodes. In other words, the donor and

acceptor phases have to form an interpenertrating, bicontinuous network. To date, the

best performance of organic solar cells ever reported is based on bulk heterojunction

architecture. Solar cell with 6.1% power conversion efficiency was achieved using the

alternating co-polymer, PCDTBT, in bulk heterojunction composites with the fullerene

derivative ($PC_{70}BM$) (Figure 1.5) [A.J. Heeger, 2009].
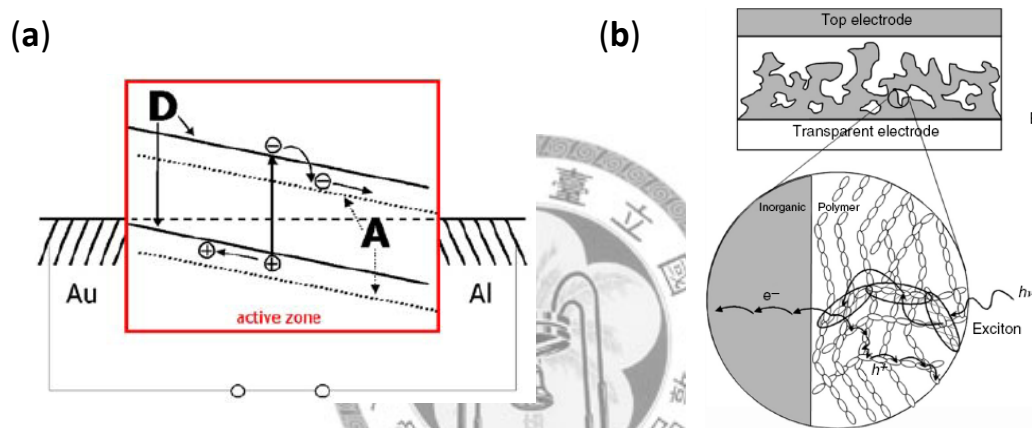
Figure 1.4 (a) Energy band diagram and (b) device architecture of bulk heterojunction
devices. In bulk heterojunction devices, charge carriers can be dissociated throughout
the volume of the active layer. Thus every absorbed photon in the active layer can
potentially contribute to the photocurrent. [H. Hoppe, 2007]
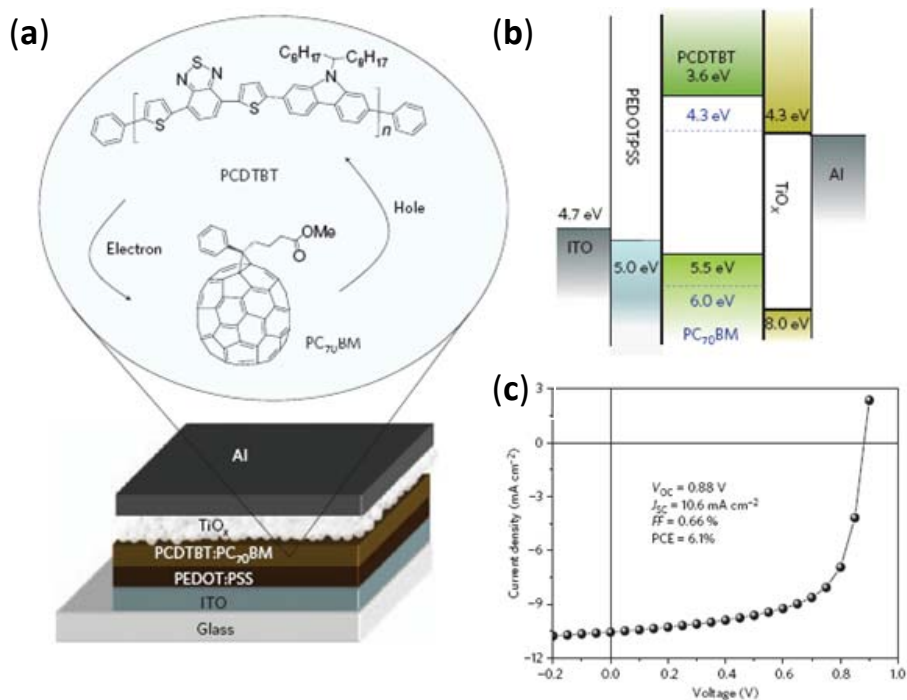
Figure 1.5 (a) Device structure and (b) energy level diagram of the device components. The inset shows the transfer of photo-generated electrons from PCDTBT to $PC_{70}BM$. The titanium oxide (TiOx) layer is introduced as an optical spacer on top of the BHJ layer. (c) J–V characteristics of a PCDTBT: $PC_{70}BM$ solar cell under AM 1.5 G irradiation with an intensity of 100 mWcm^{-2}. [A. J. Heeger, 2009]

1.5 Materials in organic solar cells

Organic solar cells are composed of donor materials (hole transporter with a low ionization potential) and acceptor materials (electron transporter with a high electron affinity). Quite a few donor/acceptor combinations have been proposed to fabricate an organic photovoltaic, such as polymer/polymer blends, polymer/small molecule bilayers and blends, and combinations of organic/inorganic materials. Common donor materials and acceptor materials are discussed in the following:

1.5.1 Donor materials

Common donor materials are organic semiconductors such as conjugated polymers and small molecules. They typically have relatively high absorption coefficients (usually $>10^5 cm^{-1}$) [N.S. Sariciftci, 2004] and long-lived charge carriers [J. R. Durrant, 2003], which partly balance their low mobilities as compared to inorganic semiconductors. In fact, charge carrier mobilities obtained recently in polymer and fullerene films are comparable to those obtained in amorphous silicon films [R. H. Friend, 1999]. In the active layer of organic solar cells, donor materials often serve as the major light absorber. An organic layer with a thickness of about 100nm is necessary to absorb 60% to 90% of photons if a reflective back electrode is used [J.M. Nunzi, 2002]. Moreover, the functionality of organic semiconductors can be tailored readily by molecular design and chemical synthesis, providing the possibility for tuning their optical bandgaps and solubility to solvents.

Among all organic semiconductors, conjugated polymers are of special interest for the following reasons: cheap solution processes (such as screen-printing, doctor blading and spin coating) are possible for fabricating thin films. Owing to the ease of solution processing, forming material blends to make bulk heterojunction devices is also facilitated. On the other hand, small molecules are often less soluble than polymers, so thermal evaporation rather than solution processes is typically employed to form a thin

film. Several conjugated polymers for photovoltaic applications are shown in Figure

1.6.
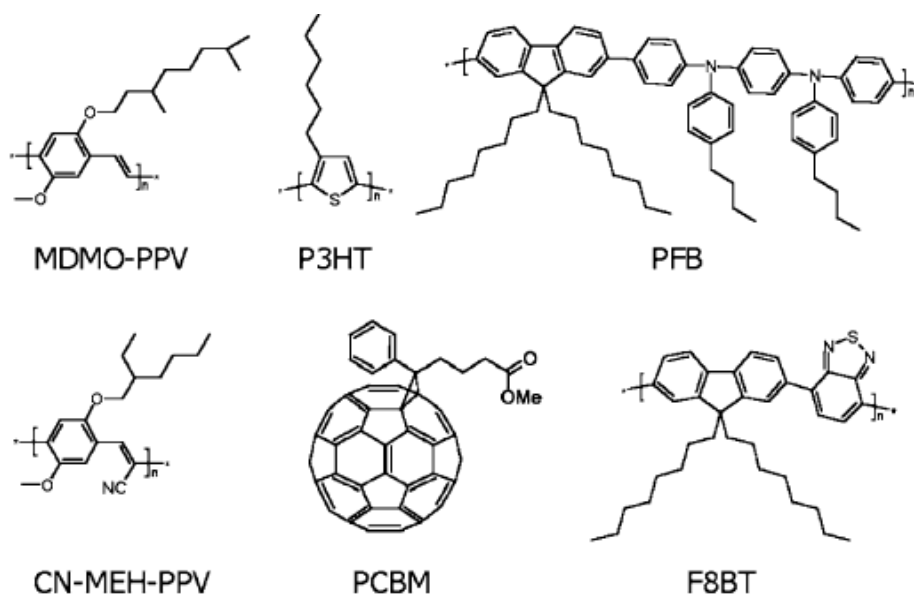
Figure 1.6 Structures of conjugated polymers and a soluble C_{60} derivative commonly applied in polymer-based solar cells. [H. Hoppe, 2007]

1.5.2 Acceptor materials

Common acceptor materials are organic small molecules and inorganic

semiconductors. Representative organic small molecules are fullerenes, which have

relatively high charge carrier mobility and electron affinity among acceptor materials.

Nevertheless, fullerenes are not so soluble in solvents, which is a limitation when

solution based processes are employed. Therefore, a soluble derivative of fullerenes,

PCBM ([6,6]-phenyl C_{61}-butiric acid methyl ester), was synthesized (Figure 1.6) [F.

Wudl, 1992] and have achieved relatively high power conversion efficiencies (4-5%) in

polymer solar cells when combined with P3HT [Y. Yang, 2005][J. Nelson, 2006], and have caused much attention. Another group of acceptor materials are inorganic semiconductors (such as TiO_2 [W-F Su, 2006], ZnO [R. A. J. Janssen, 2006], CdSe [A.P. Alivisatos, 2002], CdS [A.P. Alivisatos, 1996], PbS [H. Sargent, 2005] and $CuInS_2$ [N.S. Sariciftci, 2003]), which can be tailored to be nano-structured configurations or nanocrystals. They generally possess promising properties of high electron mobility, high electron affinity and good chemical and physical stability. Moreover, the sizes and shapes (such as particles, elongated rods and tetrapods) of inorganic nanocrystals can be changed via different synthetic routes [A.P. Alivisatos, 2002] [A.P. Alivisatos, 2005], providing the possibility to alter their optical bandgaps and charge transporting properties. The major limitation of the inorganic semiconductors arises from their relatively low efficiency when applied to solar cell applications, probably because of the imcompatibility between the organic and inorganic phases.

1.6 Improving solar cell performance by surface modification

1.6.1 A brief introduction to surface modification

Solids are composed of a bulk material covered by a surface. The surface of a solid can interact with the surrounding environment, exhibiting quite different characteristics.

The physical and chemical properties of a surface often play a significant role in material science, which often deals with the interface of several phases in condensed state. In nanoscale science, the surface part of a solid becomes more and more important owing to the largely increased specific surface area. For these reasons, surface engineering is of crucial importance as materials in nano scale are tackled.

Surface modification, as one of the typical subjects concerned in surface engineering, involves the application of a thin layer of small molecules (could be mono-layered or multi-layered) to vary or modify the properties of a surface. The molecular interface modifiers (IMs) can be either physically or chemically bonded to a surface, or even just in contact with the surface. The modified surface can be a flat dense film (in this condition the IMs are often termed "self-assembled monolayer", SAM) , a mesoporous surface or even the surface of nano-crystals.

Surface modification has found many applications in varied fields. To name a few, in semiconductor industry, surface modification of the silicon oxide substrate by the interface modifier of hexamethyldisilizane (HMDS) is typically performed to promote the adhesion between the spin-casted photo resists and silicon oxide substrates. Moreover, in the growing steps of nano-crystals, interface modifiers can passivate certain crystal planes by adsorbing to these planes, leading to anisotropic crystal growth. The shape of the growing crystals can be controlled accordingly (Figure 1.7) [A.P.

Alivisatos, 2005]. Furthermore, as conjugated polymers are being studied extensively in recent years, surface modification is also employed in the fabrication processes of organic devices to enhance the performance of these devices. In 1998, R.H. Friend presented the findings that treating the silica substrate with HMDS can enhance the charge-carrier mobility of P3HT in organic thin film transistor (OTFT) by a factor of two [R.H. Friend, 1998]. Some other groups also noticed that surface treatment of the gate dielectric can improve the mobility of P3HT and poly[5,58-bis(3-alkyl-2-thienyl)-2,28-bithiophene)] (PQT) [A. Salleo, 2004]. In 2006, M.D. McGehee et al. explained the reasons for the enhanced mobility [M.D. McGehee, 2006]. They examined the crystal structure of P3HT at the buried interface between P3HT and the gate dielectric treated by HMDS and octadecyltrichlorosilane (OTS) with the aid of X-ray diffraction rocking curves. The authors reported that there were many highly oriented crystals near the interface in P3HT thin films, especially for the OTS-treated samples. The preferentially oriented crystals had lots of grain boundaries with (010) and (001) faces, leading to highly facilitated charge transport in the direction paralleled to the substrate. These results suggested that surface modification is an effective way to enhance the performance of OTFTs, mainly through the improved charge-carrier mobility induced by the interaction between conducting polymer and the interface modifiers.
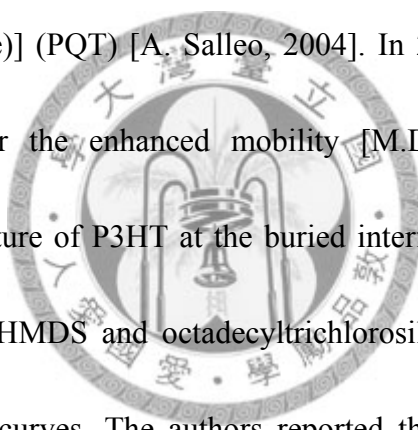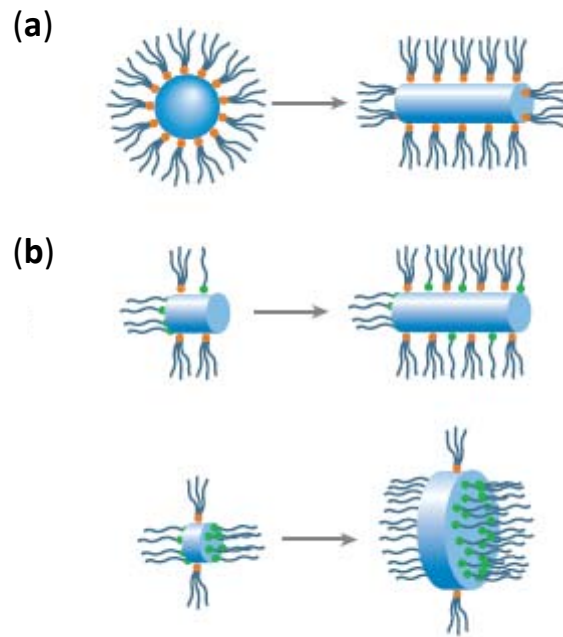
Figure 1.7   Shape control of colloidal nanocrystals. (a) Kinetic shape control at high growth rate. The high-energy facets grow more quickly than low energy facets in a kinetic regime. (b) Kinetic shape control through selective adhesion. The introduction of an organic molecule that selectively adheres to a particular crystal facet can be used to slow the growth of that side relative to others, leading to the formation of rod- or disk-shaped nanocrystals. [A.P. Alivisatos, 2005]

Surface modification has also been employed as a way to improve the performance of organic solar cells. Typically, this is accomplished by three different ways through applying surface treatment processes to different parts of a solar cell. The three different ways are: surface modification of the top metal electrode, surface modification of the transparent conductive oxide (ITO or FTO) as the bottom electrode, and surface modification of the active layer materials. The reported literatures in relation to these three ways are reviewed separately as follows:

1.6.2 *Surface modification of the top metal electrode*

Surface modification of the top metal electrode is accomplished by inserting a thin layer of self-assembled molecules between the metal electrode and the active layer materials. Generally, the metal surface in contact with the active layer cannot be modified or treated during or after the metal deposition. Thus, some techniques have been figured out to perform surface modification of the top metal electrode. Hong H. Lee et al. proposed a method to carry out surface engineering of gold electrode in a P3HT/PCBM bulk-heterojunction solar cell by a "soft contact lamination" technique, as illustrated schematically in Figure 1.8 (a) [H.H. Lee, 2008]. The gold electrode was formed on a substrate, and surface modification of the exposed metal surface was performed subsequently. The modified metal layer was then transferred from the substrate to the top of organic active layer to combine the solar cell. The improvement in the device performance as surface modification was carried out was evident [Figure 1.8 (b)]. The improved efficiency was attributed to the increase in V_{oc} caused by the application of SAMs.

(a)

(b)
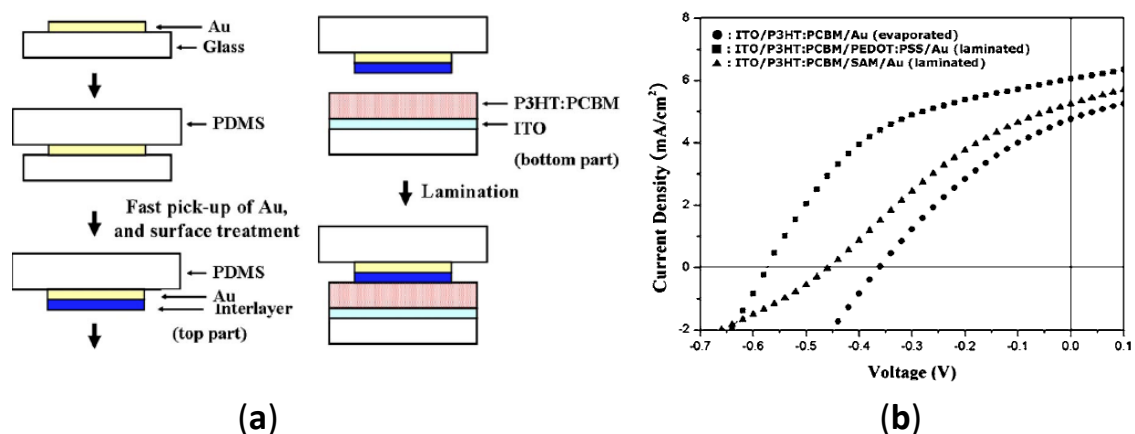
Figure 1.8 (a) Schematic illustration of fabrication of bulk heterojunction solar cell by soft contact lamination method. (b) Effects of surface engineering on *J-V* characteristics of BHJ solar cells. [H.H. Lee, 2008]

The cause of the improvement in device performance as surface modification of the top electrode was performed was further investigated by Alex K. Y. Jen et al. [A.K.Y. Jen, 2008]. A SAM-modified ZnO/metal cathode was incorporated in the P3HT/PCBM hybrid devices, and a series of parasubstituted benzoic acids (BA-X) with different dipole moments were adopted as the SAMs, as shown in Figure 1.9 (a). The authors suggested the observed changes in device characteristics were the effect of the modified work function of the metal electrode caused by the net dipole formed at the ZnO/SAM/metal junctions [Figure 1.9 (b)]. When the net interfacial dipole directed away from the metal surface as molecules with negative dipoles were applied, the modified work function of metal matched well with the conduction band of ZnO, leading to optimized current injection and internal electric field across the device, so the performance of devices was enhanced. This mechanism is rather similar to the effect of

the frequently employed method to improve the efficiency of organic solar cells first

applied by N. S. Sariciftci [N.S. Sariciftci, 2002]: inserting a thin interlayer of LiF under

the metal electrode also forms a dipole moment across the junction, leading to a change

in the metal work function and facilitated charge collection at the metal electrode. The

efficiency of devices is improved thereby.
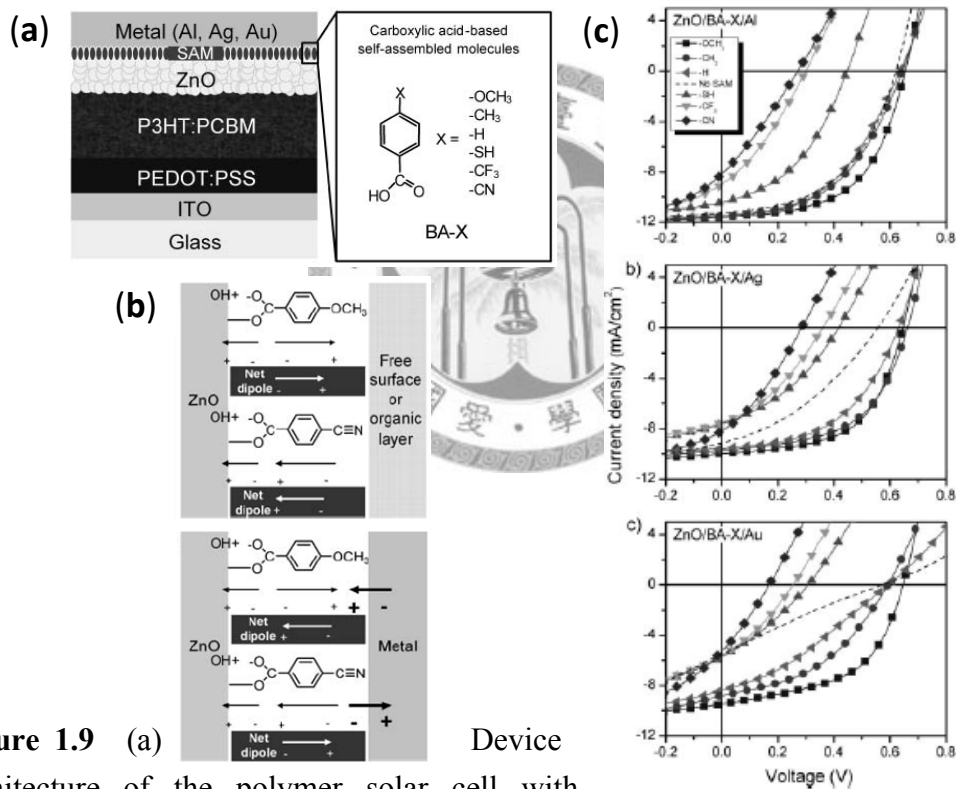
Figure 1.9 (a) Device architecture of the polymer solar cell with SAM-modified ZnO/metal bilayer cathodes; (b) Schematic illustration of the net interfacial dipole formed between a ZnO/SAM/free surface or organic layer (top) and ZnO/SAM/metal junctions (bottom). (c) J-V characteristics of polymer solar cells with a series of SAM-modified cathodes. [A.K.Y. Jen, 2008]

1.6.3 *Surface modification of the bottom electrode of transparent conductive oxide*

Surface modification of the bottom electrode of the transparent conductive oxide (ITO or FTO, typically) is accomplished by applying a thin buffer layer to the electrode or using SAMs to adsorb to the surface of the electrode. Modification of bottom electrode is relatively simple, so the method is frequently employed to enhance the performance of photovoltaics. The most commonly used buffer layer material is the doped conductive polymer, poly(3,4-ethylenedioxythiophene) poly(styrenesulfonate) (PEDOT:PSS) (Figure 1.10), which can not only serve as the electron blocking layer in solar cell devices but also can smoothen the surface of the transparent conductive oxide to make a better contact with the active layer, and thus the interfacial series resistance is lowered [C.J. Brabec, 2001].
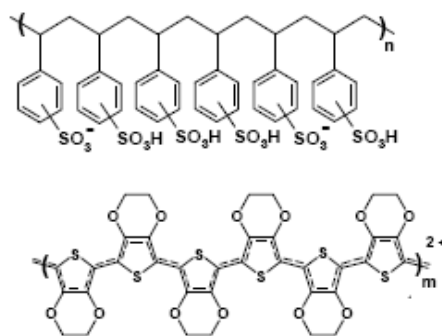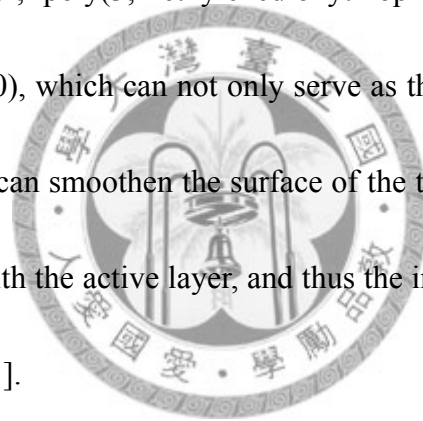
Figure 1.10 The chemical structure of PEDOT:PSS.

On the other hand, modification of the transparent conductive oxide by SAMs is carried out by using molecules with a permanent dipole moment to tune the work function of the electrode. Kilwon Cho et al. have investigated the effect of a series of

SAMs on the work function of ITO and the resulted solar cell efficiency [Kilwon Cho, 2007]. The authors found that the work function of ITO was shifted as a result of the addition of SAMs with $-NH_2$, $-CH_3$ and $-CF_3$ terminal groups, as observed by using secondary electron emission spectroscopy (Figure 1.11). It was found that SAMs with electron withdrawing groups (the CF_3 SAM) increase the work function of ITO more than SAMs with electron donating groups (the CH_3 SAM and the NH_2 SAM), making the ITO work function close to the active layer's highest occupied molecular orbital (HOMO) level, and thus hole injection from the active layer to the anode of ITO is facilitated. The OPV devices with the CH_3 SAM treated anode exhibited the highest efficiency, being quite consistent with the author's expectation. Very similar observations were made by T.S. Jones et al. [T.S. Jones, 2006]. In Jones' research, several SAM molecules with a dipole moment of appropriate direction and magnitude were employed to modify the surface of ITO anode in solar cells based on a CuPc:C_{60} heterojunction. The increased J_{sc}, fill factor and power conversion efficiency for devices with SAM treated anode were attributed primarily to the enhanced interfacial charge transfer rate at the anode, due to both a decrease in the interfacial energy step between the anode energy level and the HOMO level of the organic layer, and a better compatibility of the SAM-modified electrodes with the subsequently deposited organic layers, which increased the density of active sites for charge transfer (Figure 1.12).
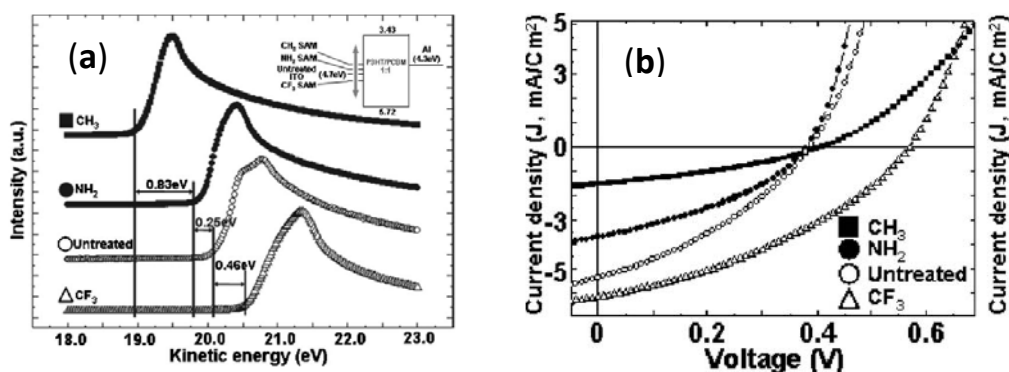
Figure 1.11 (a) Secondary electron emission spectra for the various ITO substrates. The inset shows schematic energy diagram of the electron-donating and electron withdrawing SAM treated ITOs; (b) J-V characteristics of the OPV devices with the various SAM-treated ITO substrates. [Kilwon Cho, 2007]
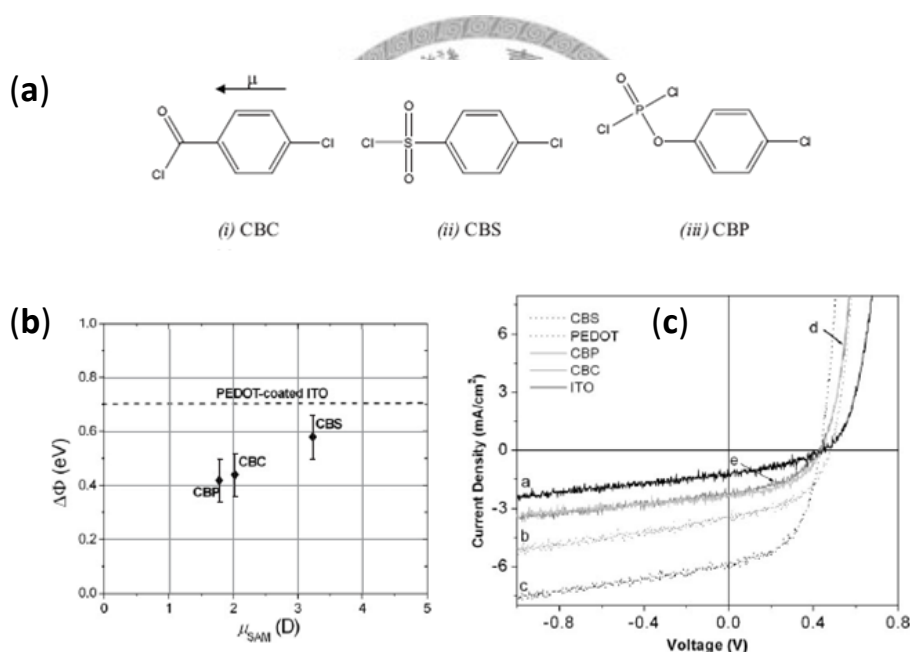
Figure 1.12 (a) Chemical structures of the SAMs used in this study; (b) Experimentally measured change of anode work function relative to that of untreated ITO; (c) J–V characteristics of devices under simulated AM1.5 irradiance (100mWcm^{-2}). [T.S. Jones, 2006]

In a brief summary, the enhancement in the performance of organic photovoltaics as surface modification of the cathode/anode is performed typically stems from two

reasons: one is the improved electrical contact between the electrodes and the active layer materials; the other is the decreased charge injection barrier between the electrodes and the active layer, owing to that the energy levels between them match better as surface modification is performed.

1.6.4 Surface modification of the active layer materials

One of the many advantages of organic/inorganic hybrid solar cells is that the surface of the inorganic component (typically inorganic semiconductor nanocrystals) can be modified readily by organic molecules such that the chemical properties of the inorganic nanocrystals and the physical characteristics of devices can be tuned by choosing appropriate interface modifiers (IMs). Surface modification of the active layer materials by IMs could have significant effect on the performance of photovoltaics, for that the active layer is the place where several dominant processes for power generation occur (such as light harvesting, exciton dissociation and charge transfer). This is quite true for devices with bulk heterojuction architecture that the properties of the great donor/acceptor interface area influence the efficiency of the device tremendously.

Interface modifiers in a hybrid solar cell can typically have several beneficial effects, as reviewed from the literatures: light harvest improvement, dipole impartation, charge transfer improvement, charge recombination reduction and morphology alteration.

These effects will be reviewed one by one in the following.

(i) Light harvest improvement

In a dye-sensitized solar cell (DSC), a photosensitized anode (typically mesoporous TiO$_2$) and an electrolyte are employed to form a photoelectrochemical system [M. Grätzel, 2001]. Dye molecules, as the photo-sensitizer on the surface of TiO$_2$, can be excited by absorbing the incident light and then transfer the photo-excited electrons to the TiO$_2$ anode. These dye molecules, which are virtually the surface modifiers of TiO$_2$, can serve as the light absorber to improve the harvest of light in DSCs. In the newly developed solid state dye sensitized solar cells [L. Schmidt-Mende, 2005], the liquid electrolyte in DSCs is replaced by solid state small molecules (such as: Spiro-MeOTAD) as the hole transporter. The working concept of solid state DSC is rather close to that of the organic/inorganic hybrid solar cells except that the major light absorbers in solid state DSCs are the dye molecules instead of the conjugated polymer. Actually, as inspired by the working concepts of solid state DSCs, it is possible to improve the harvest of light in organic/inorganic hybrid solar cells by choosing appropriate interface modifiers as the light absorber. The molecules whose absorption spectra are complementary to the absorption spectrum of the conjugated polymer can serve as promising interface modifiers to improve the harvest of light.

(ii) Dipole impartation

Quite similar to the effect that SAMs on the electrodes can tune the work function and the relative energy levels in a solar cell, interface modifiers with permanent dipole moment can also change the energy offset at the donor/acceptor interface. For instance, M. D. McGehee et al. employed a series of para-substituted benzoic acids with varying dipoles to modify the interface of P3HT/TiO$_2$ devices (Figure 1.13) [M. D. McGehee, 2007]. They found that the energy offset at the TiO$_2$/polymer interface and thus the open-circuit voltage of devices can be tuned by as large as 0.25 volt. The same authors presented another work that interface modification of the planar TiO$_2$/polymer photovoltaic cells was performed by applying two carboxylated polythiophenes having different densities of carboxylic acid groups [M. D. McGehee, 2006]. Both of the interface modifiers increased the photocurrent of the cells but lowered the open-circuit voltage, owing to the increased TiO$_2$ work function induced by the formation of interfacial dipoles pointing toward the TiO$_2$ surface. According to these results, it is suggested that care must be taken when carboxylic-group containing molecules are employed as the IMs. By incorporating IMs with proper amount of carboxylic groups, the photocurrent of devices can be increased without substantially decreasing the open-circuit voltage.

(a)

-R Group	Dipole Moment (D)
-SO₂F	4.5
-NO₂	3.8
-CN	3.4
-Br	1.4
-H	-2.1
-OCH₃	-3.9
-NH₂	-4.5
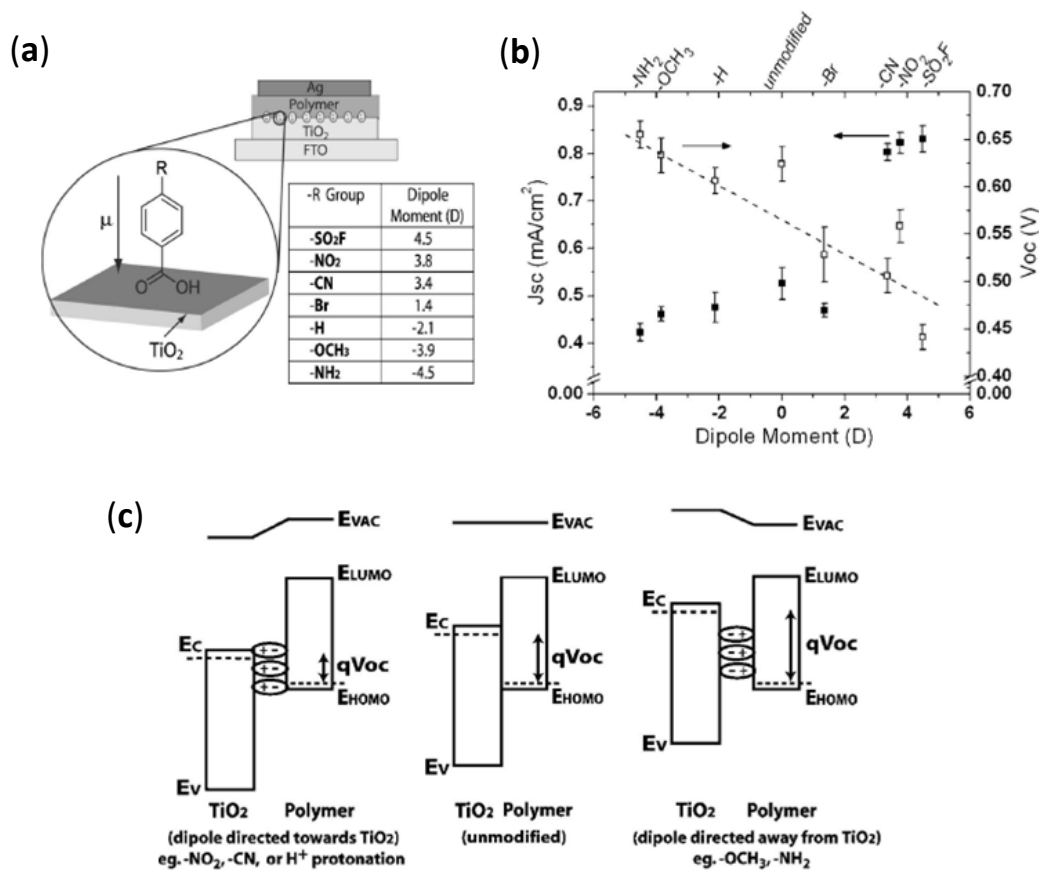
Figure 1.13 (a) Schematic of bilayer TiO₂/polymer devices with dipolar modification of titania surface. The table lists the substituent −R group on the para position of the benzoic acid accompanied with calculated dipole moment. (b) V_{oc} and J_{sc} of TiO₂/P3HT bilayer devices with and without interface modifications employing para-substituted benzoic acid derivatives plotted against dipole moment of the modifiers. (c) Schematics of band diagram of TiO₂ /polymer cell at flatband with interfacial dipoles pointing toward TiO₂ (left), without any modification (middle) and with interfacial dipoles pointing away from TiO₂ (right). Quasi-Fermi levels are drawn as dash lines and the split between them dictates the V_{oc}. [M. D. McGehee, 2006]

(iii) Charge transfer improvement

As the photo-generated excitons reach the donor/acceptor interface within its lifetime, photo-induced charge transfer can occur. In the charge transfer processes, excitons are dissociated by the strong local electric field at the interface. However, the bulky or

insulating organic molecules existed at the surface of the as-synthesized nanocrystals usually hinder the charge transfer processes. Hence, surface modification of the nanocrystals is often carried out to replace the insulating molecules to more conducting ones to improve the charge transfer at the donor/acceptor interface. Wei-fang Su et al. have reported that the employment of the hole accepting ligands for replacing the highly insulated trioctylphosphine oxide (TOPO) molecules can enhance photoluminescence quenching of CdSe quantum dots (Figure 1.14) [W-F Su, 2008]. In addition, the same group has demonstrated the improved performance of polymer/TiO$_2$ nanorod bulk heterojunction photovoltaic devices by interface modification [C-W Chen, 2008]. The enhanced solar cell efficiency is arisen partially from the improved charge separation efficiency, as inferred from the more pronounced PL quenching (Figure 1.15). Moreover, Leeyih Wang et al. have employed a series of interface modifier molecules with varied numbers of thiophene rings and varied alkyl chain lengths to investigate the structural effect of modifiers on the performance of organic/inorganic photovoltaic devices [L-Y Wang, 2009]. The authors found that higher efficiency of charge separation at the P3HT/TiO$_2$ interface can be achieved by choosing interface modifiers with either shorter insulating main-chain or longer conjugated backbone.
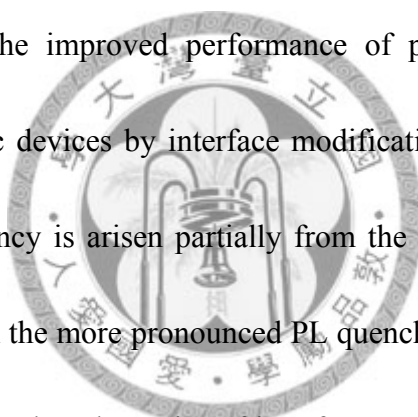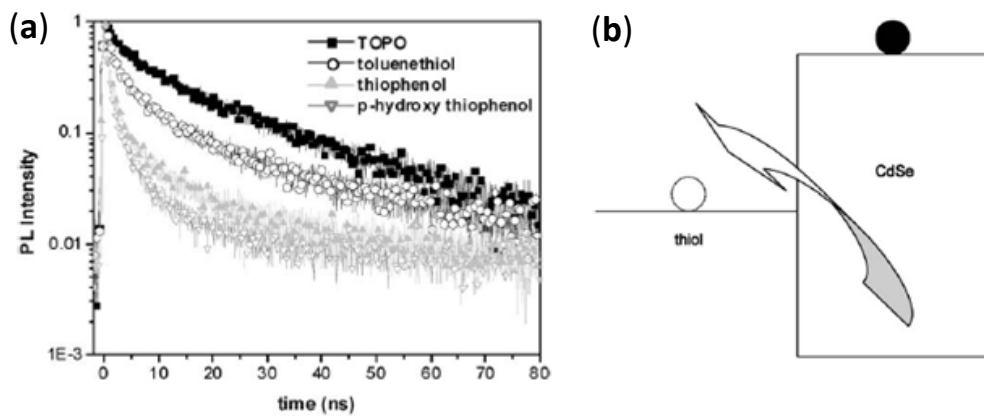
Figure 1.14 (a) PL lifetime decay of CdSe quantum dots with different ligands; (b) A schematic diagram of the energy levels and charge separation of excitons at the surface of a thiol capped CdSe quantum dot. [W-F Su, 2008]
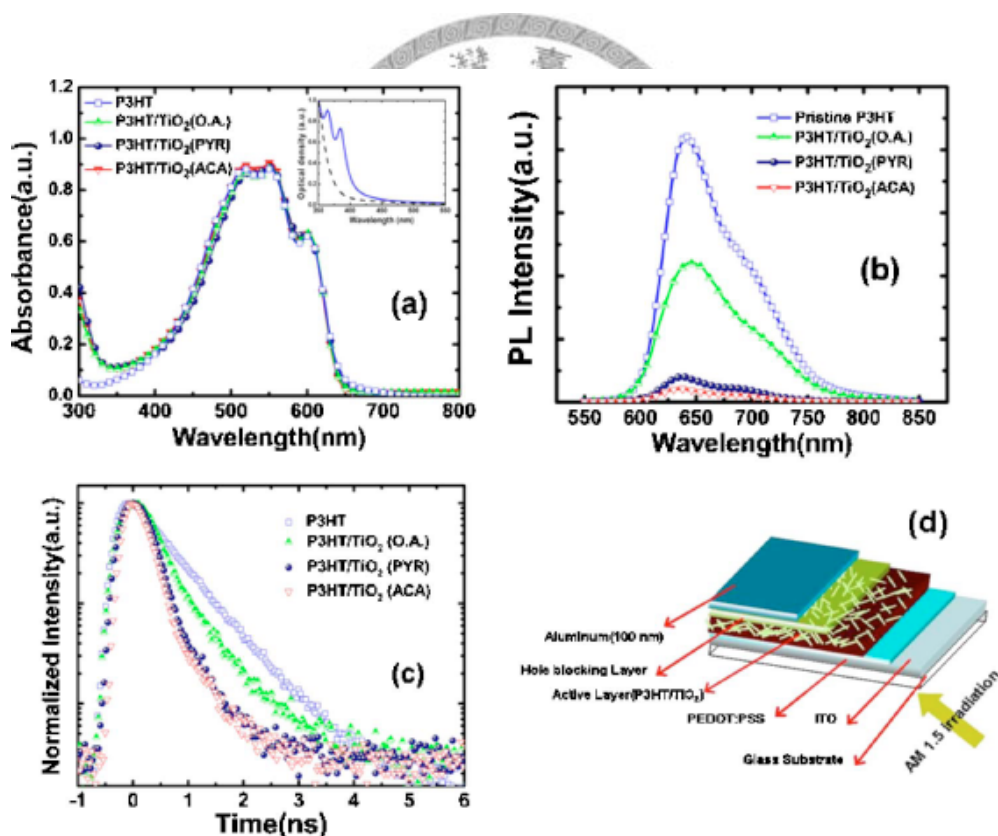
Figure 1.15 (a) UV-visible absorption, (b) PL intensity, and (c) time-resolved PL spectroscopy of the hybrid materials with different surface ligand molecules. The inset in (a) shows absorption spectra of as-synthesized (dash line) and ACA capped TiO_2 nanorods (solid line). (d) Schematic representation of the photovoltaic device based on the hybrid material. [C-W Chen, 2008]

(iv) Charge recombination reduction

Once the charge carriers are successfully separated via the charge transfer processes, they have to transport to the respective electrodes to generate an external photo-current. However, as the electrons and holes in their respective transporting material domains meet together, they may experience the fate of recombination. The introduction of the interface modifier molecules between the donor and the acceptor is expected to suppress the recombination of charge carriers, for the IMs can effectively form an energy barrier and spacial obstacle for recombination of electrons and holes. C.W. Chen et al. have investigated the effect of interface modification on the performance of polymer/TiO_2 nanorod bulk heterojunction solar cells [C-W Chen, 2009]. The substantial improvement in device efficiency was mainly attributed to the suppression of recombination at P3HT/TiO_2 nanorod interfaces by the attachment of effective interface modifier molecules (Figure 1.16). A very promising efficiency of 2.2% had been achieved. Triggered by this work, we can choose IM molecules with proper chemical structure or spacial conformation to impose a high recombination barrier to the photovoltaic system to improve its efficiency.
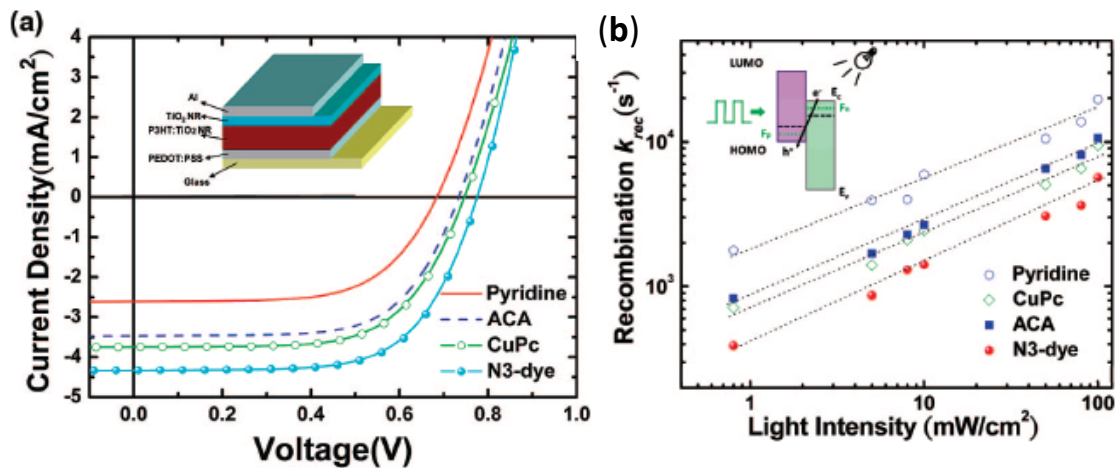
Figure 1.16 (a) Current-voltage characteristics of the photovoltaic devices using different interface modifier molecules under A.M. 1.5 (100 mW/cm^2) irradiation; (b) Charge recombination rate constant k_{rec} versus light intensity at V_{oc} determined by TOCVD measurement. The inset schematically depicts the recombination mechanism and TOCVD setup. [C-W Chen, 2009]

(v)   Morphology alteration

The nanocryatals adsorbed by distinct interface modifiers in the polymer/nanocrystal hybrid typically exhibit different tendency for self aggregation. In addition, the interface modifiers in the hybrid may interact with the neighboring polymer chains, resulting in varied polymer conformation and crystallinity. Therefore, the nano-scaled morphology and the degree of phase separation in the polymer/nanocrystal hybrid, which are crucial factors determining the mobility of charge carriers and the overall device efficiency, can be significantly influenced by the employed interface modifiers. As an example, S.A. Carter et al. have studied the effect of the capping ligands of CdSe nanorods on the behavior of devices [S.A. Carter, 2009]. They found that ligand choice can substantially

affect phase separation condition in the active layer, which in turn influenced short-circuit currents of the devices (Figure 1.17). The reason is that efficient exciton dissociation could not be achieved as huge domains are presented in the active layer, for the diffusion length of excitons is at most tens of nanometers, so the generation of photocurrent is limited. Moreover, Jean M. J. Fre´chet has presented a study to control the morphology of polymer/nanocrystal composites in hybrid solar cell by employing end-functional polythiophene as a surface modifier [Jean M. J. Fre´chet, 2004]. As shown in Figure 1.18, the end-functionalized P3HT can enhance the performance of P3HT/CdSe solar cells by increasing the dispersion of CdSe nanocrystal in hybrid films.
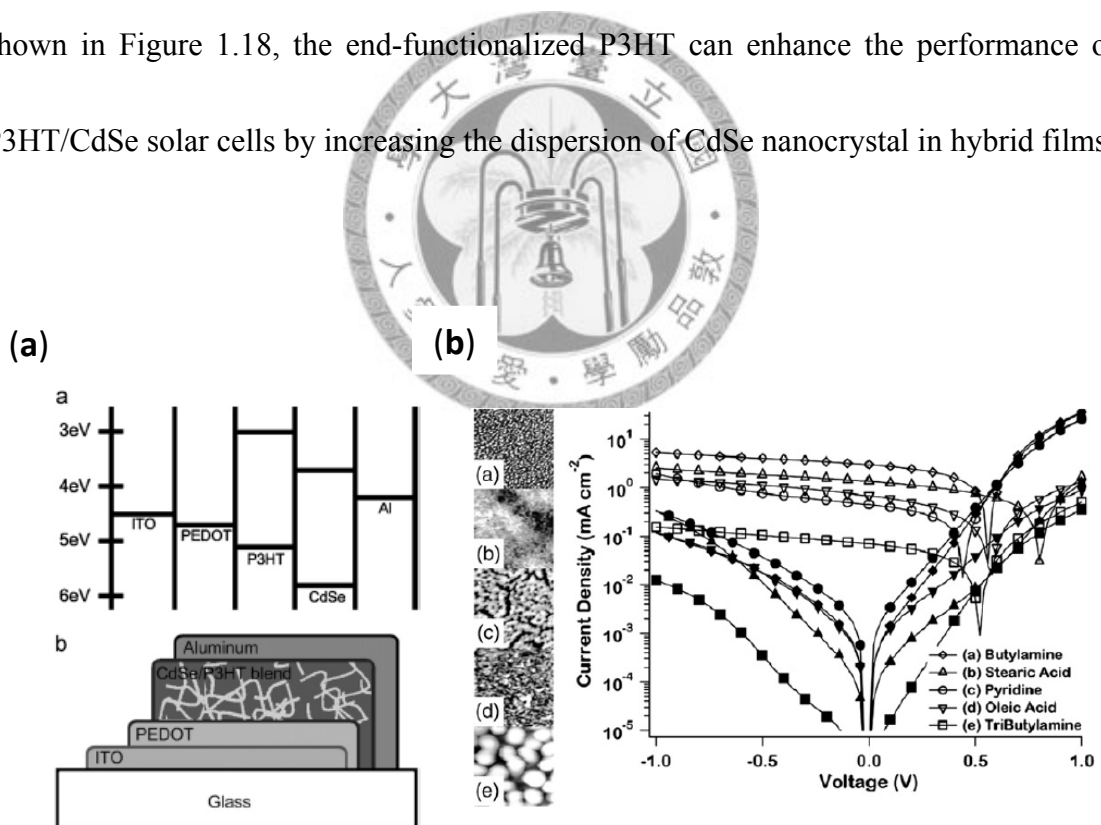
Figure 1.17 (a) Energy diagram and schematic of CdSe/P3HT blended devices; (b) AFM images (left) and J-V characteristics (right) of NC/P3HT films identical in preparation except for the NC capping ligand. [S.A. Carter, 2009]
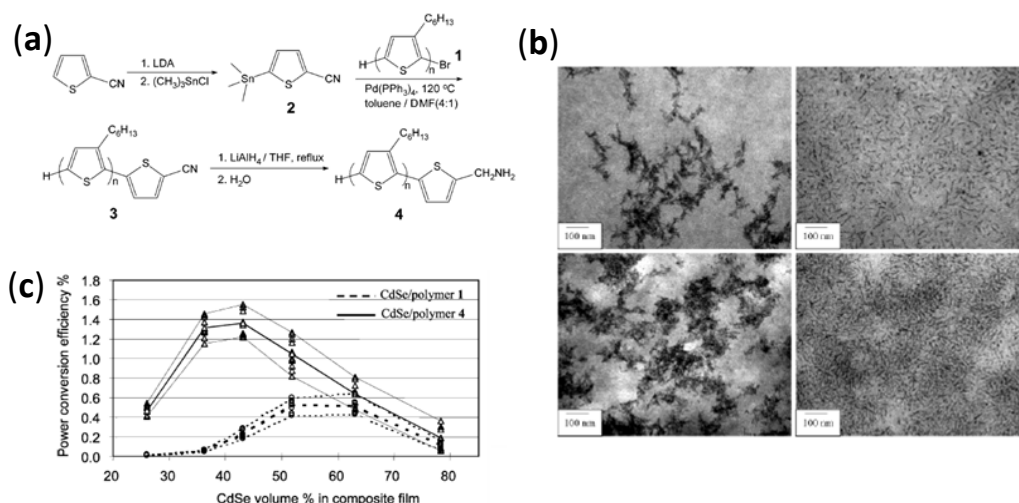
Figure 1.18 (a) Synthesis of P3HT with amino end-functionality; (b) TEM images of four films consisting of CdSe (20 wt %)/polymer **1** (top left), CdSe (20 wt %)/polymer **4** (top right), CdSe (40 wt %)/polymer **1** (bottom left), and CdSe (40 wt %)/polymer **4** (bottom right), respectively; (c) Plots of power conversion efficiency (AM 1.5) versus the volume ratio of CdSe in the active layer of the devices made using polymer **4** (solid lines) and polymer **1** (dashed lines). [Jean M. J. Fre´chet, 2004]

1.7 Research motivations

From the previous review, it can be realized that surface modification of the donor/acceptor interface could have various beneficial effects on the performance of photovoltaic devices. The exhibited effect of IMs significantly depends on the chemical structures and intrinsic properties of them. Choosing appropriate organic molecules as IMs is a key issue for achieving promising power conversion efficiency for a solar cell. According to the previous review, a desirable IM should at least fulfill the following requirements: first of all, the bonding between the IM molecule and the nanocrystal acceptor should be strong enough to form a uniform monolayer. Molecules with

carboxylate end groups could have several strong binding modes to the surface of TiO$_2$ [C. Pe´rez Leo´n, 2006] and are among our choices. Nevertheless, small molecules bearing multiple carboxylate groups should be avoided for that they could have a great tendency to self-aggregate, largely deteriorating photocurrent of a solar cell [Lei L. Kerr, 2008]. Moreover, IMs with multiple carboxylate groups could lead to decreased V$_{oc}$ [M. D. McGehee, 2006][M. Grätzel, 2003]. Secondly, the IM molecules should be highly conductive and do not possess long insulating mainchain such that the energy barrier and spacial obstacle at the donor/acceptor interface could be lowered and charge separation is facilitated. Lastly, the employed IM should be highly compatible to both donor and acceptor to yield a well-intermixed active layer without causing large scale phase segregation.
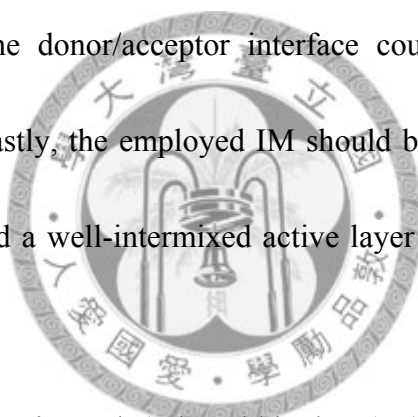
In the study of this thesis, poly(3-hexylthiophene) (P3HT) was chosen as the hole-conducting material for its high charge carrier mobility of up to 0.1 cm^2 V^{-1} s^{-1} [R. H. Friend, 1998] and the excellent self-assembling properties; TiO$_2$ nanorod was selected as the electron conductor owing to the promising chemical stability and the high electron mobility among inorganic nanocrystals. In addition, the high aspect ratio of TiO$_2$ nanorod makes it a better choice for charge transport as compared to TiO$_2$ nanoparticle. From our previous works, we have systematically studied the effect of several parameters (such as the molecular weight of P3HT, the solvent type, the hybrid

compositions, film thicknesses, process conditions, and so on) on the performance of P3HT/TiO$_2$ nanorods bulk heterojunction solar cells [W-F Su, 2009]. Now we turn to examine the effect of surface modification of TiO$_2$ nanorods, expecting to further enhance the performance of devices. Based on the previously mentioned requirements for IMs, we are proposing two novel interface modifiers, Cudye (a derivative of copper phthalocyanine) and oligomer 3HT-COOH (a regioregular 3-hexylthiophene oligomer with carboxylic end functional groups), to modify the surface of TiO$_2$. Qualitative and quantitative methods for characterizing the surface modified TiO$_2$ nanorods were carried out to provide a systematic way for studying surface modification of nanocrystals. Moreover, the effect of applying Cudye and oligomer 3HT-COOH as the IMs in P3HT/surface modified TiO$_2$ nanorod hybrid system was investigated, hoping to provide a clarified way to make more efficient solar cell devices.
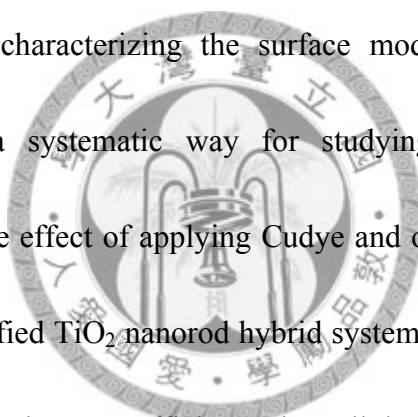
Chapter 2 Experimental section

2.1 Chemicals

All the chemicals are used as received and are summarized in Table 1.

Table 1 Chemicals used in the experiments.

Chemicals	Chemical formula	Purity	Producer
Acetonitrile	C_2H_3N	99.5%	Acros
Ammonia	$NH_{3(aq)}$	30%	Panreac
Chloroform	$CHCl_3$	99+%	Acros
Chlorobenzene	C_6H_5Cl	99+%	Acros
Dichloromethane	CH_2Cl_2	99.99%	Acros
Ethanol	C_2H_5OH	99.99%	Fisher Scientific
Hexane	C_6H_{14}	95%	J.T. Baker
Ferrocene	$C_{10}H_{10}Fe$	98%	Acros
Hydrogen peroxide	$H_2O_{2(aq)}$	35%	Acros
Isopropanol	C_3H_7OH	99.96%	Acros
Methanol	CH_3OH	99.99%	Acros
Methyldicyclohexylamine	Cy_2NMe	99+%	Aldrich
Oleic acid	$C_{18}H_{33}CO_2H$	90%	Aldrich
Pyridine	C_5H_5N	99+%	Acros
Tetrahydrofuran	C_4H_8O	99.99%	J.T. Baker
Tetra-n-butylammonium hexafluorophosphate	$C_{16}H_{36}F_6NP$	98%	Aldrich
Titanium(IV) isopropoxide	$Ti(OCH(CH_3)CH_3)_4$	98%	Aldrich
Trimethylamino-N-oxide dihydrate	$(CH_3)_3NO$	98%	Acros
Tris(dibenzylideneacetone) dipalladium	$Pd_2(dba)_3$	99+%	Aldrich
Tri-tert-butylphosphine	$P(tBu)_3$	99+%	Aldrich

2.2   Preparation of materials

2.2.1   *Synthesis of TiO₂ nanorods*

The synthesis of TiO₂ nanorods was accomplished by hydrolyzing titanium tetraisopropoxide according to our previously published literature [W-F Su, 2006]. Oleic acid (120 g) was put into a three-neck flask and heated at 120℃ for one hour under vigorous stirring and Ar flow to remove moisture. The reactant was allowed to cool to 98℃ and titanium tetraisopropoxide (17 mmol), as the precursor, was then added into the flask and stirred for 5 minutes to well mixed with the oleic acid. Trimethylamine-*N*-oxide dihydrate (34 mmol) in 17 ml water was then rapidly injected into the flask to catalyze the polycondensation reaction. After reacted for 9 hours to complete crystallization, the reactant was cooled to room temperature and the mixture of oleic acid and TiO₂ nanorods could be obtained. To remove any non-reacted oleic acid or impurities, the mixture were washed by methanol or ethanol and precipitated for several times. After subsequent centrifugation and drying, TiO₂ nanorods end-capped with oleic acid can be obtained as the white powder. The flow chart for synthesizing TiO₂ nanorods is shown in Figure 2.1:

```
Oleic acid (OA)(120g)
        │  Put into 250mL three-neck flask purged with Ar
        ▼  Heated at 120℃ for 1 hour under vigorous stirring
        │  Cooled down to 98℃
        ▼
Purified oleic acid
        │  Added ← Titanium tetraisopropoxide (TTIP)(17mmol)
        ▼
OA-TTIP complex (120g)
        │  Rapid injection ← Trimethylamine-N-oxide dihydrate (34 mmol)/H₂O (17mL)
        ▼  Reacted for 9 hours, then cooled to RT
TiO₂(oleic acid) solution
        │  Washed by ethanol and precipitated for several times
        ▼
TiO₂ nanocrystal powder
```

Figure 2.1 Flow chart for synthesizing TiO_2 nanorods.

2.2.2 Synthesis of the oligomer with carboxylate terminated 3-hexylthiophene (oligomer 3HT-COOH)

The oligomer 3HT-COOH was synthesized through Heck reaction using vinyl terminated 3-hexylthiophene oligomer and 1,4-dibromo-3-carboxylic thiophene. The α-vinyl-ω-phenyl end functional P3HT (compound 1, Figure 2.2) and 2, 5-Dibromo thiophene-3-carboxylic acid (compound 2, Figure 2.2) were first synthesized by following the literature [W-F Su, 2007][M. Pomerantz, 2003]. In a dry box, we combined the compound 2 (0.15g, 0.70mmol) and the compound 1 (Mn = 5000, 1.00g, 0.2 mmol) in a glass reaction tube equipped with a stir bar. Then we added $Pd_2(dba)_3$

38

(160mg), tri(*t*-butyl)phosphine (0.15mL), methyldicyclohexylamine (10mL), and anhydrous THF (100 mL) into the mixture. The tube was sealed and removed from the dry box. The mixture was stirred at 55℃ for 24 h, and then cooled to room temperature. Finally, the solution was precipitated with methanol (500mL) to give purplish polymer whisker and it was further washed with methanol in a Soxhlet apparatus. The purified polymer was dried in vacuum overnight and afforded as a dark purple material (yield: 75%).
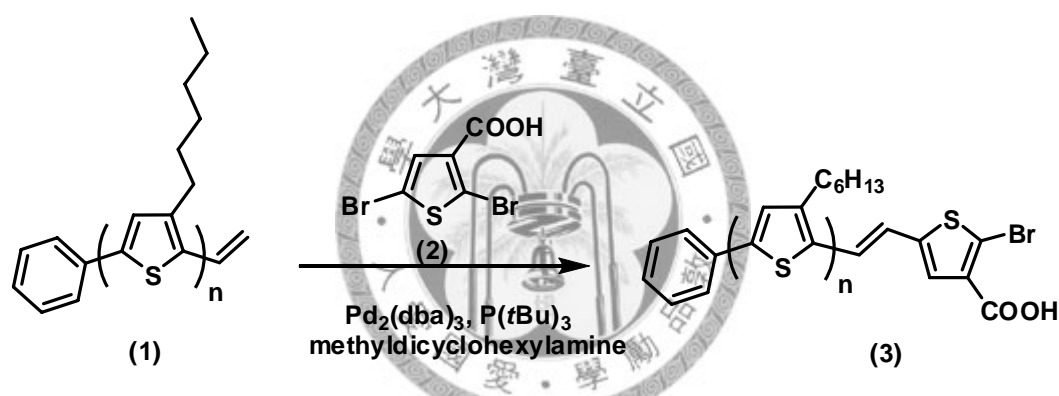
Figure 2.2 The synthesis of oligomer 3HT-COOH (Mw=5000) through Heck reaction.

2.2.3 *Surface modification of TiO$_2$ nanorods*

The as synthesized TiO$_2$ nanorods are end-capped with oleic acids as surfactant. Oleic acid, as a nonconductive molecule with long alkyl chain which could obstruct charge transport, is not a promising surface ligand for photovoltaic applications. For this reasnon, we employed surface modification (or ligand exchange) procedures to replace oleic acids with the more conductive interface modifiers. Figure 2.3 shows the chemical

structures of the surface ligands or interface modifiers involved in the modification procedures. There were two main steps involved in the surface modification processes. The first step was to react the oleic acid end-capped TiO_2 nanorods with pyridine to remove oleic acid and obtain a cleaner surface and the second step was to adsorb interface modifier molecules onto the surface of TiO_2.
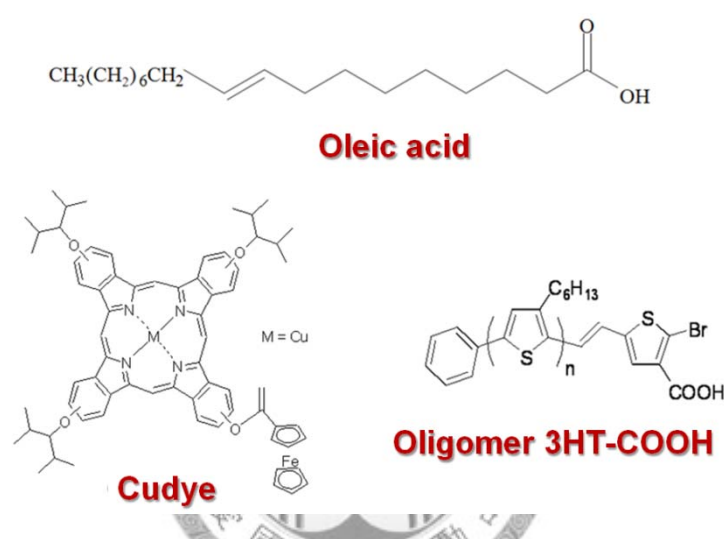
Figure 2.3 Chemical structures of interface modifiers involved in the surface modification processes.

In the first step, the mixture liquid of oleic acid and TiO_2 nanorods (20mL) was washed and precipitated by methanol or ethanol (20mL) for 3 to 5 times to remove oleic acid molecules that were not tightly bonded to the surface of TiO_2 nanorods. Then pyridine (20mL) was added to mix uniformly with TiO_2 nanorods with the aid of ultrasonic homogenizer. The mixture was then put into a three-neck flask and refluxed at 70℃ for 24 hours in nitrogen to obtain the transparent solution. Oleic acid molecules on the surface of TiO_2 could be further removed in this step, as shown schematically in

Figure 2.4.
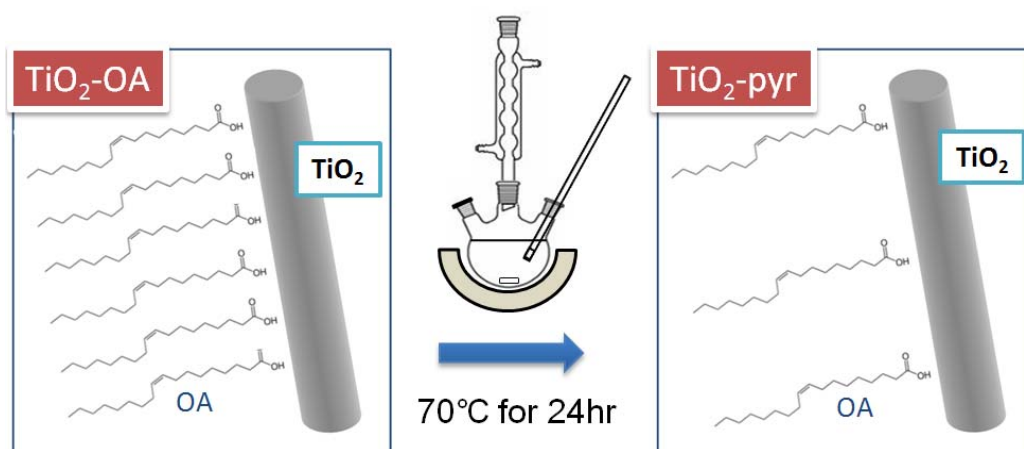
Figure 2.4 Pyridine treatment of the oleic acid end-capped TiO_2 nanorods.

In the second step, two kinds of interface modifiers were chosen to modify the surface of TiO_2 nanorods: oligomer 3HT-COOH and Cudye. Adequate amount of interface modifiers (32mg for oligomer 3HT-COOH; 4mg for copper dye) were dissolved into the pyridine solution of TiO_2 nanorods (20mL). The solution was then heated to 70℃ and stirred for 24 hours to allow the complete adsorption of interface modifiers onto the surface of TiO_2. After that, the solution was cooled to room temperature. Excess amount of hexane was used to precipitate TiO_2 and to wash out the non-adsorbed interface modifiers. Surface modified TiO_2 nanorods could be collected after subsequent centrifugation and drying processes. The processes are shown schematically in Figure 2.5.
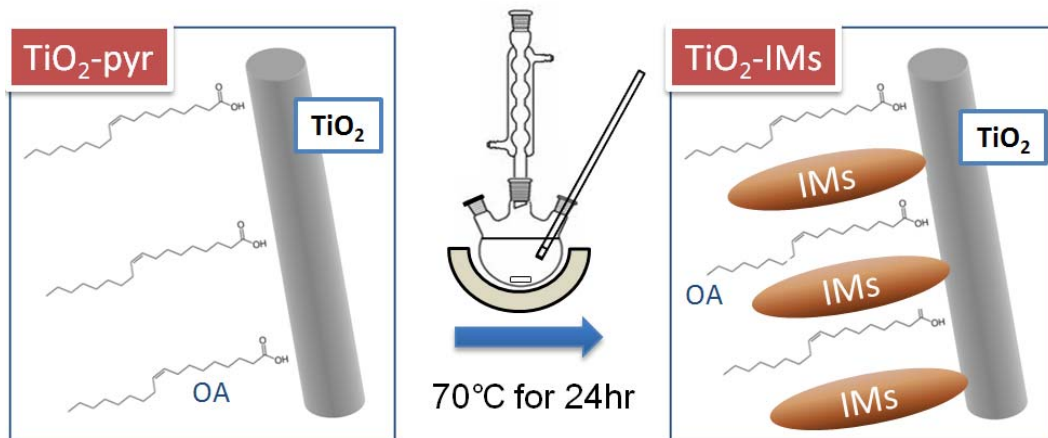
Figure 2.5   Adsorption of the interface modifiers onto the surface of

2.3   Preparation of samples

2.3.1   Preparation of P3HT/TiO₂ hybrid films

P3HT/TiO$_2$ hybrid films, as the active layer in the solar cell devices, were prepared

on glass substrate for the study of UV-vis absorption spectrum, photoluminescence

spectrum, atomic force microscope and transient photo-voltage measurements. The

preparation processes of the hybrid films consisted of glass substrates cleaning, hybrid

solution preparation and spin coating.

(1) The cleaning of glass substrate

Glass substrates with an area of 1.5cm^2 were put into staining jars and immersed into

the solution mixture of ammonia, hydrogen peroxide and de-ionized water (1:1:5 by

volume ratio) and cleaned by ultrasonic homogenizer for about 2 hours, followed by

immersing the glass substrates into isopropanol and agitated for 30 minutes.

(2) Hybrid solution preparation and spin coating

Adequate amount of P3HT (Mw = 55000 g mol^{-1}, PDI =1.5, and regioregularity greater than 99% as determined by NMR, from Industrial Technology Research Institute, Taiwan) was dissolved in chlorobenzene (30mg/mL) and agitated by ultrasonic homogenizer until the color became bright orange to ensure complete dissolution. Excess amount of hexane was added into the pyridine solution of surface modified TiO$_2$ nanorods to precipitate TiO$_2$. After centrifugation, the TiO$_2$ precipitate was added with solvent mixture comprised of pyridine, dichloromethane and chloroform (pyridine : dichloromethane : chloroform = 1:2:3 , volume ratio) to form TiO$_2$ solution with a concentration of 12.5mg/mL. The P3HT solution and the TiO$_2$ nanorods solution were then mixed together (the ratio of P3HT/TiO$_2$ is 47/53 in weight percent) to form the hybrid solution. The hybrid solution was then agitated by ultrasonic homogenizer for about 30 minutes to ensure that there was no apparent aggregation in the solution. Then the hybrid solution was spin coated onto the cleaned glass substrate with controlled spin speed such that the film thickness was about 120nm. The flow chart for P3HT/TiO$_2$-IM hybrid film preparation is shown in Figure 2.6.
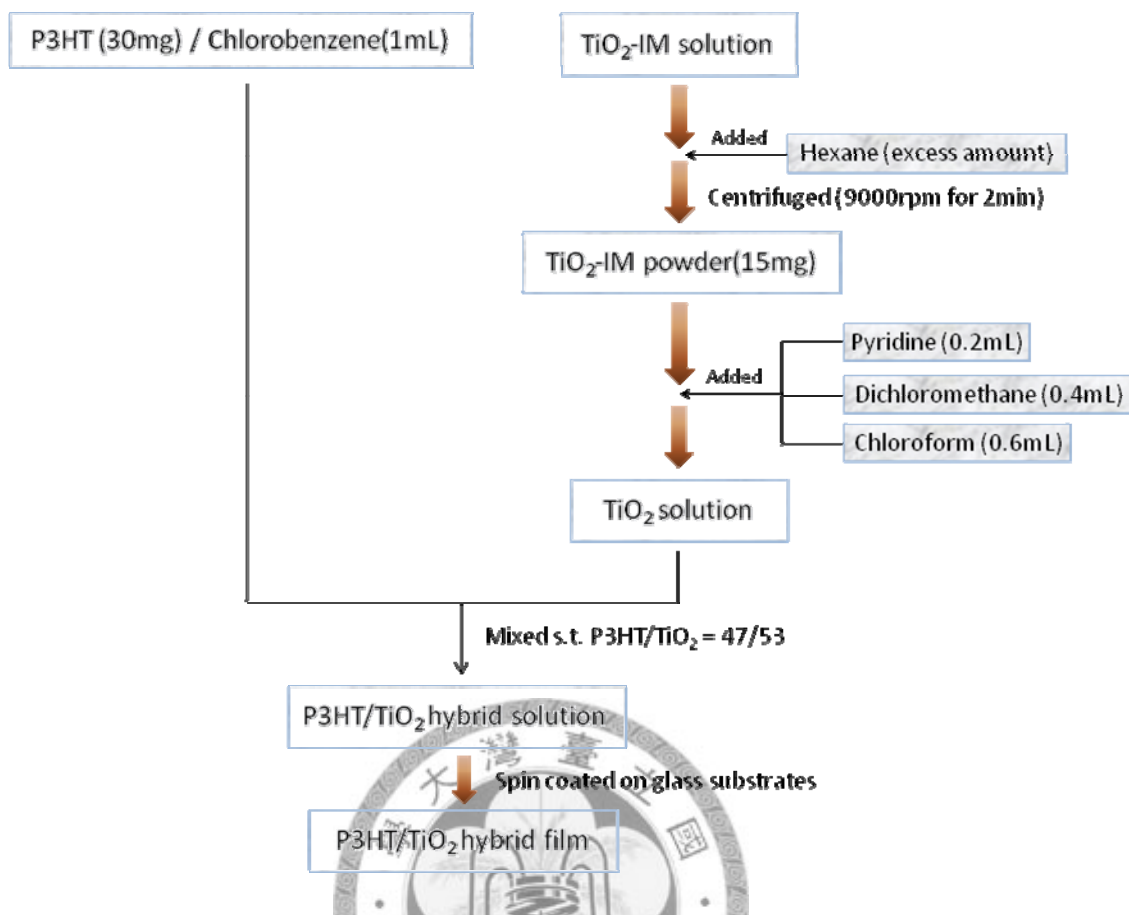
Figure 2.6 Flow chart for preparation of P3HT/TiO$_2$-IM hybrid films.

2.4 Material characterizations and surface characterizations
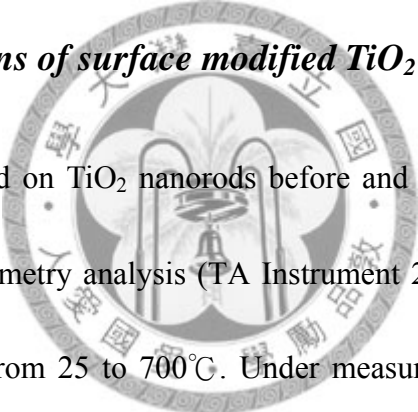
2.4.1 *Characterizations of TiO$_2$ nanorods*

The crystalline structure of TiO$_2$ nanorods was studies using X-ray diffraction (XRD) (PANalytical X' Pert PRO with filtered Cu Kα radiation (λ=1.54056 Å)) and the TEM images of TiO$_2$ nanorods were obtained using a JOEL JEM-1230 transmission electron microscope.

2.4.2 Characterizations of the oligomer with carboxylate terminated 3-hexylthiophene (oligomer 3HT-COOH)

FT-IR spectroscopy (PerkinElmer Spectrum100) was used to characterize the end-functional groups of oligomer 3HT-COOH. Ultraviolet-visible absorption spectra of oligomer 3HT-COOH were obtained by UV-visible spectrometer (PerkinElmer Lambda 35).

2.4.3 Characterizations of surface modified TiO$_2$ nanorods

The amount of oleic acid on TiO$_2$ nanorods before and after surface treatment was determined by thermogravimetry analysis (TA Instrument 2950) under N$_2$ flow with a heating rate of 10℃/min from 25 to 700℃. Under measurement the powder samples were maintained at around 100℃ for 20 minutes to eliminate moisture before further heating. High resolution X-ray photoelectron spectroscopy (PHI 5600) was used to study the surface chemistry of ligand-capped TiO$_2$ nanorods using drop-casted TiO$_2$ nanorods samples on silicon substrate. The experiments were conducted under ultra high vacuum. Typical surveys were collected for 15 min.

The amount of interface modifiers adsorbed on TiO$_2$ nanorods was estimated according to the Beer-Lambert law:

$$A = \log \frac{I_0}{I} = \epsilon c l$$

where A is the absorbance; I_0 is the intensity of the incident light; I is the intensity of the leaving light; c is the molar concentration of the absorber; l is the length of the sample cell; ϵ is the molar absorbtivity of the absorber. From the Beer-Lambert law, the absorbance, which can be derived from UV-visible absorption spectra, is proportional to the concentration of the absorber, provided that the light paths are the same. A calibration line can thus be made to correlate the absorbance of the interface modifier to the concentration of it. The amount of interface modifier on the surface of TiO_2 can then be calculated according the calibration line. The experimental details were as following: different amount of interface modifiers were dissolved in 30mL hexane and the absorption spectra were recorded. The absorption peak values were plotted as the function of concentration, and by linear fitting the calibration line could be obtained. Furthermore, different amount of interface modifiers were added to a fixed amount of TiO_2 to perform the surface modification processes. Then the interface modifier adsorbed TiO_2 was precipitated by 30mL hexane and the centrifugal liquid containing non-adsorbed interface modifiers could be obtained. The amount of adsorbed interface modifiers could be derived from subtracting the non-adsorbed amount (estimated from the calibration line) from the added amount.

2.4.4 *Characterizations of the properties of P3HT/TiO₂-IM hybrid system*

The film thickness was determined by a α-stepper (Veeco, Dektak 6M 24383). Ultraviolet-visible absorption spectra were obtained by UV-visible spectrometer (PerkinElmer Lambda 35). The steady-state photoluminescence spectra were measured by spectro-fluorometer (PerkinElmer LS-55). The surface hydrophobicity of TiO_2 nanorods before and after surface modification was evaluated by a contact angle goniometer (First Ten Angstron FTA-125) using drop-casted TiO_2 nanorods samples on glass substrate and de-ionized water as the testing liquid. The nano-scaled surface morphology of P3HT films blended with TiO_2 nanorods with different interface modifiers were characterized by atomic force microscopy (Digital Instrument Nanoscope III A) in tapping mode. For the transient photo-voltage measurement, the P3HT/TiO_2 hybrid layer was prepared on ITO substrates, and the Al electrode was then deposited by thermal evaporation in vacuum at a pressure of around $2x10^{-6}$ torr to complete the fabrication of the samples (Figure 2.7). Under measurement the samples were illuminated by a white light to generate carriers and were operated at open circuit voltage condition. A small perturbation generated by a frequency-doubled Nd:YAG pulse laser (λ =532nm, repetition rate 10Hz, duration ~5ns) was used to generate extra electrons and holes in hybrids. The transient decay signals were recorded by a digital oscilloscope (Tetronix TDS5052B).
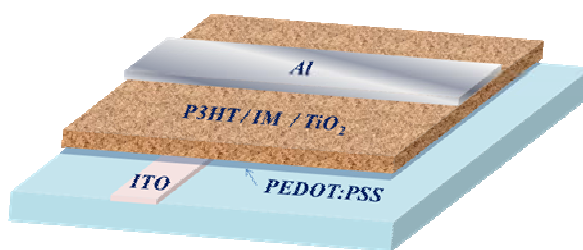
Figure 2.7 Structure of samples for transient photo-voltage measurement.

CV measurements were performed to determine the highest occupied molecular orbital (HOMO) energy level and lowest unoccupied molecular orbital (LOMO) energy level of P3HT and interface modifier molecules and were performed on electrochemical work station (CHI 600B). To measure the CV curves of organic molecules in solution, the organic molecules were dissolved in solvent mixture of tetrahydrofuran and dry acetonitrile with a volume ratio of 1:2. Tetra-n-butylammonium hexafluorophosphate (TBAPF6, 0.1 M) was used as the supporting electrolyte. A glass carbon electrode, a no aqueous $Ag/AgNO_3$ electrode, and a platinum wire were used as the working, reference, and counter electrodes, respectively. The scan rate was 100mV s^{-1} for all experiments. Ferrocene/ferrocinium (Fc/Fct) couple was used as the internal reference, and all potentials were calibrated with Fc/Fct. The HOMO energy levels were calculated based on the following equation:
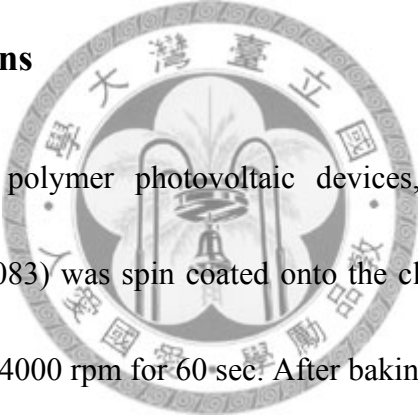
$$E_{HOMO} = -4.80 - E_{ox}(\text{onset potential vs. Fc/Fc}^+)$$

The LUMO energy levels can be estimated by the equation:

$$E_{LUMO} = E_{HOMO} + E_g$$

where E_g is the band gap of organic molecules estimated from the absorption threshold of the UV-vis absorption spectrum.

2.5 Device fabrications

For the fabrication of polymer photovoltaic devices, a 40 nm-thick layer of PEDOT:PSS (Baytron P, 4083) was spin coated onto the cleaned ITO substrate at 200 rpm for 10 sec followed by 4000 rpm for 60 sec. After baking at 120^oC for 30 min in the oven, the samples were moved into a nitrogen-purged glove-box for subsequent depositions. The thin active P3HT/TiO$_2$ nanorod hybrid layer (~120 nm), obtained from a 30 mg/ml solution at 47:53 weight ratio of P3HT to TiO$_2$ in the mixed solvent, was then deposited by using spin coating. An additional layer of TiO$_2$ nanorods was deposited between the active layer and the Al electrode to act as a hole blocking layer and also as an optical spacer. The Al electrode was then deposited onto the TiO$_2$ nanorod layer by thermal evaporation in vacuum at pressure around 2×10^{-6} torr.

Chapter 3   Results and Discussion

3.1   Characterizations of TiO$_2$ nanorods

UV-visible absorption spectrum, X-ray diffraction and TEM were applied to characterize the synthesized TiO$_2$ nanorods. UV-visible absorption spectrum was used to determine the absorption band of TiO$_2$ nanorods from which the band gap of TiO$_2$ can be calculated. XRD was used to examine the crystallinity (revealed from the full width at half maximum, FWHM) and crystal structure (revealed from peak position) of TiO$_2$ nano-crystals. Scherrer's formula could also be applied to determine the size of nano-crystals from the XRD results. TEM images were derived to observe the size and aspect ratio of TiO$_2$ nanorods.
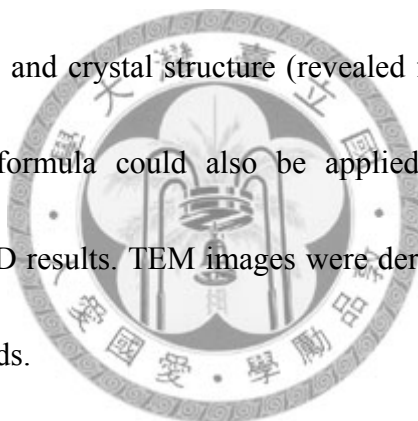
The absorption spectrum in Figure 3.1 shows that the absorption band of TiO$_2$ is in ultraviolet region and the absorption threshold is about 350nm. The sharp X-ray diffraction peaks shown in Figure 3.2 indicates good crystallinity of TiO$_2$ nanorods. From the peak position it can be inferred that the TiO$_2$ nanorods are anatase phase, whose conductivity is better in all the three crystal structures (anatase, rutile and brookite) of TiO$_2$, and is promising for solar cell applications. The aspect ratio of TiO$_2$ nanorods can be determined from the intensity ratio of the (004) peak (corresponded to the crystal plane of the longitudinal direction) to the (200) peak (corresponded to the

crystal plane of the transverse direction). From the TEM image shown in Figure 3.3, it can be seen that the TiO$_2$ nanorods are 20-40nm in length and 4-5 nm in diameter.
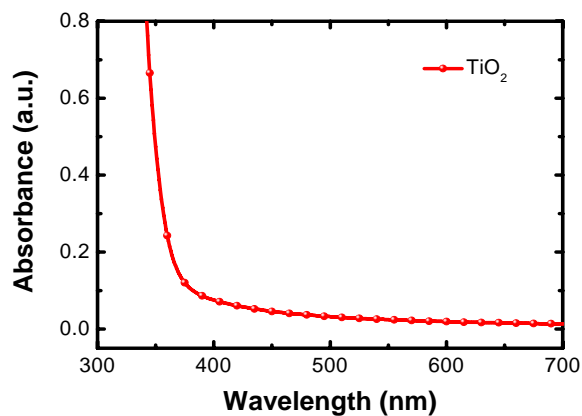
Figure 3.1   UV-visible absorption spectrum of TiO$_2$ nanorods.
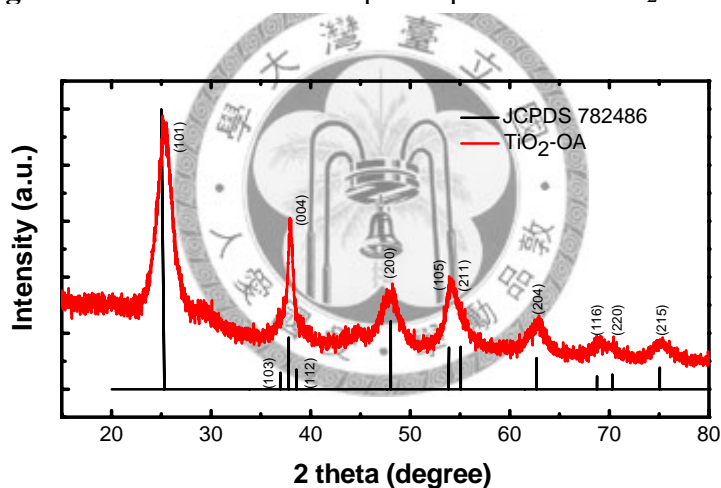
Figure 3.2   X-ray diffraction pattern of TiO$_2$ nanorods (anatase). Standard diffraction
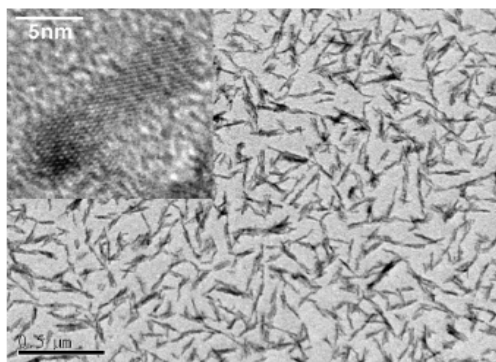
Figure 3.3   TEM image of anatase TiO$_2$ nanorods. HRTEM image is shown in the inset. [W-F Su, 2006]

3.2 Characterizations of the oligomer with carboxylate terminated 3-hexylthiophene (oligomer 3HT-COOH)

Figure 3.4 depicts the FT-IR spectrum of oligomer 3HT-COOH (Mw=5000) together with the spectrum of P3HT of similar molecular weight. P3HT and oligomer 3HT-COOH have several absorption bands in common: the strong bands at 2856cm^{-1} and 2927cm^{-1} can be assigned respectively to the symmetric and asymmetric -CH$_2$ stretches of the hydrocarbon moiety; the shoulder at 2955cm^{-1} is due to the asymmetric stretch of the terminal -CH$_3$ group of the hexyl chain; the band at 1456cm^{-1} can be associated with the -CH$_2$ deformation (δ_{CH2}) [P. J. Thistlethwaite, 2000]. Compared to the spectrum of P3HT, the oligomer 3HT-COOH spectrum has several additional signals: the band at 1650 cm^{-1} can be associated with the C=O group; the several bands in the finger print region from 1000cm^{-1} to 1300cm^{-1} may relate to the C-O-H in-plane bend (δ_{C-O-H}), and the C-OH stretch (ν_{C-OH}) of the carboxylate group [M. Thelakkat, 2009]. The broad band centered at around 3300cm^{-1} can be resulted from the adsorbed moisture (the carboxylate group may form hydrogen bonds readily with H$_2$O). These bands are the strong evidences that the carboxylate- group-containing 1,4-dibromo-3-carboxylic thiophene is successfully attached to the end of 3-hexylthiophene oligomer through Heck reaction to form the oligomer with carboxylate terminated 3-hexylthiophene.
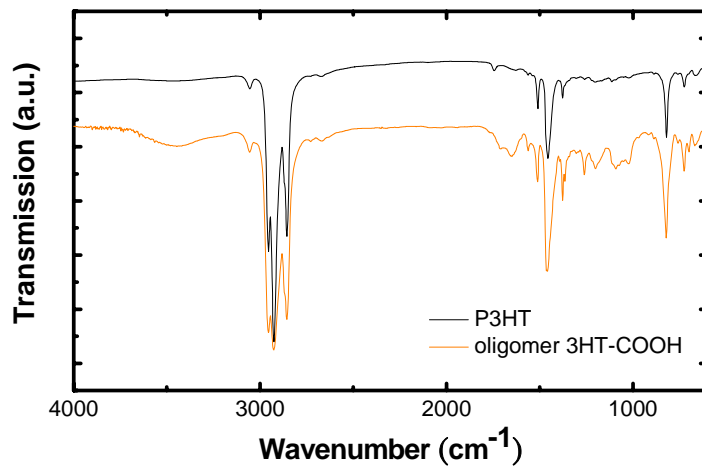
Figure 3.4 Fourier transform infrared spectra of P3HT and oligomer 3HT-COOH.

The absorption spectrum of oligomer 3HT-COOH (Mw=5000) and P3HT of similar molecular weight are shown in Figure 3.5. As compared to P3HT, the absorption of oligomer 3HT-COOH is substantially blue shifted, and its vibronic features become much less prominent, indicating the shorter π-π^* conjugation length and the lower crystallinity of oligomer 3HT-COOH. This can be due to the following reason: oligomer 3HT-COOH can form hydrogen bonds with each other through the carboxylate end functional groups, which hinders their crystallization.
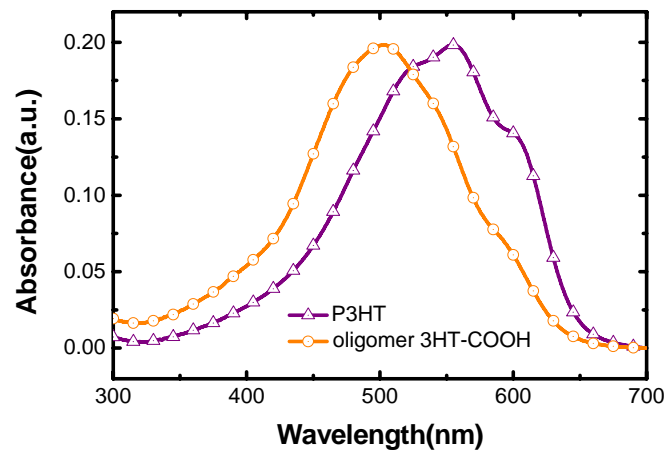
Figure 3.5 UV-visible absorption spectra of P3HT and oligomer 3HT-COOH.

3.3 Characterizations of surface modified TiO₂ nanorods

3.3.1 Fundamental surface properties

Surface modification processes were performed to exchange or replace the non-conductive oleic acids on the as-synthesized TiO_2 surface to more conductive ones (Cudye and oligomer 3HT-COOH). The processes consist of two major steps. The first step is to treat the oleic acid end-capped TiO_2 with pyridine after repeated ethanol washing to eliminate oleic acids as many as possible. The second step is to adsorb interface modifier molecules (IMs) onto the surface of TiO_2. In the first step, it should be demonstrated that oleic acids on TiO_2 surface were effectively washed out, and thermogravimetry analysis (TGA) and X-ray photoelectron spectra (XPS) measurement were undertaken to prove this.

Figure 3.6 plots the weight loss curve of TiO_2 nanorods before (TiO_2-OA) and after (TiO_2-pyr) pyridine treatment obtained from TGA. The amount of oleic acid on the surface of TiO_2 can be estimated from the overall weight loss. Before pyridine treatment, the oleic acid content on TiO_2 nanorods was 32 wt%. This number decreased to 20 wt% after pyridine treatment. This is related to the fact that oleic acids are partially removed from the surface of TiO_2. The residual oleic acid bound tightly on the surface reduces surface defects [M. Grätzel, 2003].
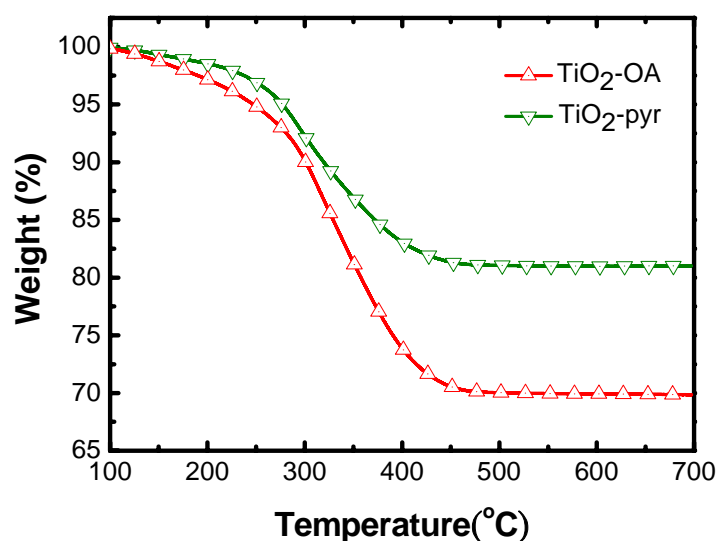
Figure 3.6   Thermalgravimetric results of TiO_2-OA and TiO_2-pyr.

High resolution XPS was used to study the surface chemistry of modifier-end-capped TiO_2 nanorods. As a powerful surface analyzing tool, XPS collects photo-electrons escaped from the top 0.1 to several nanometers of the material being illuminated by a beam of X-ray. XPS is a quantitative spectroscopic technique that can detect the elemental composition, chemical state and electronic state of the elements existed in a material. The elements a sample contains can be identified qualitatively by the specific binding energy of the electrons in certain orbital of the element.

Figure 3.7 shows the results of XPS of TiO_2 before (TiO_2-OA) and after (TiO_2-pyr) pyridine treatment. The oleic acid capped TiO_2 nanorods have C1s peak ranged from 284 to 286eV, with a normal distribution centered at 285 eV [Figure 3.7 (a)]; Ti 2p3/2 peak ranged from 458 to 460eV, with a normal distribution centered at 458.8 eV; Ti 2p1/2 peak ranged from 463 to 466 eV, with a normal distribution centered at 464.4eV

[(Figure 3.7 (b)]. The positions of these peaks are all consistent with previously reported data [D. Borgmann, 1993][N. Fourches, 1993]. The decrease of C 1s signal after pyridine treatment indicates that organic surface ligands (OA) are partially removed in the surface treatment processes. Owing to the removal of oleic acids, the electrons from Ti 2p3/2 and Ti 2p1/2 orbital can easily escape from sample and are detected more easily (can be realized as the diminishing of the "sheltering effect" of oleic acids), causing the increase of intensity of these two peaks. Besides, XPS spectra of O region were also taken [Figure 3.7 (c)]. Electrons from O 1s orbital of TiO_2 have lower binding energy, and the corresponding peak is ranged from 529 to 532eV, centered at 530.1eV; electrons from O 1s orbital of carboxylate group (-COOH) have higher binding energy, and the corresponding peak is ranged from 531 to 534eV, being consistent with previously reported data [Norman M. D. Brown., 1992]. The decrease of the O 1s peak from –COOH can be interpreted as the removal of the carboxylate-group-containing oleic acid. Note that the peak position is slightly shifted after pyridine treatment. This may imply that the chemical states of related electrons are different after the treatment. The increase of the O 1s peak from TiO_2 is originated from the diminishing of the "sheltering effect" of oleic acid after treated by pyridine. From the TGA and XPS results, it is undoubtedly to say that a cleaner TiO_2 surface has been yielded after the first step of surface modification process.
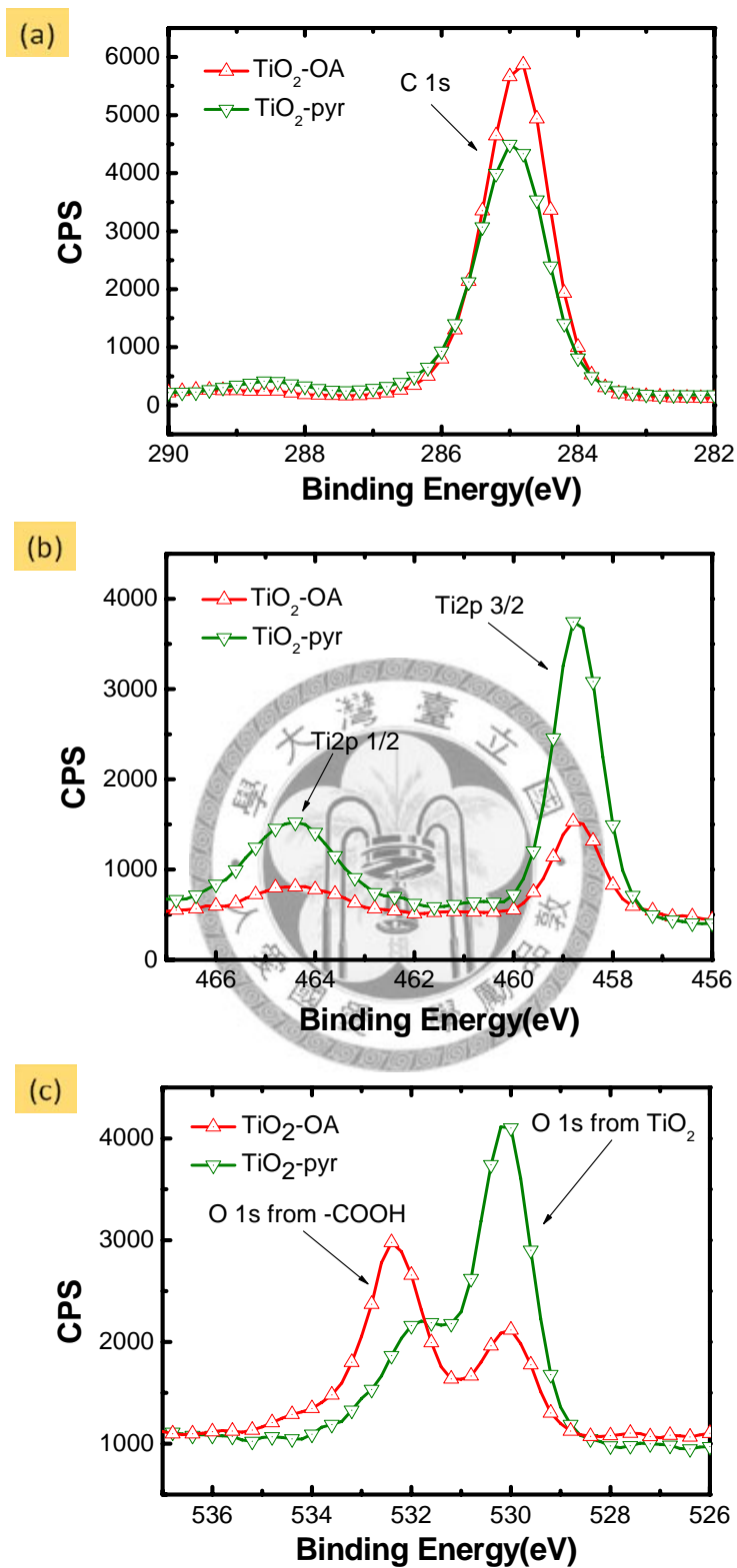
Figure 3.7 XPS results of TiO$_2$ nanorod before (TiO$_2$-OA) and after (TiO$_2$-pyr) pyridine reatment for (a) C1s orbital, (b) Ti2p 3/2 orbital and (c)O1s orbital.

In the second step of the surface modification processes, Cudye and oligomer 3HT-COOH were adsorbed on the surface of TiO_2 nanorod. It is crucial to confirm that the adsorption reaction of IMs are effectively carried out, so XPS measurement was empolyed to ensure the adsorption of interface modifiers. Signals of specific atoms that could only originate from interface modifier molecules were examined. As shown in Figure 3.8, TiO_2 nanorods modified with oligomer 3HT-COOH have an S 2p3/2 peak centered at 168.5eV, which comes from the sulfur atom of the thiophene ring in oligomer 3HT-COOH. Comparably, no signal can be observed at the same position for pyridine-treated TiO_2. The adsorption of oligomer 3HT-COOH on TiO_2 is therefore clearly elucidated. However, for TiO_2 nanorods modified with Cudye, unfortunately no apparent peak of Cu 2p3/2 centered at about 935eV can be observed, probably owing to that the concentration of Cu atom was below the detection limit of the detector (for oligomer 3HT-COOH, 1.93×10^{-1} mmol of S atom was added into 20mL pyridine solution of TiO_2, but only 2.84×10^{-3} mmol of Cu atom was added to the same amount of TiO_2). Other ways should be figured out to assure the adsorption of Cudye. The absorption spectrum is the simplest and easiest way and would be discussed in the next section.
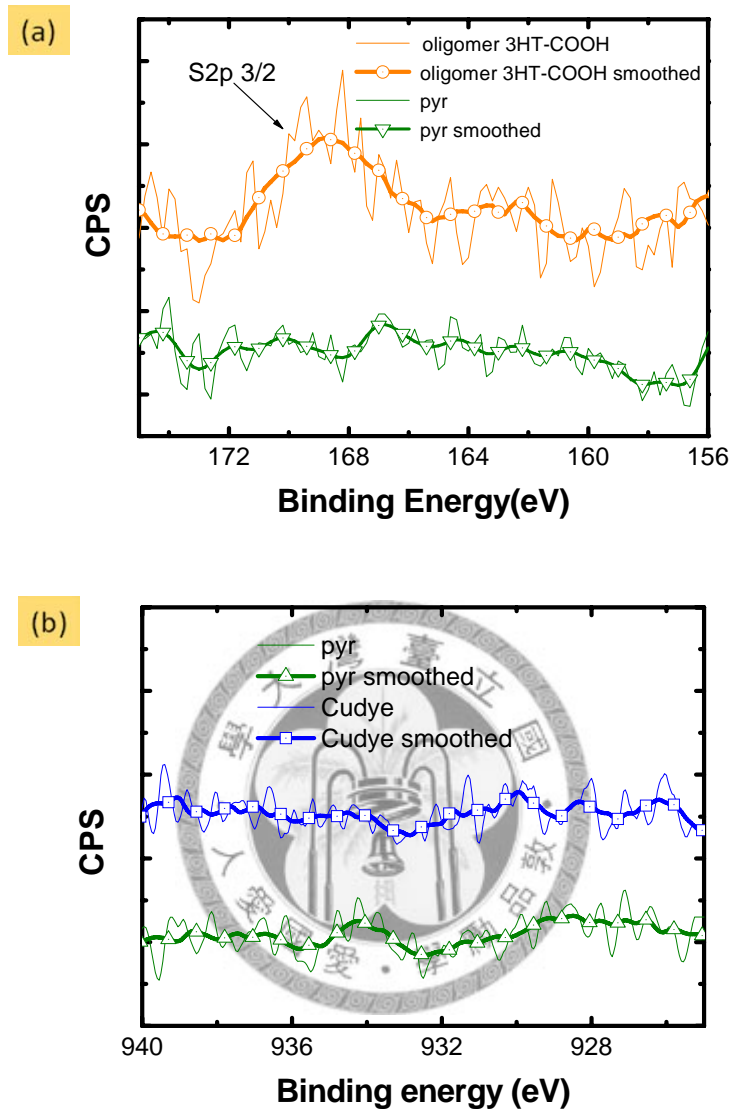
Figure 3.8 XPS results of TiO$_2$ modified by (a) oligomer 3HT-COOH and (b) Cudye.

The TEM images of surface modified TiO$_2$ nanorods dispersed in chloroform are shown in Figure 3.9. We can observe that TiO$_2$ nanorods merely treated by pyridine (without the existence of IMs on the surface) exhibit an obvious tendency to aggregate [Figure 3.9 (a)]. Several nanorods tend to gather together side by side to form a secondary particle. On the contrary, TiO$_2$ nanorods modified by Cudye [Figure 3.9 (b)]

and oligomer 3HT-COOH [Figure 3.9 (c)] can disperse well without apparent aggregation. This phenomenon is related to the fact that IMs can form spacial barriers between TiO_2 nanocrystals to stabilize them, as illustrated in the right part of Figure 3.9. From this result it can be expected that with surface modification, aggregation of TiO_2 nanorods can be suppressed in P3HT/TiO_2 hybrid films, leading to more effective contact between P3HT and TiO_2.
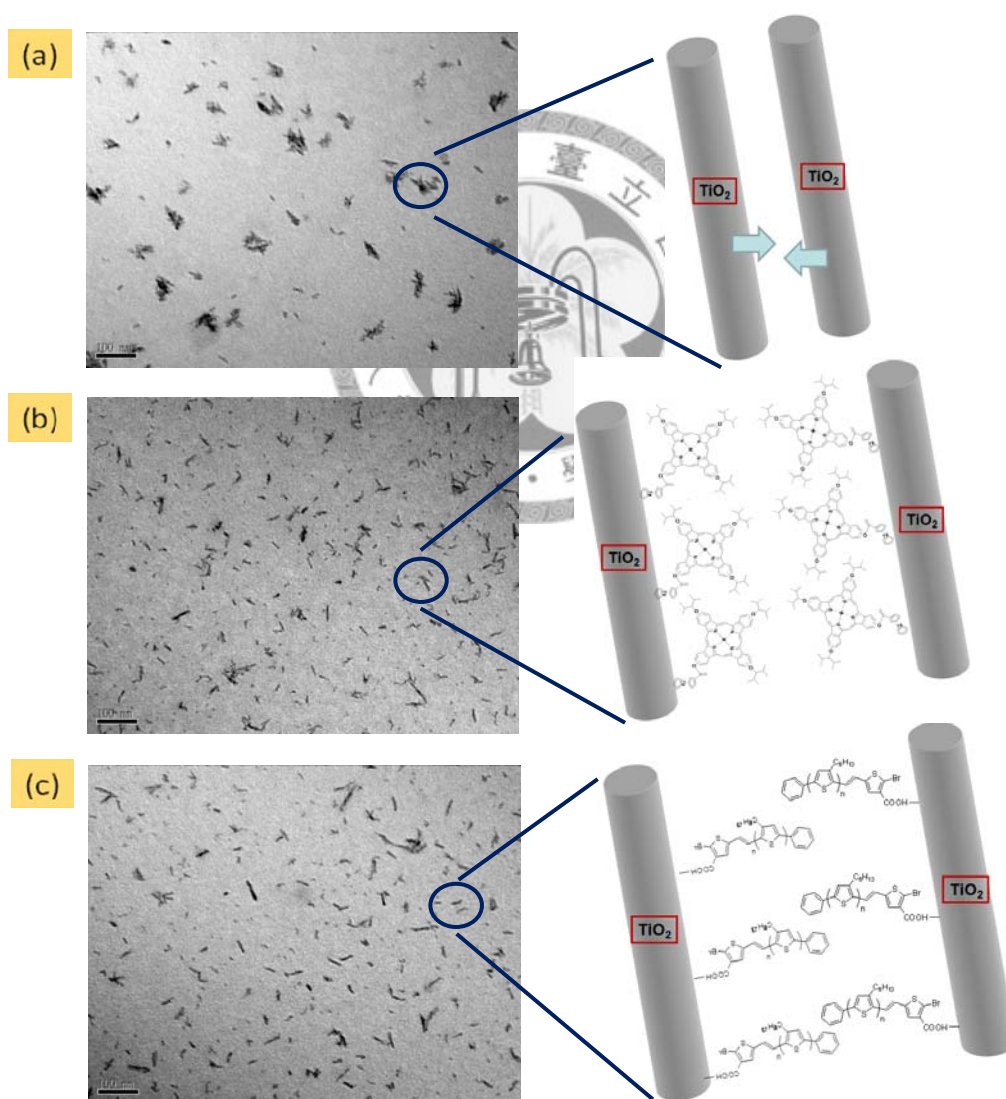
Figure 3.9 TEM images of (a) TiO_2-pyr, (b) TiO_2-Cudye and (c) TiO_2-(oligomer 3HT-COOH). The modified TiO_2 nanorods are shown schematically in the right part of the figure.

3.3.2 Desorption test of interface modifiers

As surface modification was performed, it is relevant to demonstrate that the adsorption of IMs is strong enough such that desorption processes would not take place readily as TiO_2 nanorods are employed to fabricate devices. An experiment was designed to monitor the desorption behavior of IMs. The experimental procedures are as follows: TiO_2 nanorods were mixed with extra amount of hexane, which is a good solvent for both Cudye and oligomer 3HT-COOH. The mixture was agitated by ultrasonic homogenizer to desorb the loosely attached IMs and centrifugation was performed subsequently. The washing steps were repeated for several times and the absorption spectra were recorded to monitor the remaining amount of IMs on TiO_2.

Figure 3.10(a) and Figure 3.10(b) show the UV-visible absorption spectrum of TiO_2-Cudye and TiO_2-(oligomer 3HT-COOH) after repeated washing steps, respectively. The absorption spectrum of the mixture of P3HT (Mw=8k) and TiO_2 is also shown for comparison [Figure 3.10 (c)]. As demonstrated by the figure, there was nearly no desorption of the Cudye molecules after repeated washing steps, while desorption of oligomer 3HT-COOH did occur to some extent after 4 times of washing. The percentage of the remaining amount of IMs on TiO_2 after washing can be plotted in relation to the washing times, as showed in Figure 3.11. From the figure we can see that up to 97% of Cudye was remained on the surface of TiO_2 without significant desorption, showing that

the attachment of Cudye was strong enough. Comparably, about 20% oligomer 3HT-COOH was desorbed after the first 2 times of washing, while no apparent desorption can be observed in the subsequent washing steps. Evidently, there were two parts of oligomer 3HT-COOH with different adsorption characteristics in the adsorbed layer: one part was the chemically adsorbed oligomer 3HT-COOH that formed chemical bonds to the surface of TiO_2 via carboxylate groups (the chemical bonding was strong enough such that desorption would not take place easily); the other part of oligomer 3HT-COOH was attached only by entangling with the chemically adsorbed layer, being easy to be removed after times of washing. Also noted that the P3HT molecules mixed with TiO_2 were almost entirely washed out after 2 times of washing owing to the fact that no chemical bonding or entanglement was formed between them. These results exhibit that the adsorption of IMs are strong enough (at least in part for oligomer 3HT-COOH) and are hard to be removed during the processing steps.
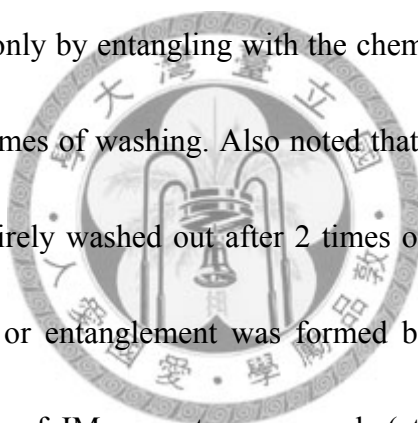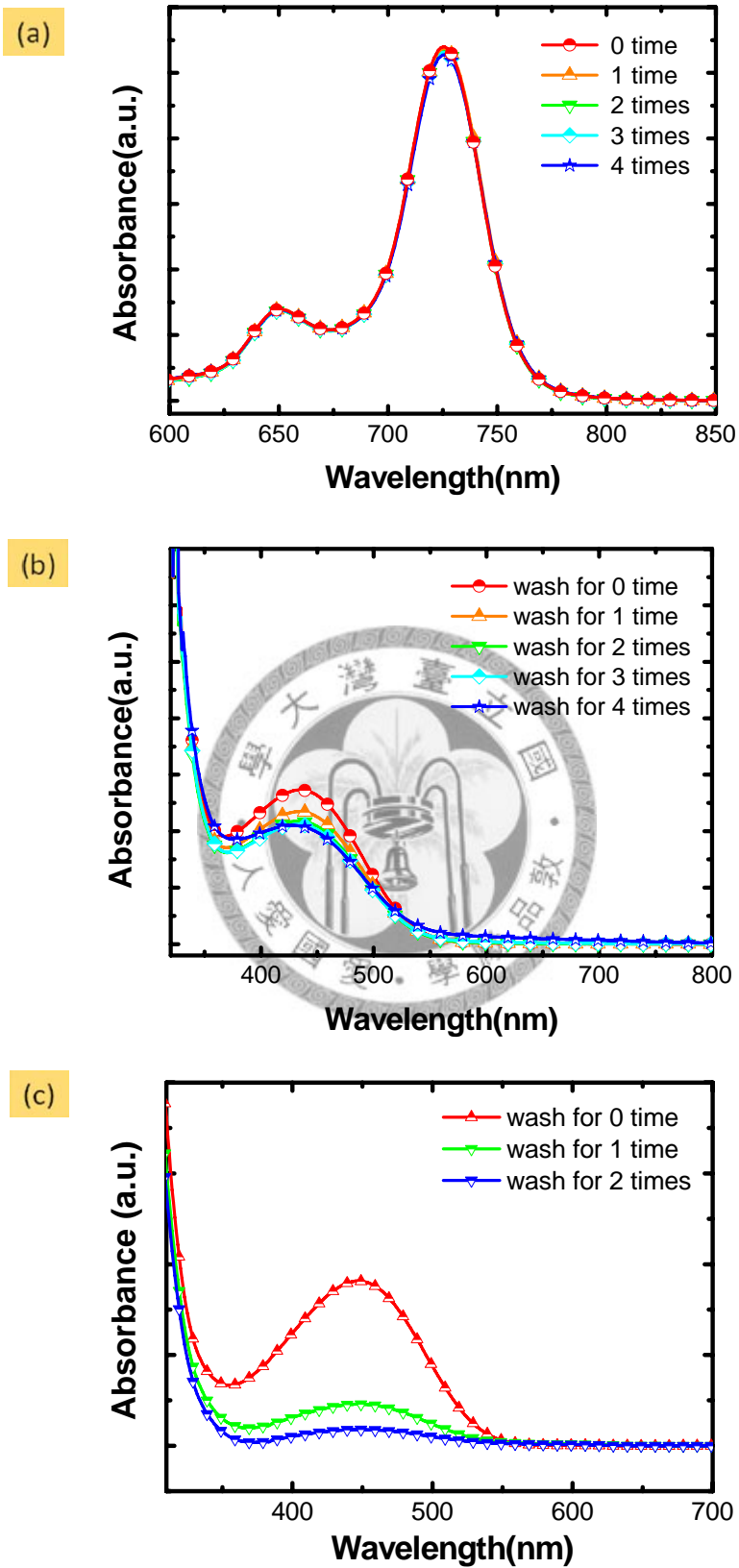
Figure 3.10 UV-visible absorption spectrum of (a) TiO_2-Cudye, (b) TiO_2-(oligomer 3HT-COOH) and (c) TiO_2/P3HT after repeated washing steps.
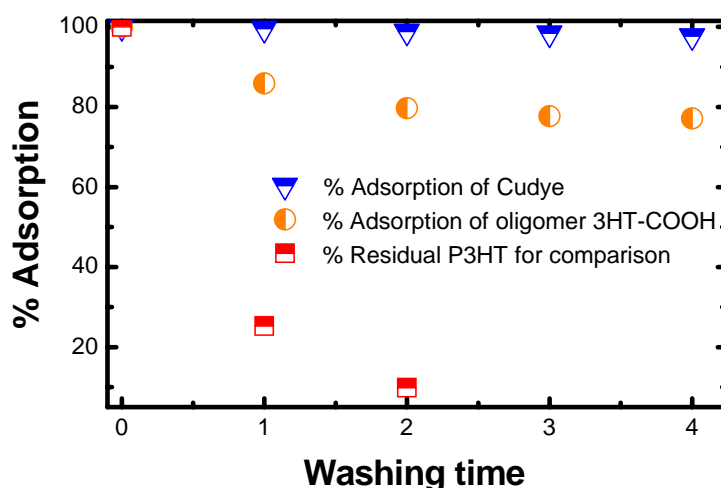
Figure 3.11 Remaining amount of interface modifiers on TiO$_2$ after repeated washing steps.

3.3.3 Quantitative evaluations of the adsorbed interface modifiers

Benefited by the knowledge of dye-sensitized solar cells (DSSCs), we know that the

adsorption amount of dye (or interface modifier) is closely related to the modification

concentration and the temperature in the modification processes [Lei L. Kerr, 2008]. In

order to quantitatively determine the amount of the adsorbed interface modifiers, which

is an important issue in the modification processes, the methodology related to

Beer-Lambert law has been established, as mentioned in the experimental section.

According to this methodology, the calibration lines that show the relationship between

the concentration of IMs and the corresponding absorbance are created (being linear

theoretically). Based on the created calibration lines, the amount of the adsorbed IMs

can be calculated and related to the modification concentration to establish the

adsorption curve of interface modifiers. The calibration lines and the adsorption curves

for Cudye and oligomer 3HT-COOH are shown in Figure 3.12 and Figure 3.13, respectively. It can be seen from Figure 3.12 that the adsorption curve of Cudye is basically linear before the adding amount of Cudye reaches 2.03×10^{-4} mmol, gradually reaching saturation condition as the adding amount exceeds 4.14×10^{-4} mmol. The saturation effect indicates that the adsorption of Cudye on the surface of TiO_2 nanorods virtually forms a monolayer. The amount of Cudye on TiO_2 nanorods applied to device fabrication is estimated from the adsorption curve and is calculated to be 0.012mg Cudye/mg TiO_2 or 7.95×10^{-4} mol Cudye/mol TiO_2.
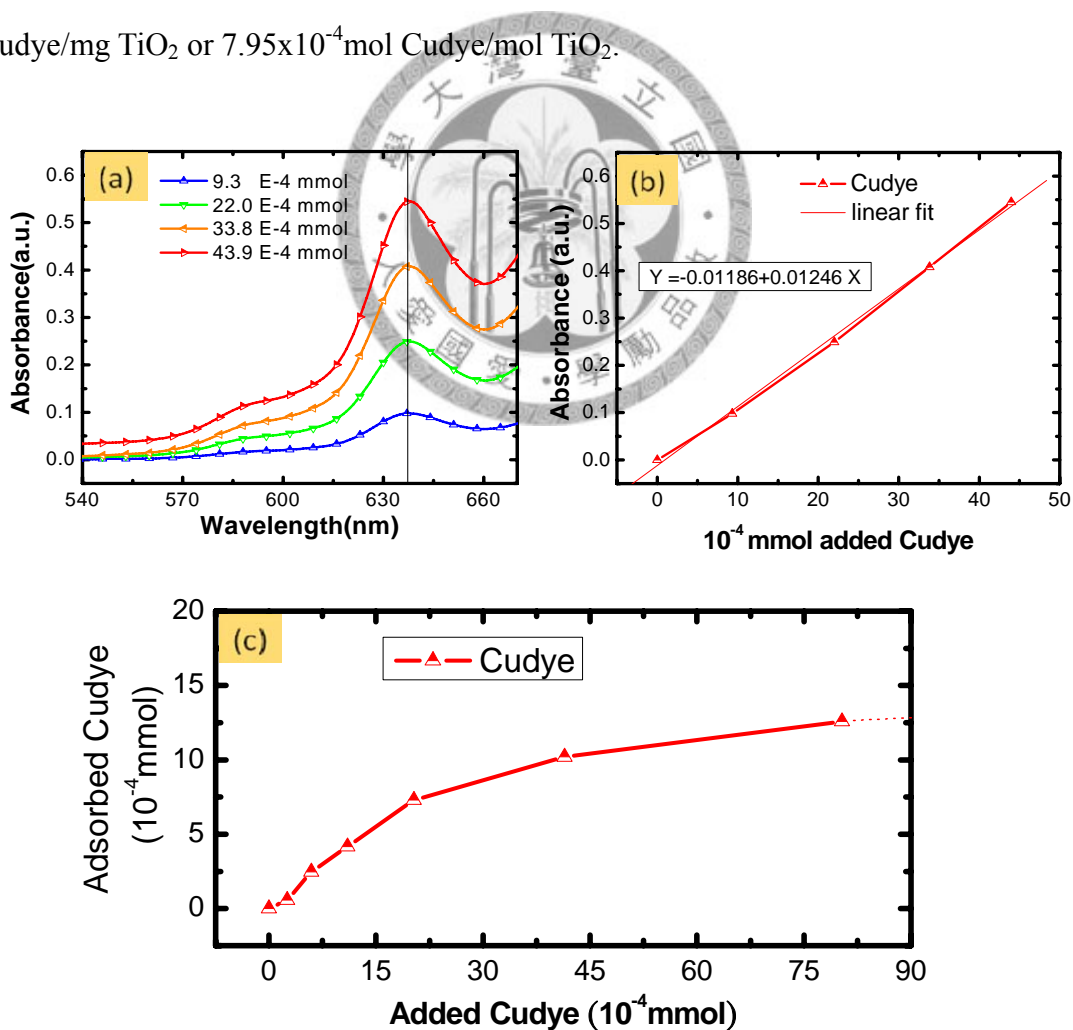
Figure 3.12 According to the calibration line [(a), (b)], the adsorption curve for Cudye shown in (c) can be made.

As for the interface modifier of oligomer 3HT-COOH, it can be seen from Figure 3.13 that the adsorption curve is virtually linear before the solubility limit is reached. The amount of oligomer 3HT-COOH adsorbed on TiO_2 nanorods applied to device fabrication can be calculated from the adsorption curve to be 0.023mg oligomer 3HT-COOH/mg TiO_2 or 3.96×10^{-4}mol oligomer 3HT-COOH/mol TiO_2. According to these calculations, we can know that while the powder of TiO_2 nanorods modified with IMs is colorful as observed by eyes, the amount of the adsorbed IMs is relatively small.
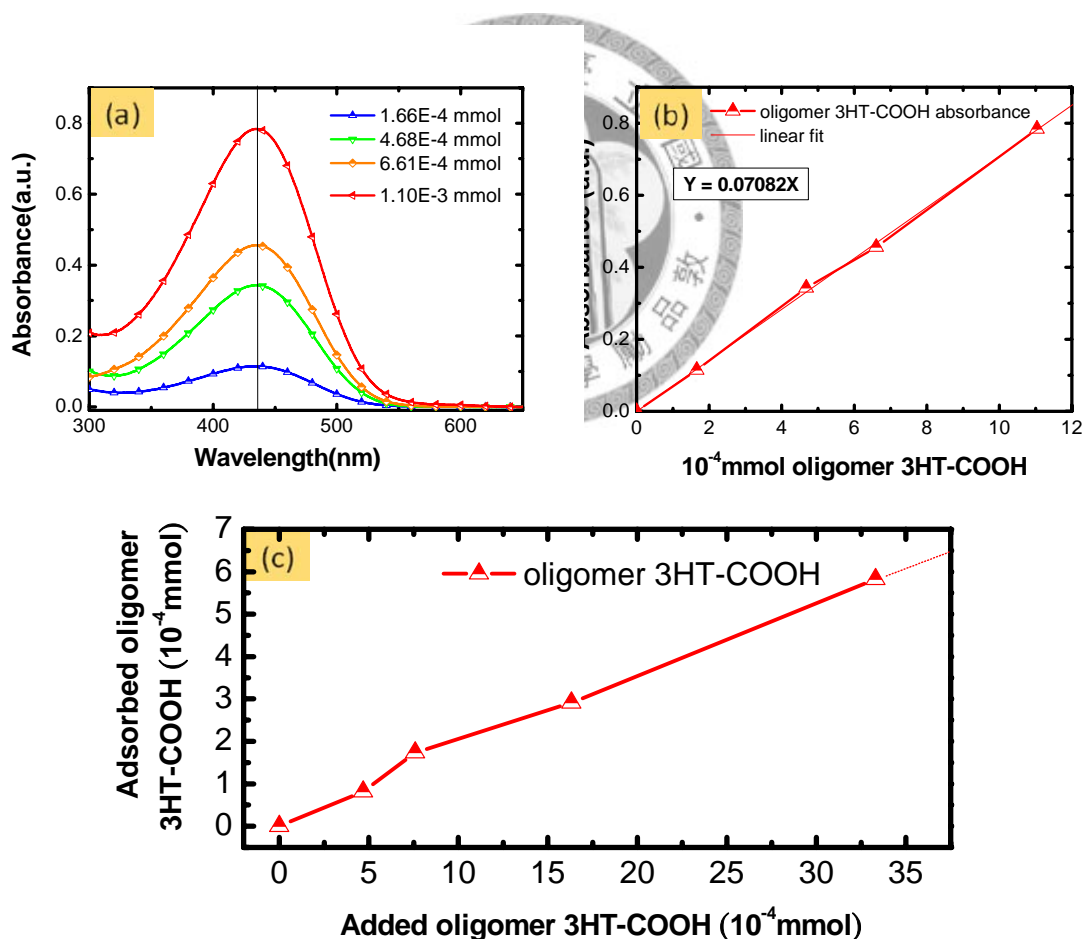
Figure 3.13   According to the calibration line [(a), (b)], the adsorption curve for oligomer 3HT-COOH shown in (c) can be made.

3.4 Effect of TiO₂ surface modification in P3HT/surface modified TiO₂ hybrid system

3.4.1 Energy band structure of P3HT/surface modified TiO₂ hybrid system

Energy band diagram is of significant importance in studying device physics and charge injection properties at material interfaces of solar cells. In P3HT/TiO₂ hybrid system, it is well known that the open circuit voltage of device is theoretically equal to the energy gap between the conduction band (E_c) of TiO₂ and the highest occupied molecular orbital (HOMO) of P3HT; the short circuit current is close related to the energy difference between the lowest unoccupied molecular orbital (LUMO) of P3HT and the conduction band of TiO₂ that determines the local electric field for exciton dissociation. As surface modification of TiO₂ nanorod is performed, a key issue is that what the band structure would be as IMs are introduced to insert between P3HT and TiO₂. The determination of energy band diagram of P3HT/IM/TiO₂ system is therefore essential to investigate the physics in the hybrid system.

The HOMO levels of P3HT and IMs were determined from cyclic voltammetry and the corresponding LUMO levels are obtained by subtracting the bandgaps estimated from the absorption threshold of the UV-visible absorption spectra. The energy levels of TiO₂ were taken from literature [Weiyou Chen, 2008]. The measurement data are shown in Figure 3.14. The calculated energy levels are summarized in Table 2 and the band

diagram of P3HT/IM/TiO$_2$ system is depicted in Figure 3.15. It can be seen that the LUMO of both Cudye and oligomer 3HT-COOH lie between the LUMO of P3HT and the conduction band of TiO$_2$; the HOMO of both Cudye and oligomer 3HT-COOH lie between the HOMO of P3HT and the valence band of TiO$_2$. The energy band diagram of P3HT/IM/TiO$_2$ system is therefore a three-leveled, cascade-typed band diagram.
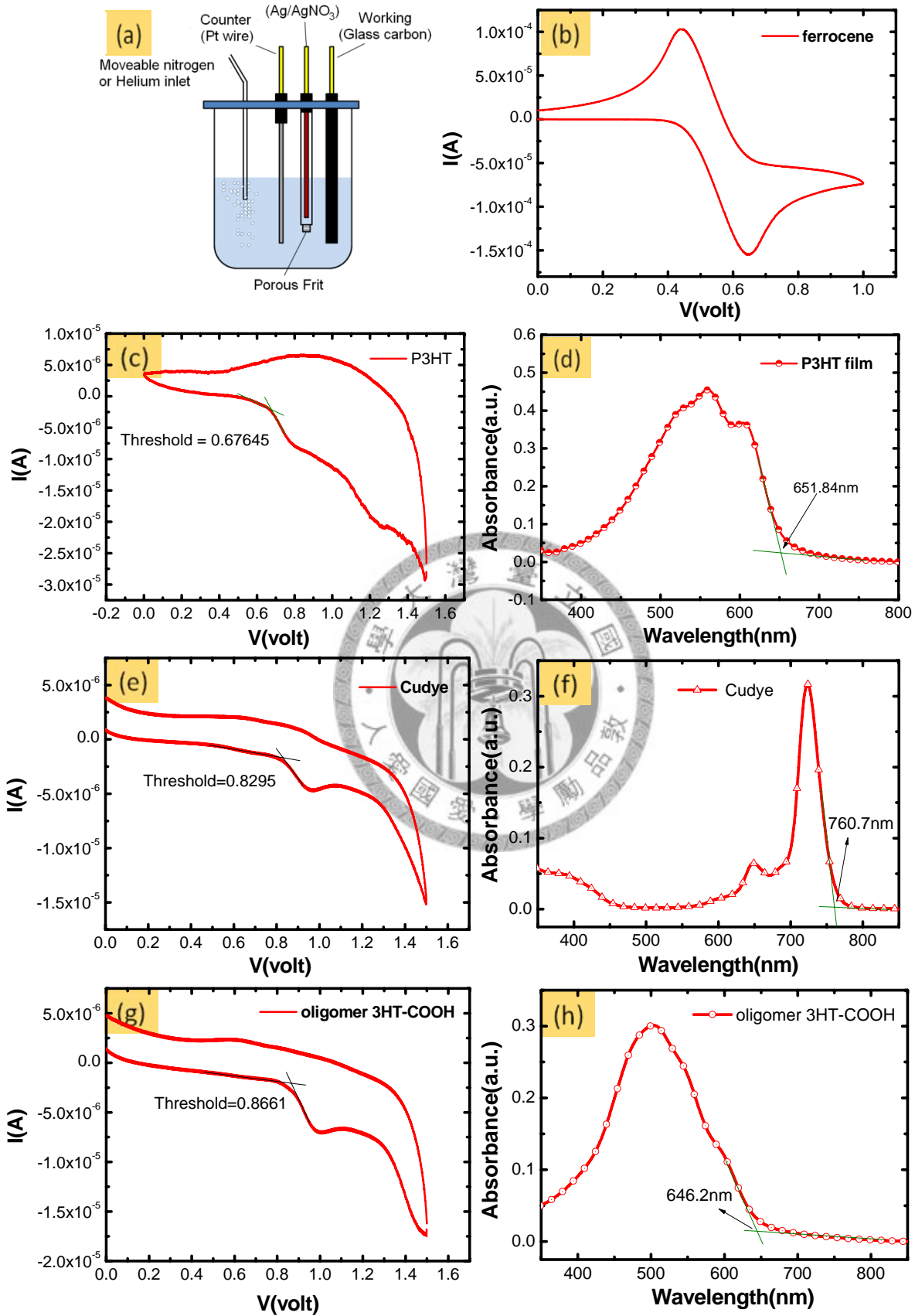
Figure 3.14 (a)Setup of cyclic voltammetry; (b) CV curve of ferrocene; oxidation curves of (c) P3HT, (e) Cudye and (g) oligomer 3HT-COOH together with the absorption spectra of (d) P3HT, (f) Cudye and (h) oligomer 3HT-COOH.
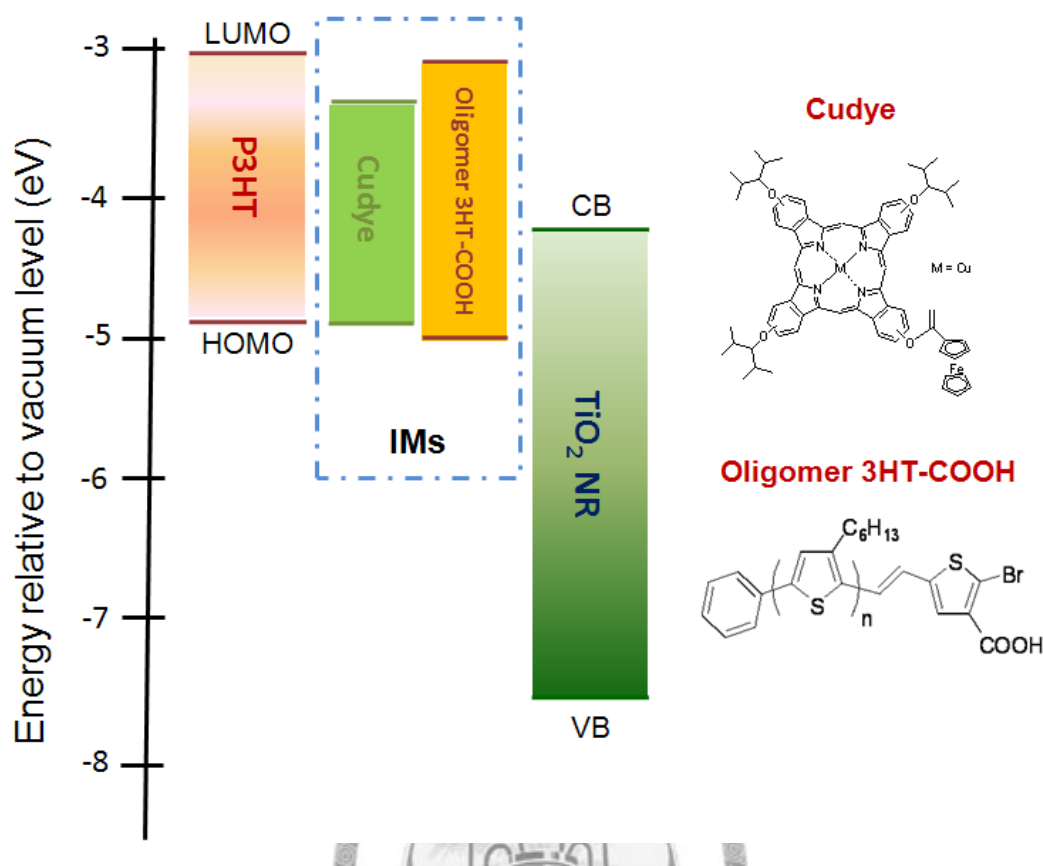
Figure 3.15 Energy band diagram of P3HT/IM/TiO$_2$ system together with the chemical structures of the IMs of Cudye and oligomer 3HT-COOH.

Table 2 Calculated energy levels and bandgaps for P3HT, Cudye and oligomer 3HT-COOH. The data of TiO$_2$ are derived from literature [Weiyou Chen, 2008].

Material	HOMO	LUMO	E$_g$ (eV)
P3HT	-4.93	-3.03	1.9
Cudye	-4.93	-3.30	1.63
oligomer 3HT-COOH	-4.97	-3.05	1.92
TiO$_2$	-7.42	-4.20	3.22

Some literatures had discussed about systems with band diagram of this type. According to the argument of S. Ramakrishna et al [S. Ramakrishna, 2008], the insertion of the light-absorbing interface modifiers between P3HT and TiO$_2$ could result

in complicated mechanisms in P3HT/TiO$_2$ hybrid solar cells, one is referred to as the "dye-regenerating" mechanism; the other is referred to as "electron-mediating" mechanism, as shown schematically in Figure 3.16. In the "dye-regenerating" mechanism, IM molecules absorb the incident light and contribute to charge generation, and P3HT transports a hole to the dye to regenerate it, acting much like dyes and the electrolyte in dye-sensitized solar cells. In this mechanism, the relative position of the HOMO level between P3HT and IMs is important. The HOMO level of IM cannot be higher than that of P3HT in the dye-regeneration process. On the other hand, in the "electron-mediating mechanism", P3HT can act as the major light absorber and is excited by the incident photons. The IM molecules at the interface of P3HT and TiO$_2$ act as the energy mediator or energy funnel to mediate electrons from P3HT to TiO$_2$. In this case, the LUMO level of dye molecule should lie between the LUMO of P3HT and the conduction band of TiO$_2$. To determine the contribution of each mechanism in our system, UV-visible absorption spectra and photoluminescence spectra were undertaken and discussed in the following section.
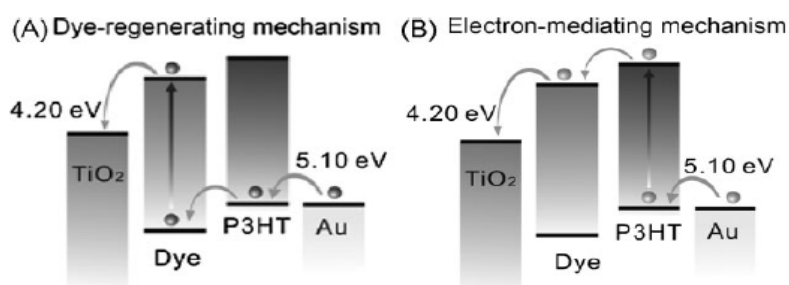
Figure 3.16   (a) ''Dye-regenerating'' and (b) ''electron-mediating'' mechanisms for the dye-modified P3HT/TiO$_2$ hybrid solar cells. [S. Ramakrishna, 2008]

3.4.2 *Light harvesting in P3HT/surface modified TiO$_2$ hybrid system*

Figure 3.17 shows the UV-visible absorption spectra of Cudye, oligomer 3HT-COOH

and surface modified TiO$_2$ nanorods. Cudye is green-colored and has two absorption

peaks at 644nm and 718nm near the IR region. oligomer 3HT-COOH has a broad

absorption band ranged from 300nm to 550nm and the absorption peak maximum is

located at 441nm, slightly blue shifted as compared to P3HT (Mw=55k), owing to its

shorter conjugation length. The absorption spectra of pyridine treated TiO$_2$ nanorods

have little difference compared to the as-synthesized TiO$_2$, having an absorption

threshold at about 350nm. The absorption of surface modified TiO$_2$ is simply the

superposition of the absorption of TiO$_2$ and the IMs, indicating the fact that the IMs are

on the surface of TiO$_2$. It was expected that the introduction of IMs would increase light

harvesting in the P3HT/IM/TiO$_2$ system. However, difference in absorption spectra

could barely be seen in the P3HT/IM/TiO$_2$ hybrid films compared to the system without

IMs, as shown in Figure 3.18. Obviously, the argument in the "dye-regenerating"

mechanism that the IMs can serve as the light absorber is not applicable in our case.
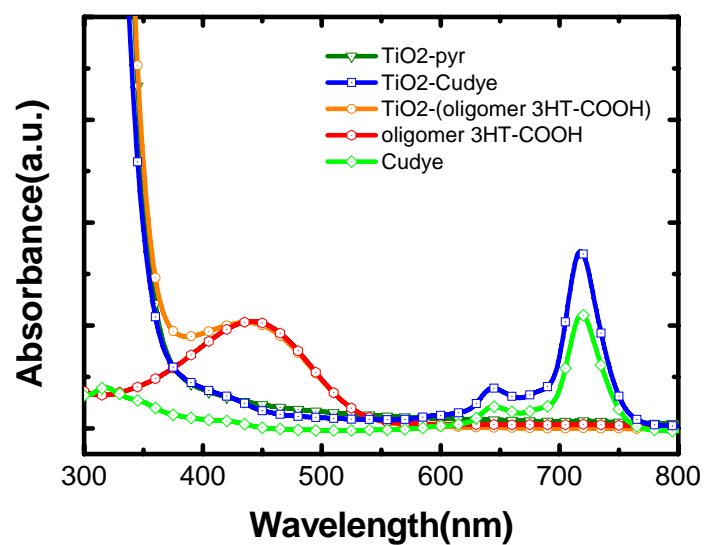
Figure 3.17 UV-visible absorption spectra of Cudye, oligomer 3HT-COOH and surface modified TiO$_2$.
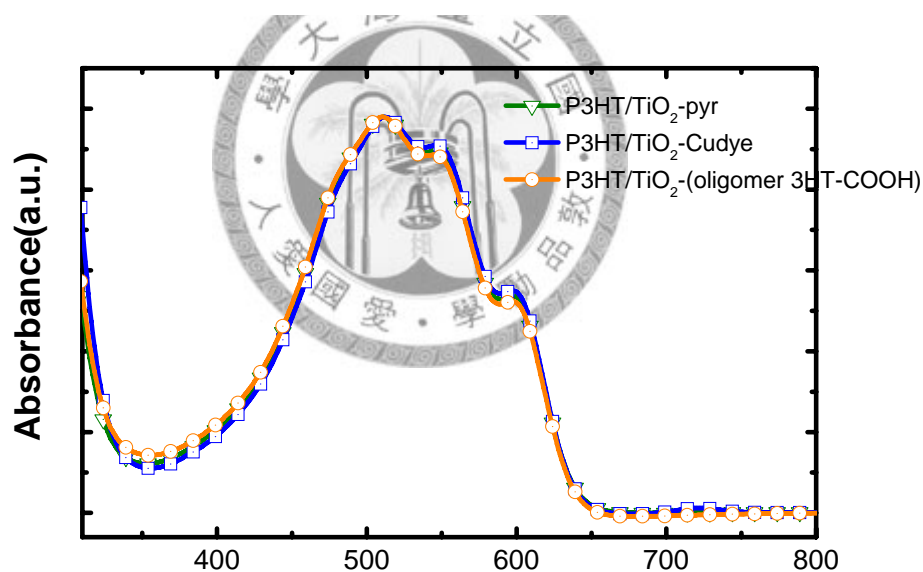
Figure 3.18 UV-visible absorption spectra of solid hybrid films of P3HT/IM/TiO$_2$.

3.4.3 Charge separation in P3HT/surface modified TiO$_2$ hybrid system

As a polymer of P3HT is excited by a photon, the electron is pumped to a higher energy state. The pumped electron can return to the ground state via either radiative or non-radiative routes. When P3HT as a donor material is hybrided with the acceptor,

TiO$_2$, the excited electron in P3HT can transfer readily to TiO$_2$ (termed "photo-induced charge transfer"), providing a non-radiative route for the electron to return to the ground state, and the photoluminescence of P3HT is consequently quenched. The PL quenching effect can be applied to monitor the charge separation processes in materials for solar cell applications, as discussed in the following paragraph.

Figure 3.19 depicts the PL spectra of P3HT/IM/TiO$_2$ system with the excitation wavelength of 450nm and the weight ratio of P3HT to TiO$_2$ is 1:2. The samples were made in solution state. The inset presents the corresponding UV-visible absorption spectra of the samples, showing that the absorption of different samples is virtually identical such that the PL intensity could be compared. A clear quenching effect is observed as TiO$_2$ nanorods are introduced into pristine P3HT. Thus, the photo-induced charge transfer occurs at the interface of the two phases. As different IMs are attached to the surface of TiO$_2$, varied quenching effect can be observed with the order of oligomer 3HT-COOH > Cudye > pyridine > OA. PL spectra with hybrid solid film samples (P3HT/TiO$_2$ = 47/53 in wt%) were also undertaken to compare with the active layer in devices, and the results showed similar sequence of quenching efficiency (here we define the quenching efficiency as the percentage of photoluminescence that is quenched with the existence of the quencher) as compared to liquid-phased samples (quenching efficiency: Q_{pyr} = 58.3%; Q_{Cudye} = 62.2%; $Q_{oligomer\ 3HT-COOH}$ = 66.7%), as

presented in Figure 3.20. The largely reduced PL intensity of the $P3HT/TiO_2$-pyr system

as compared to the $P3HT/TiO_2$-OA system can be evidently attributed to the removal of

the oleic acid, for the insulating oleic acid existed at the D/A interface greatly hinders

the charge transfer processes. However, after the adsorption of IMs, the quenching

effect is further increased. This phenomenon can be ascribed to several reasons, as

proposed by various literatures. Jenny Nelson et al. explored the effect of the interface

layer of an amphiphilic dye (Z907) on the performance of hybrid polymer/zinc oxide

photovoltaic devices [J. Nelson, 2006]. They attributed the enhanced charge separation

in devices to the cascade energy level structure formed by ZnO, Z907 and P3HT.

Electrons can transfer down the cascade while holes are blocked. This explanation is

applicable in our case because our $P3HT/IM/TiO_2$ system also forms a three-leveled

cascade, as shown by the previously mentioned CV results. The photo-excited electrons

generated in P3HT can transfer readily down the cascade from the LUMO of P3HT to

the lower leveled LUMO of IMs, then to the even lower level of TiO_2 conduction band.

Due to the properly aligned energy levels, there is no energy barrier encountered in the

electron transfer processes. According to the PL results, it is confirmed that the

"electron-mediating" mechanism dominates the photocurrent generation in the

$P3HT/IM/TiO_2$ system. The IMs serve as electronic mediator or energy funnel that can

improve the electron injection efficiency from P3HT to TiO_2.
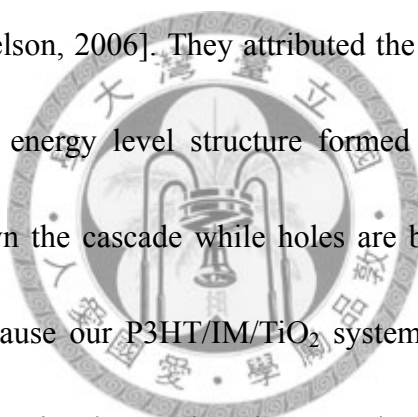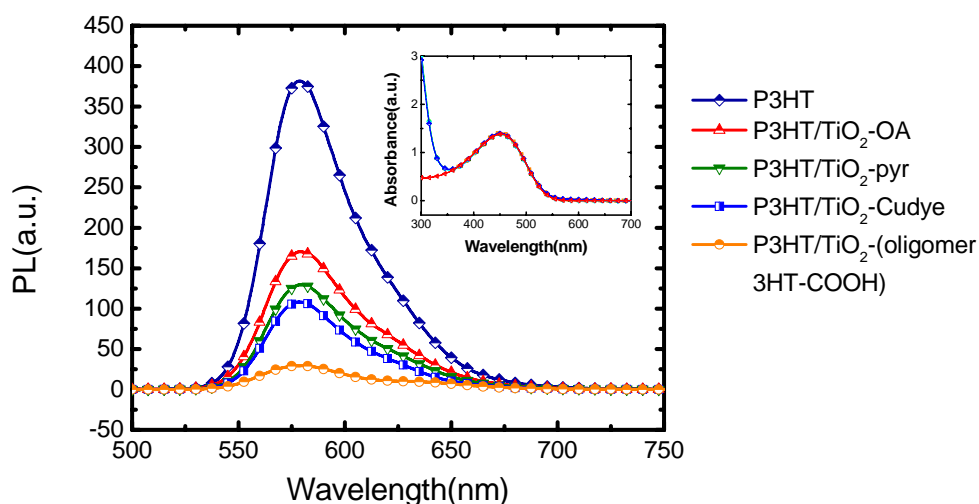
Figure 3.19 Photoluminescence spectra of P3HT/IM/TiO$_2$ system in solution state (excited at 450nm). The inset shows the absorption spectra of the samples.
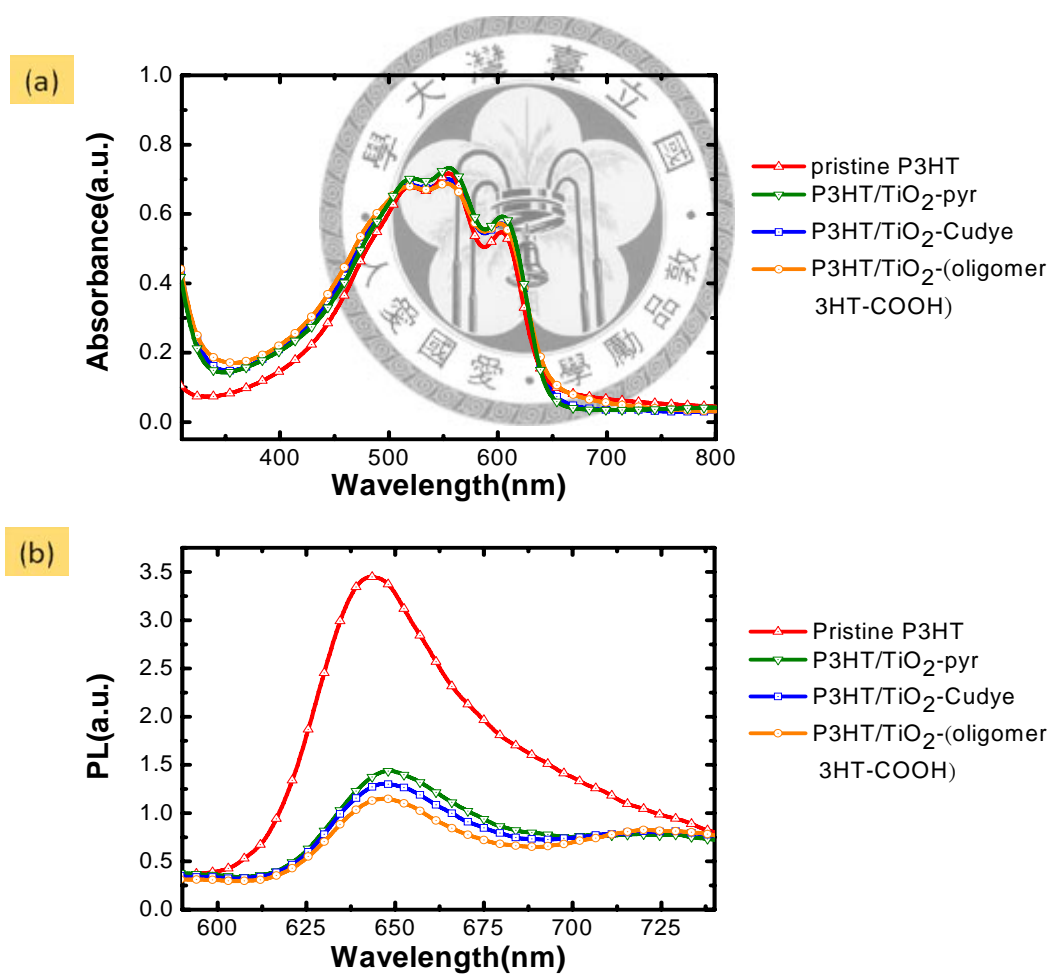
Figure 3.20 (a) UV-visible absorption spectra of hybrid films of P3HT/IM/TiO$_2$; (b) corresponding photoluminescence spectra excited at 500nm.

There are other explanations for the improved charge separation as interface modifiers are applied in solar cells. One is the removal of surface states. M. Grätzel pointed out that surface complexation of colloidal semiconductors (TiO_2) by benzene derivatives strongly enhanced interfacial electron transfer rates between TiO_2 and another phase [M. Grätzel, 1991]. These findings are rationalized in terms of removal of surface states by complexation with the absorbant. On the other hand, Ohkita et al. considered that the improved electron injection efficiency could be in virtue of the improved wetting between the polymer and the oxide surface [Ohkita, 2007]. This could also be one of the possible explanations in our case, for the results of contact angle measurement suggest the improved wetting between P3HT and TiO_2 (see page 85); the low aggregation tendency of surface modified TiO_2 nanorods from the TEM images also implies the increased contact area between P3HT and TiO_2 where charge separation can take place.

Based on the PL results, comparison between the two interface modifiers, Cudye and oligomer 3HT-COOH, are attempted to be made in terms of their different characteristics. These two surface modifiers are both conductive due to their conjugated structure, being both promising electronic mediators between P3HT and TiO_2. The Cudye is a highly symmetric, sphere-like small molecule, while oligomer 3HT-COOH has a long-chained backbone extended for several nanometers. The long-chained shape

and the conductive nature of oligomer 3HT-COOH make it an effective energy funnel to "grab" excitons from the bulk material, leading to more efficient charge separation compared to Cudye, as illustrated schematically in Figure 3.21.

In another aspect, McGehee et al. investigated the effect of carboxylate-group bearing small molecule on the energy offset at the TiO_2/polymer interface [M. D. McGehee, 2007]. The carboxylate group can change the band offset either by forming an interfacial dipole layer or by protonation of titania (in effect forms a dipole layer at the interface). The surface dipole pointed from P3HT to TiO_2 facilitate the transfer of electrons, thus the charge separation efficiency is enhanced. This accounts for the high PL quenching efficiency for oligomer 3HT-COOH. As for the Cudye, the charge separation efficiency is less prominent without the existing of strong dipole.
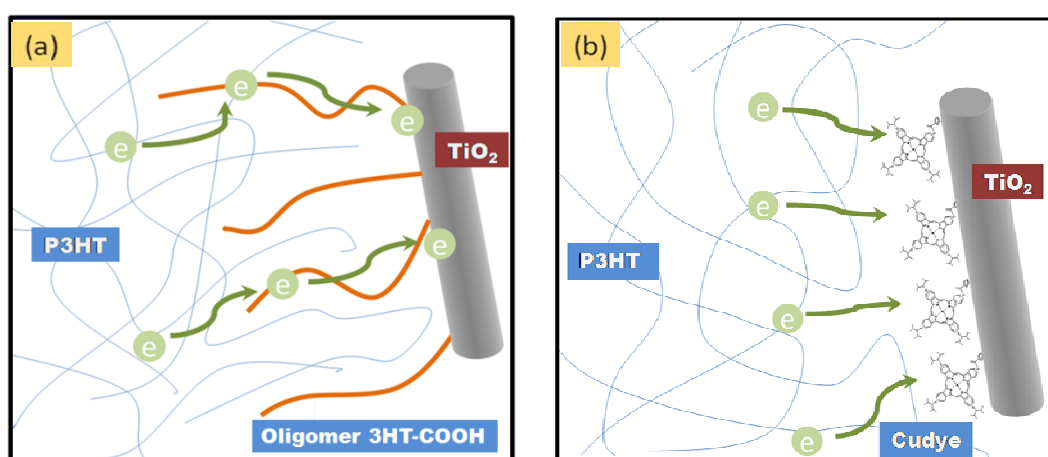
Figure 3.21 Schematic illustration of charge transport properties at the donor/acceptor interface of (a) P3HT/TiO_2-(oligomer 3HT-COOH) system and (b) P3HT/TiO_2-Cudye system.

3.4.4 Charge recombination in P3HT/surface modified TiO₂ hybrid system

When donor and acceptor materials are hybrid together to form a bulk-heterojunction, a highly interpenetrating network in nanoscale is created. The large interface area between donor and acceptor facilitates the exciton dissociation process. However, the recombination of electrons and holes (virtually a reverse process of charge separation) is also enhanced owing to the large interface, for the charge carriers in their respective transporting materials meet more easily at the interface. Recombination of charge carriers largely deteriorates the efficiency and photocurrent generation in the solar cell. For this reason, tackling the problem of charge recombination is a significant issue to improve the performance of bulk-heterojunction solar cells. Treating the donor/acceptor interface with IMs may serve as a possible solution to this problem. In our previous discussion, we have demonstrated that the insertion of the interface modifier layer between P3HT and TiO₂ can assist charge separation according to the PL results. Now we turn to investigate the effect of IMs on charge recombination in the P3HT/IM/TiO₂ system, with the aid of transient photo-voltage measurement.

In the study of recombination kinetics by transient photo-voltage measurement, devices are held in flat band condition by applying a voltage equaled to V_{oc} and under the illumination of a white bias lamp. A pulsed light transiently generates electrons and holes, imposing a small perturbation to the system, resulting in a transient increase in

V_{oc}. After the pulsed light illumination, the charge carrier density in materials decreases via recombination of electrons and holes across the heterojunction interface. The quasi-Fermi levels are away from the band edges, leading to the decrease of V_{oc} which is determined by the difference between the quasi-Fermi levels. Since in flat band condition the photo excited charges cannot be extracted by the electrodes, the decreasing of the transiently generated photo-voltage can be only related to the recombination of charge carriers. The decay curve of V_{oc} can be fitted to monoexponential decay to obtain the charge carrier lifetime, τ. The recombination rate, k_{rec}, is decided by the reciprocal of τ. Figure 3.22 shows the results of transient photo-voltage measurement of P3HT/TiO$_2$ hybrid samples with different interface modifiers, and the calculated results of charge carrier lifetimes and recombination rates are showed in Table 3.
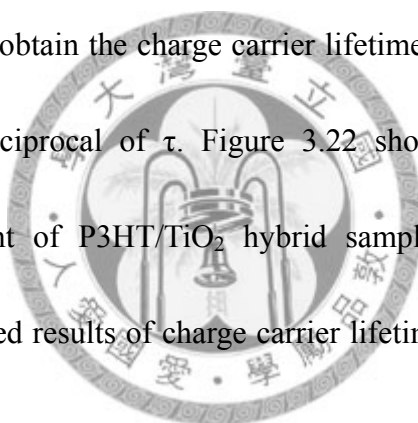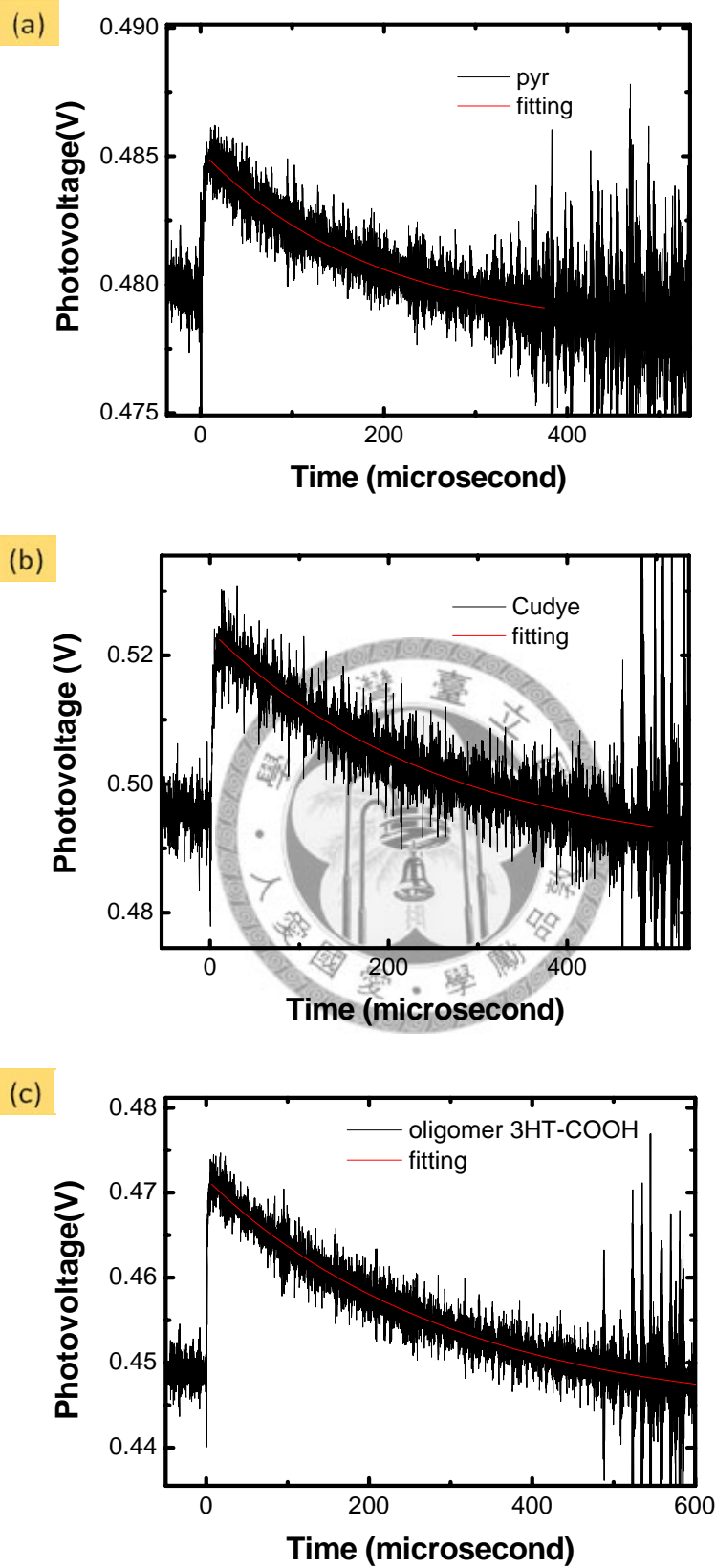
Figure 3.22 Photo-voltage transient curves for (a) P3HT/TiO$_2$-pyr, (b) P3HT/TiO$_2$-Cudye and (c) P3HT/TiO$_2$-(oligomer 3HT-COOH).

Table 3 Charge carrier lifetime and recombination constant of P3HT/TiO$_2$-IM system.

Interface modifier	Charge carrier lifetime $\tau(\mu s)$	Recombination constant $k_{rec}(s^{-1})$
pyridine	190.2	5.26×10^3
Cudye	259.5	3.85×10^3
oligomer 3HT-COOH	300.9	3.32×10^3

As can be seen from the table, the charge carrier lifetime increased as surface modification of different IMs was carried out, with an increasing order of pyridine, Cudye, oligomer 3HT-COOH. The fact that the P3HT/TiO$_2$-(oligomer 3HT-COOH) system have the longest charge carrier lifetime are quite expectable owing to the following reasons: oligomer 3HT-COOH with a molecular weight of about 5000 is a giant molecule. Existing between P3HT and TiO$_2$, oligomer 3HT-COOH effectively forms an energy barrier and spacial obstacle for recombination of electrons and holes in their respective transporting materials, resulting in the largely suppressed recombination rate. As for Cudye, its effect of inhibiting recombination is not as apparent as oligomer 3HT-COOH because of its smaller molecular size. For the P3HT/TiO$_2$-pyr system, the direct contact between P3HT and TiO$_2$ leads to extensive recombination sites at the interface, resulting in the shortest charge carrier lifetime. By the way, since charge separation is more efficient with the existing of IMs, one may expect a faster charge recombination rate when IMs are applied, assuming that these two processes are virtually reverse to each other. However, we believe that charge separation is a

multiple-stepped process involving electron transfer from P3HT to the IM as an intermediate, followed by rapid electron injection to the acceptor material across this 3-leveled potential cascade, while recombination requires direct contact between the donor/acceptor, being suppressed as IMs are inserted in between. In such case, faster charge separation rate does not necessarily lead to rapid charge recombination.

The observations that charge recombination in solar cells is reduced by the implement of interface modification by small molecules have been reported by several groups. M. Grätzel et al. [M. Grätzel, 2007] observed that charge recombination in solid state dye-sensitized solar cells was reduced by the presence of a series of Ruthenium-based bipyridyl complex molecules on the surface of TiO_2. They found that the electron-hole recombination lifetime was dependent on the different pendent side chains in these molecules, owing to the different distance between the hole conductor and TiO_2 and the different potential barrier resulted from the side chains. Ohkita et al. [Ohkita, 2007] pointed out that the charge recombination in P3HT/TiO_2 hybrid solar cells was efficiently suppressed by the chemical modification of organic dyes, suggested by the increased V_{oc}. As reported by the authors, this is probably because that the organic dyes at the surface of TiO_2 separated P3HT from it, preventing the direct contact between them. C.W. Chen et al. [C-W Chen, 2009] examined the influence of interface modifier on the performance of hybrid solar cells composed of P3HT and vertically aligned ZnO

nanorods. The improved device efficiency was found to partially due to the reduced

back recombination at P3HT/ZnO interfaces. These findings about the effect of

interface modifiers are in substantial agreement with our results.

3.4.5　　Hybrid morphology and surface properties in P3HT/surface modified TiO₂ hybrid system

3.4.5.1　　Hydrophobicity of the surface modified TiO$_2$

To monitor the adsorption of interface modifiers and the change in surface

hydrophobicity of TiO$_2$ nanorod after surface modification, water contact angle

measurements were performed. Contact angle measurement is the most direct and

commonly employed method for measuring surface hydrophobicity or hydrophilicity,

and has been widely applied to monitor the adsorption of self-assembled monolayer on

the substrates [R. T. Collins, 2008][L-Y Wang, 2009]. This method involves the

placement of a droplet of liquid (water here) onto a horizontal surface and measuring

the contact angle via the analysis of a digital image of the droplet on the surface. The

contact angle θ obeys Young's equation shown as follow:

$$\gamma_{LV} \cos\theta = \gamma_{SV} - \gamma_{SL}$$

where γ_{LV} is the surface tension between the interface between the water droplet and

the surrounding atmosphere, γ_{SV} is the surface tension between the surface and the

surrounding atmosphere, γ_{SL} is the surface tension between the surface and the liquid.

These vector forces balance each other at the interface of the three phases as shown

schematically in Figure 3.23 thus the contact angle is determined. As the surface of the

films of TiO$_2$ nanorod is modified by different IMs, the surface free energy is changed,

so does the surface tension γ, bringing about the change in hydrophobicity and contact

angle. Table 4 summarizes the results of contact angle measurement of films modified

by Cudye and oligomer 3HT-COOH with different modification concentration. After the

surface modification, the water contact angles increase with increasing IM

concentration. These results indicate that the IMs were absorbed on the TiO$_2$ surface and

the surface becomes more hydrophobic.
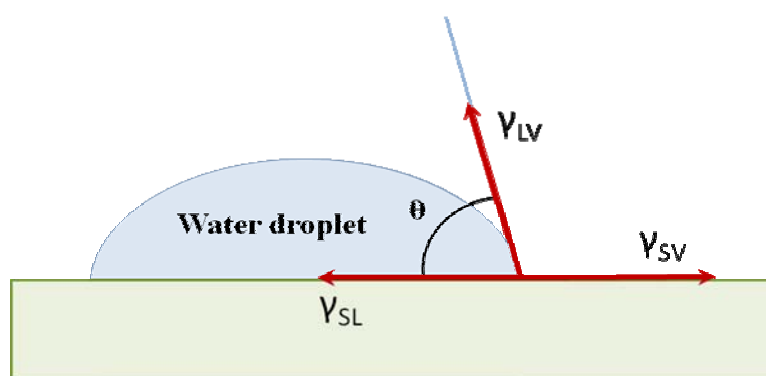
Figure 3.23   Illustration of the vector forces present at the solid-liquid interface. The measured contact angle (θ) is shown.

Table 4 Contact angles of modified TiO$_2$ with different interface modifiers and modification concentrations.

Interface modifiers on TiO$_2$ NR film		Contact angle
pyridine		95.38° ± 1.06°
Cudye 1wt%		100.01° ± 1.83°
Cudye 2wt%		101.93° ± 1.37°
Cudye 4wt%		106.09° ± 1.28°
oligomer 3HT-COOH	4wt%	107.01° ± 1.94°
oligomer 3HT-COOH	8wt%	111.80° ± 1.69°
oligomer 3HT-COOH	16wt%	115.80° ± 1.06°

3.4.5.2 Surface morphology of P3HT/surface modified TiO$_2$ hybrid films

P3HT, as an alkyl group bearing macromolecule, is highly hydrophobic as casted into films. On the contrary, the surface of TiO$_2$ nanorod is intrinsically hydrophilic if no surface ligands were attached as the consequence of its hydroxyl group bearing surface. Tremendous phase segregation will be resulted as the hydrophobic organic molecule (P3HT) and the hydrophilic inorganic quantum dots (TiO$_2$) are hybrid together without further surface treatment to form the active layer of a photovoltaic. Large scale phase segregation deteriorates solar cell efficiency for the aggregates not only cause destruction of the inter-penetrated network formed by Donor/Acceptor phases but also lead to inefficient contact between the two phases. For this reason, interface modifiers are introduced to improve the compatibility of P3HT and TiO$_2$ and prevent TiO$_2$ nanorods from large scale aggregation. From the results of contact angle measurement,

we expect that the compatibility between P3HT and TiO_2 was enhanced after surface modification, according to the fact that a more hydrophobic surface of TiO_2 was exhibited with the adsorption of IMs. Contact mode AFM was adopted to investigate the effect of IMs on the nano scale morphology of $P3HT/IM/TiO_2$ hybrid films, and the results are shown in Figure 3.24:
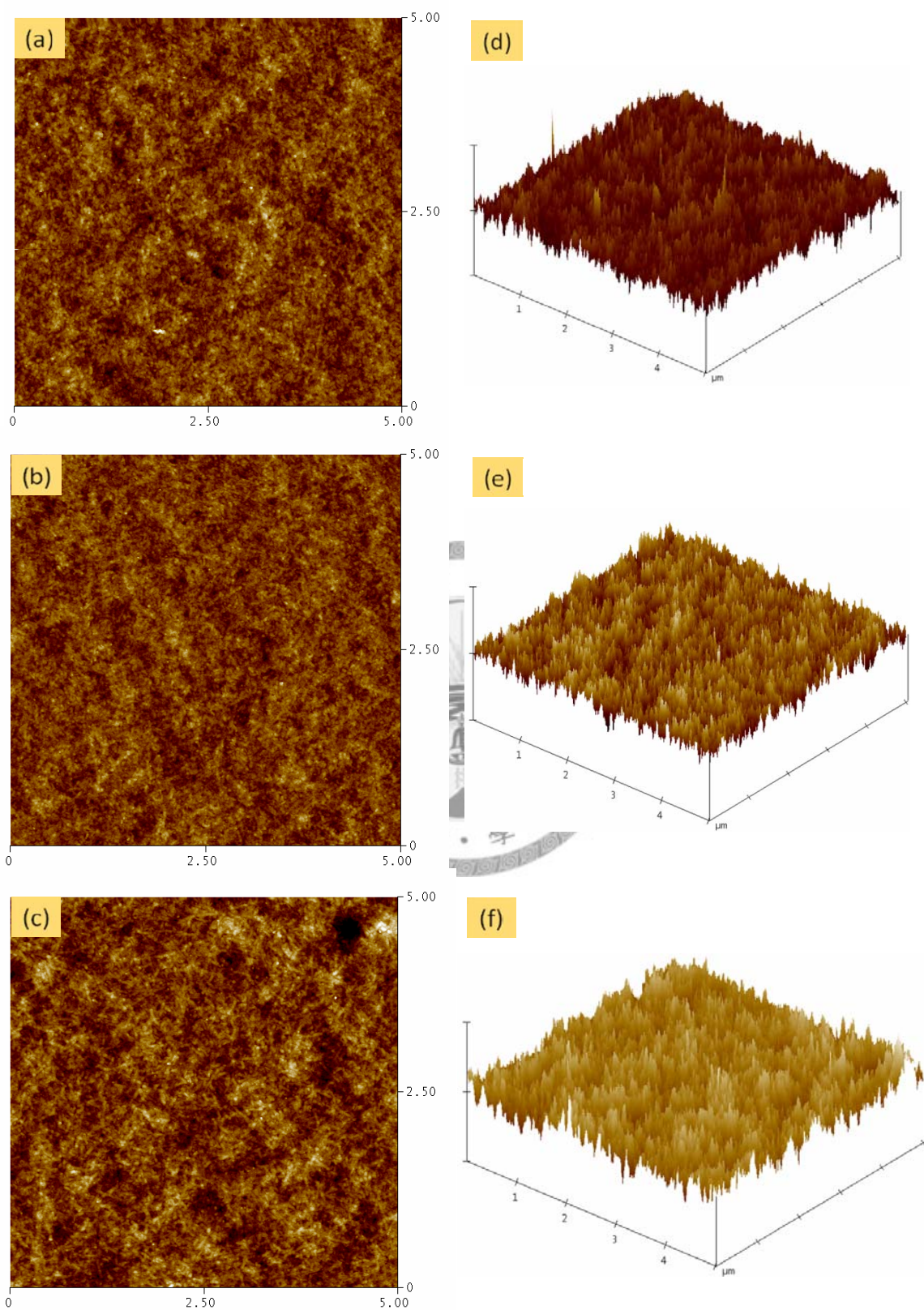
Figure 3.24 Topographic images of P3HT/TiO$_2$-pyr hybrid film [(a), (d)], P3HT/TiO$_2$-Cudye hybrid film [(b), (e)] and P3HT/TiO$_2$-(oligomer 3HT-COOH) hybrid film [(c), (f)].

As revealed by the AFM images, the blend film of P3HT/TiO$_2$-pyr exhibited a root-mean-square (RMS) roughness of 4.8nm. After surface treatment by Cudye, the RMS roughness of P3HT/TiO$_2$-Cudye blend film reduced to 4.3nm. The more smoothed surface morphology after interface modification of Cudye tallied with our expectation that a more compatible P3HT/TiO$_2$ interface can be resulted via introducing IM molecules, as inferred from the results of contact angle measurement. The small Cudye molecule, which serves as the intermediate between P3HT and TiO$_2$, brings about more complete intermixing between these two phases without causing apparent aggregation, leading to a more smoothed surface. The finding is consistent with those reported by D. Gebeyehu et al. [D. Gebeyehu, 2002], who has investigated the effect of the adsorbed RuL2(NCS) dye on the surface morphology of solid-state organic/inorganic hybrid solar cells based on P3OT and dye–sensitized TiO$_2$ electrodes. According to their results, the nc-TiO$_2$/Ru-dye/P3OT films showed a very homogeneous surface without holes and pinholes, as compared to the much rougher surface of the nc-TiO$_2$/P3OT films. As for the oligomer 3HT-COOH modified hybrid film, surprisingly, a rougher surface morphology was revealed as the RMS roughness increased to 6.0nm. These results were quite unexpectable, for the chemical structure of oligomer 3HT-COOH was virtually identical to P3HT, being excellent intermediate molecule as attached to TiO$_2$ surface, so the smoothest surface was expected to be yielded. However, after carefully scrutinized
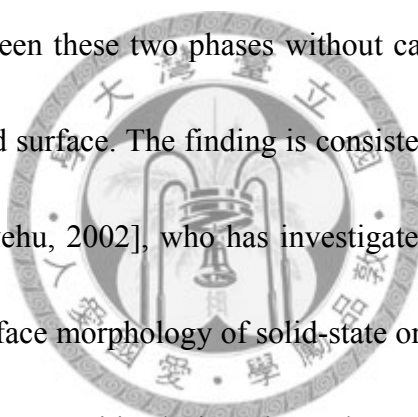
the AFM image of the P3HT/TiO$_2$-(oligomer 3HT-COOH) film, fibril structure of P3HT (corresponds to the crystalline domain), typically found in P3HT films of small molecular weight, can be observed. Note that the molecular weight of P3HT adopted to fabricate the hybrid films was about 55kD. P3HT with high molecular weight like this typically displays a nodule-like structure, exhibiting a lower tendency to crystallize as compared to P3HT with lower molecular weight. The existence of the fibril structure in the P3HT/TiO$_2$-(oligomer 3HT-COOH) film, which could not be found in pyridine or Cudye modified films, indicated that for some reasons the crystallization of P3HT (to some extent) had been induced. The cause of the induced crystallization was inferred to be the effect of IM (oligomer 3HT-COOH) attached to the surface of TiO$_2$. When introduced into P3HT film which exhibits a high tendency to crystallize via self-organization of the polymer chains, TiO$_2$ nano-crystals, as an extrinsic phase of rigid rods, can interrupt the ordering structure of P3HT. For this reason, polymer chains of P3HT to the surroundings of TiO$_2$ nanorods are expected to be amorphous, forming a disordered domain. Similar effects have been studied by Julia W.P. Hsu et al. that in P3HT/ZnO hybrid solar cells the P3HT in immediate contact with ZnO might be disordered [Julia W. P. Hsu, 2008]. This effect was verified by the blue shift in the absorption spectra when a thin (<10nm) P3HT film was deposited on ZnO. When oligomer 3HT-COOH molecules (the short-chained P3HT to a certain extent) were
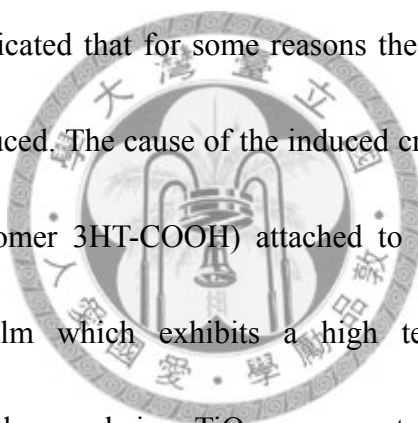
introduced to attach to the surface of TiO$_2$, they can interact with the surrounding molecular chains of P3HT in the disordered domain to arrange themselves to make a structure of higher crystallinity. The fibril structure was the indication of the improved crystallinity. The surface morphology of hybrid films was roughened by the movement of P3HT chain segments caused by the IM induced crystallization. This phenomenon is quite similar to the effect of thermal annealing on the surface morphology of P3HT film that a rougher surface is often results after annealing, owing to the forming of larger crystalline domains. More evidences and discussion about this phenomenon would be provided in the following sections.

3.4.5.3 Interface-modifier-induced ordering effect of P3HT in P3HT/surface modified TiO$_2$ hybrid films

To further validate the preceding arguments that the interface modifier of oligomer 3HT-COOH can affect the ordering structure of P3HT, UV-visible absorption spectra were employed to monitor the change of the vibronic features in the absorption spectra of P3HT, which is closely related to the π-π* stacking of the conducting polymer. Hybrid films of P3HT/TiO$_2$-pyr, P3HT/TiO$_2$-Cudye and P3HT/TiO$_2$-(oligomer 3HT-COOH) were fabricated and the thickness of the films was carefully controlled to be the same. Solvent annealing of the samples was performed in a solvent-vapor filled petri dish for about 10 minutes to allow substantial ordering of the polymer chains and

chloroform was chosen as the annealing solvent. Figure 3.25 shows the UV-visible

absorption spectra of the hybrid films before and after solvent annealing. From the

figure we can see that the absorption of hybrid films before solvent annealing was

essentially identical, inferring that the thickness of all films was controlled to be the

same. Three vibronic features associated with the ordering structure of P3HT can be

observed: two peaks at 525nm and 556nm are from intrachain π-π^* excitation and the

peak at 601nm is due to the interchain interaction of P3HT. It has been reported that the

vibronic features are extremely sensitive to the crystalline structure of the polymer [O

Inganäs, 1988][P. J. Brown, 2003]. After solvent annealing was carried out, the vibronic

features of the absorption of P3HT became more prominent for all films. The

enhancement of the vibronic features for different IM treated films was in an increasing

order of P3HT/TiO$_2$-pyr, P3HT/TiO$_2$-Cudye, and P3HT/TiO$_2$-(oligomer 3HT-COOH).

While the enhancement of the vibronic features of Cudye treated film does not have

much difference to the pyridine treated one, the change in absorption of the

P3HT/TiO$_2$-(oligomer 3HT-COOH) film is quite obvious after being solvent annealed.

Before the films were solvent annealed, the arrangement of polymer chains was in a

relatively disordered condition, for the solvent contained in the films evaporated quickly

and the polymer chain segments became immobile before they can self-organized into a

highly ordered structure. Solvent annealing treatment, which was extensively employed
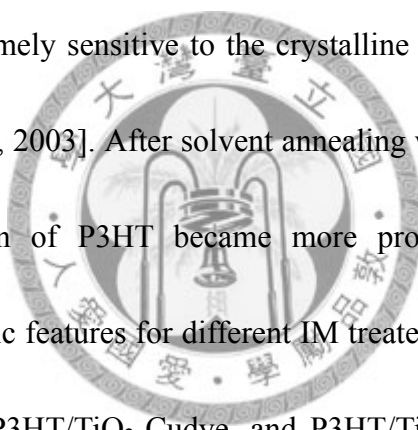
in the fabrication processes of various organic devices after film deposition [Y. Yang, 2007][Yueh-Lin Loo, 2006], imposed a driving force for the polymer chains to crystallize. The P3HT molecules in hybrid systems with high tendency to crystallize can readily organize themselves into a highly ordered structure with the aid of solvent vapor treatment. Therefore, the fact that the solvent annealed P3HT/TiO$_2$-(oligomer 3HT-COOH) film exhibited the most prominent vibronic features in the absorption spectra indicated that this system possessed the highest tendency to crystallize among all IM contained systems. Similar findings has been reported by Julia W.P. Hsu et al. that the interfacial molecules can affect the ordering structure of P3HT in P3HT/ZnO solar cells by showing distinct features in absorption spectra [Julia W. P. Hsu, 2008]. In the study of Hsu, the absorption of thin (<10nm) P3HT films was found to red shift as deposited on alkanethiol self-assembled monolayer (SAM) treated ZnO surfaces, as compared to the system without SAMs. The longer the alkanethiol molecule, the more obvious the red shift. The author pointed out that P3HT polymers were more mobile on the alkanethiol-modified surface and can reorder to form larger crystalline domains with the aid of thermal annealing. In spite of that no apparent red shift can be observed in our system owing to the much thicker films as compared to the literature, the more prominent vibronic features in the absorption spectra also account for the enhanced crystallinity in the P3HT/TiO$_2$-(oligomer 3HT-COOH) system.
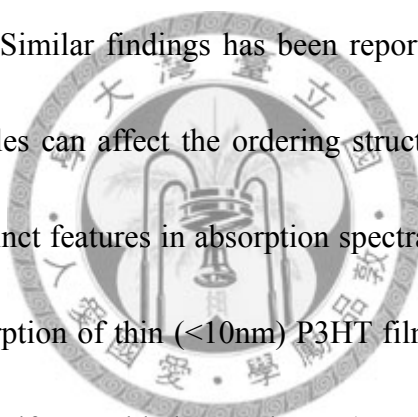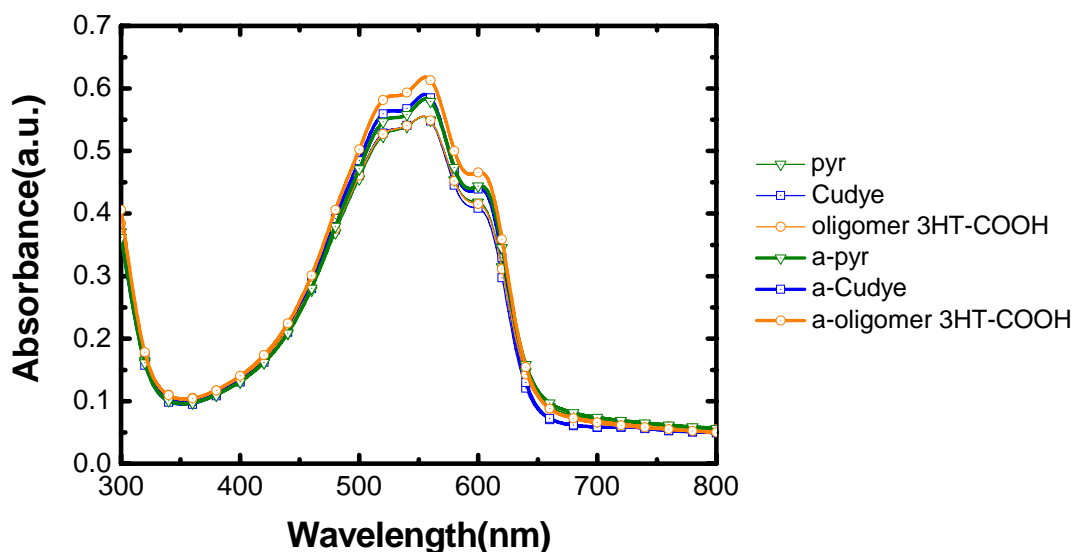
Figure 3.25 UV-visible absorption spectra of P3HT/TiO$_2$-IM films before (thin lines) and after (thick lines) solvent annealing.

To provide more convincing evidences for the preceding arguments, X-ray diffraction of the hybrid films was also performed to monitor the crystallinity of P3HT in the films. The procedures for XRD sample preparation were as follows: P3HT/IM/TiO$_2$ (the IMs were: pyridine, Cudye, oligomer 3HT-COOH) hybrid solution (chlorobenzene was chosen as the solvent) was dropped on the indium tin oxide glass substrates and allowed to dry slowly. The polymer chains in the slowly drying films had abundant time for self-arrangement before the solvent was all evaporated, so the polymer chains in these drop-casted films were highly ordered such that the XRD diffraction peaks can be revealed. Subsequently, the samples were thermal annealed at 140℃ for 60 minutes in inert atmosphere to derive more highly-crystallized films. The thickness of all films was controlled with care to be the same (all about 4.1 μm as measured by alpha stepper).

The XRD results of P3HT/IM/TiO$_2$ hybrid films are shown in Figure 3.26 (b) and

Figure 3.26 (c), together with the XRD of the blank ITO substrate [Figure 3.26 (a)]. The

diffraction peak at 5.3°, which corresponds to the (100) crystal plane of P3HT, along

with the weak diffraction signals at 10.7° ((200) plane of P3HT), 16° ((300) plane of

P3HT) and 25.3° ((010) plane of P3HT) can be revealed. The small signals at 30.4° and

35.3° were found to be originated from the ITO substrates. From Figure 3.26 (c) we can

see that the intensity of the prominent (100) diffraction peak for different samples was

in an increasing order of P3HT/TiO$_2$-pyr, P3HT/TiO$_2$-Cudye and P3HT/TiO$_2$-(oligomer

3HT-COOH), being higher in IM-contained films. This fact indicates that IM, as the

organic molecule existed on the interface of P3HT and TiO$_2$, can serve as the

intermediate to enhance the crystallinity of P3HT, especially when a driving force for

ordering of polymer chains is applied. The morphology of the hybrid films is altered

thereby (according to the results of AFM). Although the IM-induced "ordering effect"

of P3HT was not quite evident in the spin-coated P3HT/TiO$_2$-Cudye thin films as

observed by AFM and the absorption spectra, we did have some different observations

by XRD with the drop-casted thick films, owing to the fact that the sample preparation

conditions were quite different for spin-casted thin films and drop-casted thick films.
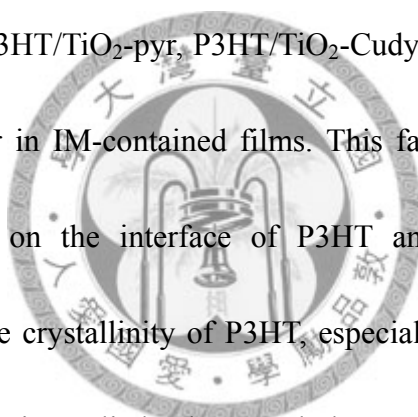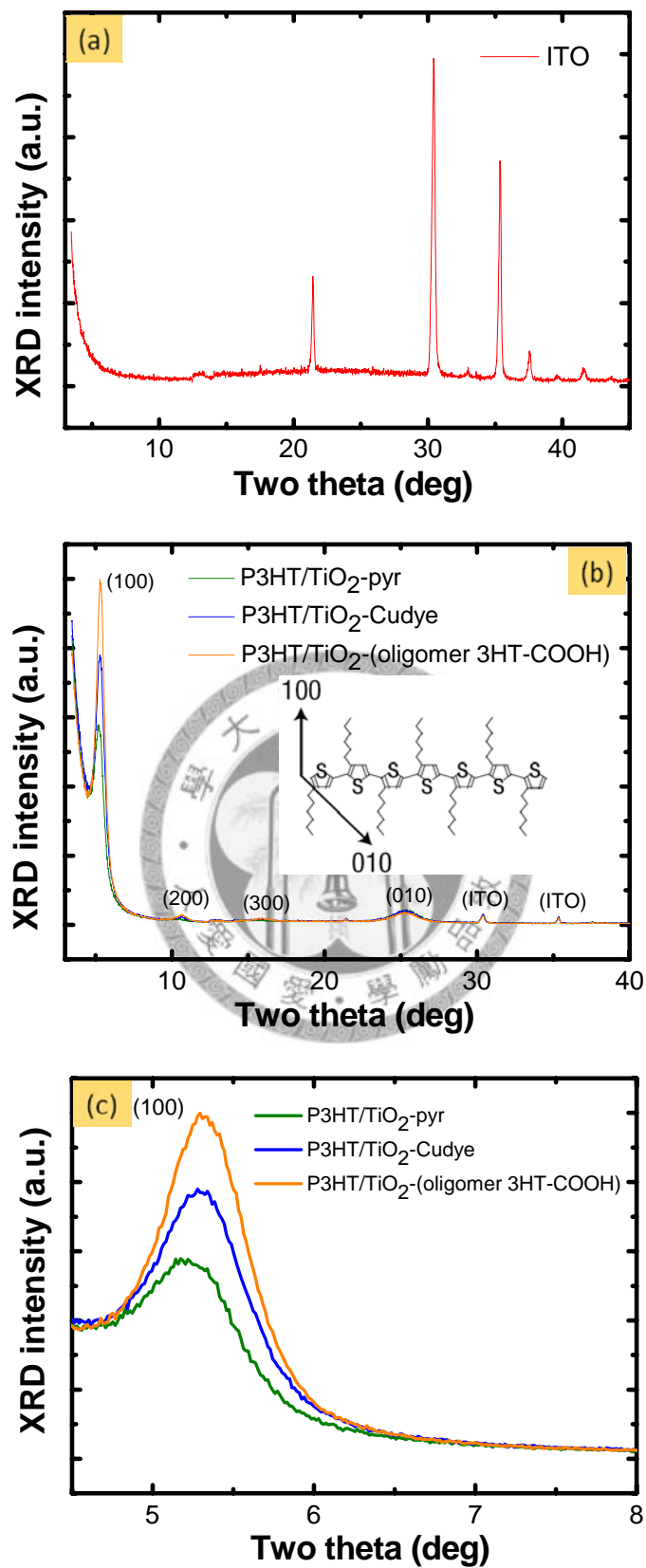
Figure 3.26 X-ray diffraction patterns of (a) ITO glass substrate and (b) drop casted P3HT/TiO$_2$-IM hybrid films after annealing. The (100) peak of P3HT is magnified and shown in (c).

3.5 Device performance

All the previous data show that the oligomer 3HT-COOH is the better performed interface modifier than Cudye. For this reason, solar cell devices based on the P3HT/TiO$_2$-(oligomer 3HT-COOH) system were fabricated, together with the P3HT/TiO$_2$-OA and P3HT/TiO$_2$-pyr system for comparison. Figure 3.27 shows the J-V curve of devices under simulated A.M. 1.5 illumination (100mW/cm^2). The device characteristics are summarized in Table 5. By removing the insulating oleic acids and replacing with suitable interface modifiers, we can enhance device performance by more than 3 folds. The enhancement is from the substantially increased J$_{sc}$, probably due to the improved charge separation and suppressed back recombination.
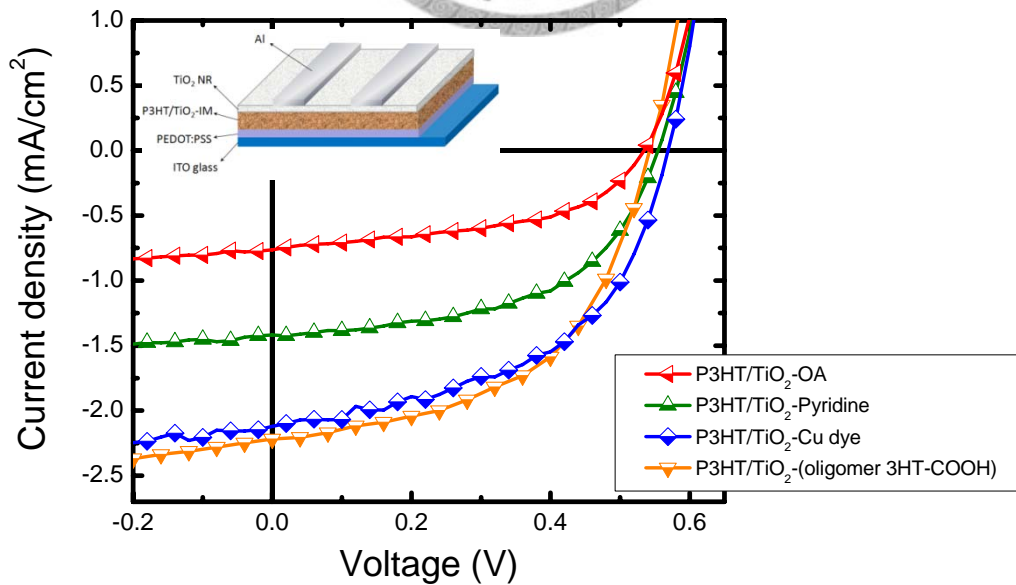
Figure 3.27 J-V characteristics of devices based on P3HT and surface modified TiO$_2$ nanorod under A.M. 1.5 (100mW/cm^2) irradiation. The architecture of device is shown in the inset.

Table 5 Device performance of P3HT/modified TiO$_2$ nanorod bulk heterojunction solar cells under A.M. 1.5 (100mW/cm^2) irradiation.

Sample	V_{oc} (V)	J_{sc} (mA/cm^2)	FF	PCE (%)
P3HT/TiO$_2$-OA	0.54	0.76	50.03	0.21
P3HT/TiO$_2$-pyr	0.58	1.42	54.97	0.43
P3HT/TiO$_2$/-Cudye	0.57	2.12	51.67	0.62
P3HT/TiO$_2$-(oligomer 3HT-COOH)	0.55	2.59	52.58	0.72

Chapter 4   Conclusion

This work has studied on the effect of surface modification of TiO_2 nanorod in P3HT/TiO_2 hybrid system for photovoltaic applications. Attempts have been made to replace the insulating ligand (oleic acid) on TiO_2 surface with more conductive interface modifiers (Cudye and oligomer 3HT-COOH). From the TGA and XPS results, it was inferred that oleic acid was partially removed from TiO_2 surface during the modification processes, yielding a cleaner surface for the interface modifiers to adsorb on. Qualitative and quantitative surveys revealed that while there was only a small amount of interface modifiers on the surface of TiO_2, the adsorption of interface modifiers was strong enough such that the surface hydrophobicity of TiO_2 and the tendency for TiO_2 to self-aggregate were effectively changed. Despite that the interface modifiers could not contribute too much to the overall light harvesting in P3HT/TiO_2-IM hybrid system for their small amount of adsorption, charge separation efficiency in this system was effectively enhanced and charge-carrier recombination was suppressed. Compared to Cudye, oligomer 3HT-COOH exhibited a better effect on facilitating charge separation and reducing recombination, probably because of its highly conductive nature and bulky molecular size. Moreover, as interfacial treatments were performed, the compatibility between P3HT and TiO_2 was enhanced by exhibiting a more similar surface

hydrophobicity and higher polymer crystallinity in the P3HT/TiO$_2$ hybrid films, especially as oligomer 3HT-COOH was employed to modify the surface of TiO$_2$. Benefited by surface modification, the efficiency of the P3HT/TiO$_2$ hybrid solar cells can be increased by more than 3 folds from the original 0.21% to 0.72% using oligomer 3HT-COOH as the interface modifier.

References

[1] N. C. Greenham, X-G Peng, and A. P. Alivisatos*, "Charge Separation and Transport in Conjugated-Polymer/Semiconductor-Nanocrystal Composites Studied by Photoluminescence Quenching and Photoconductivity," 1996, *Phys. Rev. B*, **54**, 17628-17637.

[2] W. U. Huynh, J. J. Dittmer, and A. P. Alivisatos*, "Hybrid Nanorod-Polymer Solar Cells," 2002, *Science*, **295**, 2425-2427.

[3] Y. Yin, A. P. Alivisatos*, "Colloidal Nanocrystal Synthesis and the Organic–Inorganic Interface," 2005, *Nature*, **437**, 664-670.

[4] G. Hopfengärtner, D. Borgmann*, I. Rademacher, G. Wedler, E. Hums, G. W. Spitznagel, "XPS Studies of Oxidic Model Catalysts: Internal Standards and Oxidation Numbers," 1993, *Journal of Electron Spectroscopy and Related Phenomena*, **63(2)**, 91-116.

[5] S. E. Shaheen, C. J. Brabec*, N. S. Sariciftci*, F. Padinger, T. Fromherz, and J. C. Hummelen, "2.5% Efficient Organic Plastic Solar Cells," 2001, *Appl, Phys. Lett.*, **78**, 841.

[6] N. M. D. Brown*, J. A. Hewitt, B. J. Meenan, "X-Ray-induced Beam Damage Observed During X-Ray Photoelectron Spectroscopy (XPS) Studies of Palladium Electrode Ink Materials," 1992, *Surface and Interface Analysis*, **18**, 187-198.

[7] P. J. Brown*, D. S. Thomas, A. Köhler, J. S. Wilson, J-S Kim, C. M. Ramsdale, H. Sirringhaus, and R. H. Friend, "Effect of Interchain Interactions on the Absorption and Emission of Poly(3-Hexylthiophene)," 2003, *Phys. Rev. B*, **67**, 064203.

[8] J.D. Olson, G.P. Gray, S.A. Carter*, "Optimizing Hybrid Photovoltaics through Annealing and Ligand Choice," 2009, *Solar Energy Materials and Solar Cells*, **93**, 519-523.

[9] Y-Y Lin, T-H Chu, S-S Li, C-H Chuang, C-H Chang, W-F Su, C-P Chang, M-W Chu, and C-W Chen*, "Interfacial Nanostructuring on the Performance of Polymer/TiO$_2$ Nanorod Bulk Heterojunction Solar Cells," 2009, *J. Am. Chem. Soc.*, **131**, 3644-3649.

[10] Y-Y Lin, Y-Y Lee, L-W Chang, J-J Wu, and C-W Chen*, "The Influence of Interface Modifier on the Performance of Nanostructured ZnO/Polymer Hybrid Solar Cells," 2009, *Appl. Phys. Lett.*, **94**, 063308.

[11] L. Shen, G-H Zhu, W-B Guo, C. Tao, X-D Zhang, C-X Liu, W-Y Chen*, S-P Ruan, and Z-C Zhong, "Performance Improvement of TiO$_2$/P3HT Solar Cells using CuPc as a Sensitizer," 2008, *Appl. Phys. Lett*, **92**, 073307.

[12] J-S Kim, J-H Park, J-H Lee, J. Jo, D-Y Kim, and Kilwon Cho*, "Control of the Electrode Work Function and Active Layer Morphology via Surface Modification of Indium Tin Oxide for High Efficiency Organic Photovoltaics," 2007, *Appl, Phys. Lett.*, **91**, 112111.

[13] C. G. Allen, D. J. Baker, J. M. Albin, H. E. Oertli, D. T. Gillaspie, D. C. Olson, T. E. Furtak and R. T. Collins*, "Surface Modification of ZnO using Triethoxysilane-based Molecules," 2008, *Langmuir*, **24**, 13393-13398.

[14] A. F. Nogueira, I. Montanari, J. Nelson, J. R. Durrant*, C. Winder, N. S. Sariciftci, C. Brabec, "Charge Recombination in Conjugated Polymer/Fullerene Blended Films Studied by Transient Absorption Spectroscopy," 2003, *J. Phys. Chem. B*, **107**, 1567-1573.

[15] N. Fourches*, G. Turban, B. Grolleau, "Study of DLC/Silicon Interfaces by XPS and In-situ Ellipsometry," 1993, *Applied Surface Science*, **68**, 149-160.

[16] J-S Liu, T. Tanaka, K. Sivula, A. P. Alivisatos, and J. M. J. Fre´chet*, "Employing End-Functional Polythiophene to Control the Morphology of Nanocrystal-Polymer Composites in Hybrid Solar Cells," 2004, *J. Am. Chem. Soc.*, **126**, 6550-6551.

[17] H. Sirringhaus, N. Tessler, and R. H. Friend*, "Integrated Optoelectronic Devices Based on Conjugated Polymers," 1998, *Science*, **280**, 1741-1744.

[18] H. Sirringhaus, P. J. Brown, R. H. Friend*, M. M. Nielsen, K. Bechgaard, B. M. W. Langeveld-Voss, A. J. H. Spiering, R. A. J. Janssen, E. W. Meijer, P. Herwig and D. M. de Leeuw, "Two-dimensional Charge Transport in Self-organized, High-mobility Conjugated Polymers," 1999, *Nature*, **401**, 685-688.

[19] D. Gebeyehu*, C. J. Brabec, N. S. Sariciftci, "Solid-state Organic/Inorganic Hybrid Solar Cells based on Conjugated Polymers and Dye-Sensitized TiO_2 Electrodes," 2002, *Thin Solid Films*, **403-404**, 271-274.

[20] J. Moser, S. Punchihewa, P. P. Infelta, and M. Grätzel*, "Surface Complexation of Colloidal Semiconductors Strongly Enhances Interfacial Electron-transfer rates," 1991, *Langmuir*, **7**, 3012-3018.

[21] M. Grätzel, "Photoelectrochemical Cells," 2001, *Nature*, **414**, 338-344.

[22] M. K. Nazeeruddin, R. H. Baker, P. Liska, and M. Grätzel, "Investigation of Sensitizer Adsorption and the Influence of Protons on Current and Voltage of a Dye-Sensitized Nanocrystalline TiO_2 Solar Cell," 2003, *J. Phys. Chem. B*, **107(34)**, 8981-8987.

[23] P. Wang, S. M. Zakeeruddin, P. Comte, R. Charvet, R. H. Baker, and M. Grätzel, "Enhance the Performance of Dye-Sensitized Solar Cells by Co-grafting Amphiphilic Sensitizer and Hexadecylmalonic Acid on TiO_2 Nanocrystals," 2003, *J. Phys. Chem. B*, **107(51)**, 14336-14341.

[24] H. J. Snaith, A. J. Moule, C. Klein, K. Meerholz, R. H. Friend, and M. Grätzel*, "Efficiency Enhancements in Solid-State Hybrid Solar Cells via Reduced Charge Recombination and Increased Light Capture," 2007, *Nano Lett.*, **7(11)**, 3372-3376.

[25] M. A. Green*, K. Emery, D. L. King, S. Igari, W.Warta, "Short Communication: Solar Cell Efficiency Tables (version 25)", 2005, *Progress in Photovoltaics*, **13(1)**, 49-54.

[26] B.A. Gregg*, M.C. Hanna, "Comparing Organic to Inorganic Photovoltaic Cells: Theory, Experiment, and Simulation," 2003, *J. Appl. Phys.*, **93**, 3605.

[27] P. B. Miranda, D. Moses, and A. J. Heeger*, "Ultrafast Photogeneration of Charged Polarons in Conjugated Polymers," 2001, *Phys. Rev. B*, **64**, 081201.

[28] S-H Park, A. Roy, S. Beaupre, S. Cho, N. Coates, J-S Moon, D. Moses, M. Leclerc, K-H Lee and A. J. Heeger*, "Bulk Heterojunction Solar Cells with Internal Quantum Efficiency Approaching 100%," 2009, *Nature Photonics*, **3**, 297-303.

[29] H. Hoppe*, N. S. Sariciftci, "Organic Solar Cells: An Overview," 2004, *J. Mater. Res.*, **19(7)**, 1924-1945.

[30] T. C. Monson, M. T. Lloyd, D. C. Olson, Y-J Lee, J. W. P. Hsu*, "Photocurrent Enhancement in Polythiophene- and Alkanethiol-Modified ZnO Solar Cells," 2008, *Adv. Mater.*, **20(24)**, 4755-4759.

[31] O. Inganäs*, W. R. Salaneck, J. E. Österholm, J. Laakso, "Thermochromic and Solvatochromic Effects in Poly(3-Hexylthiophene)," 1988, *Synth. Met.*, **22**, 395-406.

[32] W. J. E. Beek, M. M. Wienk, R. A. J. Janssen*, "Hybrid Solar Cells from Regioregular Polythiophene and ZnO Nanoparticles," 2006, *Adv. Funct. Mater.*, **16(8)**, 1112-1116.

[33] H-L Yip, S. K. Hau, N-S Baek, H. Ma, A. K. Y. Jen*, "Polymer Solar Cells that Use Self-assembled-monolayer-modified ZnO/Metals as Cathodes," 2008, *Adv. Mater.*, **20**, 2376-2382.

[34] S. Khodabakhsh, B. M. Sanderson, J. Nelson, T. S. Jones*, "Using Self-Assembling Dipole Molecules to Improve Charge Collection in Molecular Solar Cells," 2006, *Adv. Funct. Mater.*, **16**, 95-100.

[35] R. Zhang, J. Pan, E. P. Briggs, M. Thrash, L. L. Kerr*, "Studies on the Adsorption of RuN_3 Dye on Sheet-like Nanostructured Porous ZnO Films," 2008, *Solar Energy Materials and Solar Cells*, **92**, 425-431.

[36] Y-K Kim*, S. Cook, S. M. Tuladhar, S. A. Choulis, J. Nelson*, J. R. Durrant, D. D. C. Bradley, M. Giles, I. McCulloch, C-S Ha and M. Ree, "A Strong Regioregularity Effect in Self-Organizing Conjugated Polymer Films and High-Efficiency Polythiophene:Fullerene Solar Cells," 2006, *Nat. Mater.*, **5**, 197.

[37] J-W Kim, D-Y Khang, J-H Kim, and H-H Lee*, "The Surface Engineering of Top Electrode in Inverted Polymer Bulk-Heterojunction Solar Cells," 2008, *Appl. Phys. Lett.*, **92**, 133307.

[38] C. P. Leo´n*, L. Kador, B. Peng, and M. Thelakkat, "Characterization of the Adsorption of Ru-Bpy Dyes on Mesoporous TiO$_2$ Films with UV-Vis, Raman, and FTIR Spectroscopies," 2006, *J. Phys. Chem. B*, **110**, 8723-8730.

[39] K. C. Dickey, J. E. Anthony, and Y-L Loo*, "Improving Organic Thin-film Transistor Performance through Solvent-vapor Annealing of Solution-Processable Triethylsilylethynyl Anthradithiophene," 2006, *Adv. Mater.*, **18**, 1721-1726.

[40] R. J. Kline, M. D. McGehee* and M. F. Toney, "Highly Oriented Crystals at the Buried Interface in Polythiophene Thin-Film Transistors," 2006, *Nat. Mater.*, **5**, 222-228.

[41] Y-X Liu, S. R. Scully, M. D. McGehee*, J-S Liu, C. K. Luscombe, J. M. J. Fréchet, S. E. Shaheen, and D. S. Ginley, "Dependence of Band Offset and Open-Circuit Voltage on the Interfacial Interaction between TiO$_2$ and Carboxylated Polythiophenes," 2006, *J. Phys. Chem. B*, **110**, 3257-3261.

[42] C. Goh, S. R. Scully, and M. D. McGehee*, "Effects of Molecular Interface Modification in Hybrid Organic-Inorganic Photovoltaic Cells," 2007, *J. Appl. Phys.*, **101**, 114503.

[43] P. Ravirajan, A. M. Peiró, M. K. Nazeeruddin, M. Graetzel, D. D. C. Bradley, J. R. Durrant, and J. Nelson*, "Hybrid Polymer/Zinc Oxide Photovoltaic Devices with Vertically Oriented ZnO Nanorods and an Amphiphilic Molecular Interface Layer," 2006, *J. Phys. Chem. B*, **110**, 7635-7639.

[44] J.M. Nunzi*, "Organic Photovoltaic Materials and Devices," 2002, *C. R. Physique*, **3**, 523-542.

[45] N. Kudo, S. Honda, Y. Shimazaki, H. Ohkita*, S. Ito, and H. Benten, "Improvement of Charge Injection Efficiency in Organic-Inorganic Hybrid Solar Cells by Chemical Modification of Metal Oxides with Organic Molecules," 2007, *Appl. Phys. Lett.*, **90**, 183513.

[46] A. S. Amarasekara, M. Pomerantz*, "Synthesis and Study of Head-to-Tail Regioregular Poly(alkyl thiophene-3-carboxylates)," 2003, *Synthesis*, **14**, 2255-2258.

[47] R. Zhu, C-Y Jiang, B. Liu, S. Ramakrishna*, "Highly Efficient Nanoporous TiO₂-Polythiophene Hybrid Solar Cells based on Interfacial Modification using a Metal-free Organic Dye," 2008, *Adv. Mater.*, **21(9)**, 994-1000.

[48] A. Salleo*, T-W. Chen, A. R. Völkel, Y. Wu, P. Liu, B. S. Ong, and R. A. Street, "Intrinsic Hole Mobility and Trapping in a Regioregular Poly(Thiophene) ," 2004, *Phys. Rev. B*, **70**, 115311.

[49] L. Schmidt-Mende *, U. Bach, R. Humphry-Baker, T. Horiuchi, H. Miura, S. Ito, S. Uchida , M. Grätzel, "Organic Dye for Highly Efficient Solid-State Dye-Sensitized Solar Cells," 2005, *Adv. Mater.*, **17(7)**, 813-815.

[50] S. A. McDonald, G. Konstantatos, S-G Zhang, P. W. Cyr, E. J. D. Klem, L. Levina and E. H. Sargent*, "Solution-Processed PbS Quantum Dot Infrared Photodetectors and Photovoltaics," 2005, *Nat. Mater.*, **4**, 138-142.

[51] C. J. Brabec, S. E. Shaheen, C. Winder, N.S. Sariciftci*, and Patrick Denk, "Effect of LiF/Metal Electrodes on the Performance of Plastic Solar Cells," 2002, *Appl. Phys. Lett.*, **80(7)**, 1288-1290.

[52] E. Arici, N.S. Sariciftci*, D. Meissner, "Hybrid Solar Cells Based on Nanoparticles of CuInS₂ in Organic Matrices," 2003, *Adv. Funct. Mater.*, **13**, 165-171.

[53] H. Hoppe, N. S. Sariciftci*, "Organic Solar Cells: An Overview," 2004, *J. Mater. Res.*, **19(7)**, 1924-1944.

[54] T-W Zeng, Y-Y Lin, C-W Chen, W-F Su*, C-H Chen, S-C Liou, H-Y Huang, "A Large Interconnecting Network within Hybrid MEH-PPV/TiO₂ Nanorod Photovoltaic Devices," 2006, *Nanotechnology*, **17**, 5387–5392.

[55] I-S Liu, H-H Lo, C-T Chien, Y-Y Lin, C-W Chen, Y-F Chen*, W-F Su* and S-C Liou, "Enhancing Photoluminescence Quenching and Photoelectric Properties of CdSe Quantum Dots with Hole Accepting Ligands," 2008, *J. Mater. Chem.*, **18**, 675-682.

[56] Y-Y Lin, T-H Chu, C-W Chen*, and W-F Su*, "Improved Performance of Polymer/TiO₂ Nanorod Bulk Heterojunction Photovoltaic Devices by Interface Modification," 2008, *Appl. Phy. Lett.*, **92**, 053312.

[57] M-C Wu, H-H Lo, H-C Liao, S. Chen, Y-Y Lin, W-C Yen, T-W Zeng, Y-F Chen*, C-W Chen*, and W-F Su*, "Using Scanning Probe Microscopy to Study the Effect of Molecular Weight of Poly(3-Hexylthiophene) on the Performance of Poly(3-Hexylthiophene):TiO$_2$ Nanorod Photovoltaic Devices", 2009, *Solar Energy Materials and Solar Cells*, **93**, 869-873.

[58] C-A Dai, W-C Yen, Y-H Lee, C-C Ho, and W-F Su*, "Facile Synthesis of Well-Defined Block Copolymers Containing Regioregular Poly(3-hexyl thiophene) via Anionic Macroinitiation Method and Their Self-Assembly Behavior," 2007, *J. Am. Chem. Soc.*, **129**, 11036-11038.

[59] C-W Tang, "Two-layer Photovoltaic cell," 1986, *Appl. Phys. Lett.*, **48(2)**, 183-185.

[60] P. J. Thistlethwaite* and M. S. Hook, "Diffuse Reflectance Fourier Transform Infrared Study of the Adsorption of Oleate/Oleic Acid onto Titania," 2000, *Langmuir*, **16**, 4993-4998.

[61] R. H. Lohwasser, J. Bandara and M. Thelakkat*, "Tailor-Made Synthesis of Poly(3-Hexylthiophene) with Carboxylic End Groups and Its Application as a Polymer Sensitizer in Solid-State Dye-Sensitized Solar Cells," 2009, *J. Mater. Chem.*, **19**, 4126-4130.

[62] C-W Hsu, L-Y Wang*, W-F Su*, "Effect of Chemical Structure of Interface Modifier of TiO$_2$ on Photovoltaic Properties of Poly(3-Hexylthiophene)/TiO$_2$ Layered Solar Cells," 2009, *Journal of Colloid and Interface Science*, **329**, 182-187.

[63] F. Wudl, "The Chemical Properties of Buckminsterfullerene (C$_{60}$) and the Birth and Infancy of Fulleroids," 1992, *Acc. Chem. Res.*, **25**, 157-161.

[64] G. Li, V. Shrotriya, J-S Huang, Y. Yao, T. Moriarty, K. Emery and Y. Yang*, "High-Efficiency Solution Processable Polymer Photovoltaic Cells by Self-Organization of Polymer Blends," 2005, *Nat. Mater.*, **4**, 864.

[65] G. Li, Y. Yao, H-C Yang, V. Shrotriya, G-W Yang, and Y. Yang*, "Solvent Annealing Effect in Polymer Solar Cells based on Poly(3-hexylthiophene) and Methanofullerenes," 2007, *Adv. Funct. Mater.*, **17**, 1636-1644.